İSTANBUL TECHNICAL UNIVERSITY ★ INSTITUTE OF SCIENCE AND TECHNOLOGY

DETERMINATION OF MODE II DELAMINATION RESISTANCE OF CARBON / EPOXY LAMINATED COMPOSITES

M.Sc. Thesis by
İdil SEZER

Department : Aeronautics and Astronautics Engineering

Programme : Aeronautics and Astronautics Engineering

JUNE 2011

İSTANBUL TECHNICAL UNIVERSITY ★ INSTITUTE OF SCIENCE AND TECHNOLOGY

DETERMINATION OF MODE II DELAMINATION RESISTANCE OF CARBON / EPOXY LAMINATED COMPOSITES

M.Sc. Thesis by
İdil SEZER
(511081111)

Date of submission : 06 May 2011
Date of defence examination: 10 June 2011

Supervisor (Chairman) : Prof. Dr. Zahit MECİTOĞLU (ITU)
Members of the Examining Committee : Prof. Dr. Vedat Ziya DOĞAN (ITU)
Assoc. Prof. Dr. Şenol ATAOĞLU (ITU)

JUNE 2011

İSTANBUL TEKNİK ÜNİVERSİTESİ ★ FEN BİLİMLERİ ENSTİTÜSÜ

ÇOK KATMANLI KARBON / EPOKSİ KOMPOZİT MALZEMELERDE MOD II DELAMİNASYON DAYANIMININ ÖLÇÜLMESİ

YÜKSEK LİSANS TEZİ
İdil SEZER
(511081111)

Tezin Enstitüye Verildiği Tarih : 06 Mayıs 2011
Tezin Savunulduğu Tarih : 10 Haziran 2011

Tez Danışmanı : Prof. Dr. Zahit MECİTOĞLU (İTÜ)
Diğer Jüri Üyeleri : Prof. Dr. Vedat Ziya DOĞAN (İTÜ)
Doç. Dr. Şenol ATAOĞLU (İTÜ)

HAZİRAN 2011

FOREWORD

I would like thank my family for helping and encouraging me to this day, Astronautical Engineer Bora Büyükdoluca for his moral and technical support and my adviser Prof. Dr. Zahit Mecitoğlu for his guidance and wisdom. I also owe special thanks to Müslüm Çakır for his selfless working hours and Oras Polimer Plastik for their essential supplies donated to my study. This work is supported by ITU Institute of Science and Technology.

June 2011

İdil Sezer

(Aeronautical Engineer)

TABLE OF CONTENTS

Page

ABBREVIATIONS

FRP	**:** Fibre reinforced polymer
VCCT	**:** Virtual Crack Closure Technique
MCCI	**:** Modified Crack Closure Integral
NASA	**:** National Aeronautics and Space Administration
ASTM	**:** American Society for Testing and Materials
ESIS	**:** European Structural Integrity Society
JIS	**:** Japanese Industrial Standards
ISO	**:** International Organization for Standardization
DCB	**:** Double Cantilever Beam
ENF	**:** End Notch Flexure
SENF	**:** Stabilized End Notch Flexure
4ENF	**:** Four Point Bend End Notch Flexure
ELS	**:** End Loaded Split
ESIS TC 4	**:** ESIS Technical Committee 4
PTFE	**:** Polytetrafluorethylene
CBT	**:** Corrected Beam Theory
ECM	**:** Experimental Compliance Method

LIST OF TABLES

Page

LIST OF FIGURES

Page

DETERMINATION OF MODE II DELAMINATION RESISTANCE OF CARBON / EPOXY LAMINATED COMPOSITES

SUMMARY

Composite materials have become the modern base material of most industries today. Light structures with high performance and extensive variety are the main advantages composites offer. However, their unpredictable behavior introduces safety issues, leading to additional safety margins and higher cost. For a more effective use of composite materials, better analytical and numerical models must be developed.

Delamination is one of the failure modes of composites that require attention. It is a highly dangerous threat to composite structures for reducing the load bearing capacity of structure severely. Therefore, understanding this mode of failure is vital.

There are two main approaches when modelling delamination in composites. These are fracture mechanics based models and damage mechanics based models. There are finite element models to predict delamination initiation or growth, using various techniques of both approaches implemented into finite element codes.

One of the challenges to make composite structures safer against delamination occurrence is to come up with a proper testing method for a common ground when measuring the resistance of material to delamination.

There are three modes of delamination, which are mode I (opening mode), mode II (sliding mode) and mode III (tearing mode). Most commonly used and the only standardized test method for pure modes is mode I delamination test using DCB (double cantilever beam) specimen. For mode II and mode III testing, collaboration between several organizations is continuing. Especially for mode II testing, there are many specimens proposed; however the testing method remains highly controversial.

The subject of this thesis is mode II delamination of unidirectional carbon/epoxy composites. One of the proposed specimens for standardized test, ELS (end loaded split) specimen, is used within the experimental study according to the standardization proposal. Mode II delamination resistance of a hand-manufactured carbon/epoxy composite material is measured experimentally in accordance to this test protocol.

Geometry of the ELS specimen used in experimental study is ideally modeled within finite element software. Mechanical properties of manufactured material is obtained approximately using equations based on micromechanical analysis of composite materials and used for the material model of specimen. Cohesive zone model is used for the simulation of delamination behavior. Finite element analysis is performed under simulated test conditions.

Results of the experimental study and finite element analysis is compared. Delamination behavior in finite element results is found unlike from experimental results. Simulation of material softening in finite element results is observed to be close to experimental results.

Results are discussed and possible improvements to the study are noted.

ÇOK KATMANLI KARBON / EPOKSİ KOMPOZİT MALZEMELERDE MOD II DELAMİNASYON DAYANIMININ ÖLÇÜLMESİ

ÖZET

Kompozit malzemeler günümüzde pek çok endüstride temel yapı malzemesi haline gelmiştir. Yüksek performanslı hafif yapılar ve çok sayıda çeşit kompozit malzemelerin en büyük avantajları arasındadır. Ancak davranışlarının tahmin edilemez olması yapının güvenilirliğini azalttığından, bu sorun emniyet katsayısını arttırarak çözülmeye çalışılmaktadadır ve bu durum maliyeti arttırmaktadır. Kompozit malzemelerin daha verimli kullanılması için, daha iyi analitik ve sayısal modellerin geliştirilmesi gereklidir.

Delaminasyon (katman ayrılması), kompozit malzemelerinin göçme modlarından biri olarak ilgilenilmesi gereken bir konudur. Yapının yük taşıma kapasitesini ciddi şekilde azaltması sebebiyle kompozit yapılar için oldukça büyük bir tehdit teşkil etmektedir. Bu sebeple delaminasyonun hasar mekanizmasını anlamak oldukça önemlidir.

Delaminasyon modellemesinde, iki ana yaklaşım kullanılmaktadır. Bunlar, çatlak mekaniği tabanlı yaklaşım ile hasar mekaniği tabanlı yaklaşımlardır. Ayrıca iki yaklaşımdan da alınan çeşitli hasar tahmin teknikleri sonlu elemanlar kodlarında kullanılarak sayısal modeller oluşturulmaktadır.

Kompozit yapıları delaminasyon hasarına karşı daha güvenli hale getirmekteki en büyük zorluklardan biri, malzemenin delaminasyon dayanımını ölçmek için kullanılacak standart test metodları bulmaktır.

Delaminasyon hasarının 3 modu vardır: mod I (açılma modu), mod II (kayma modu) ve mod III (kesme modu). En yaygın kullanılan test metodu, aynı zamanda mod I, II ve III arasında standart aşamasına ulaşabilen tek test metodu olan, çift ankastre kiriş numunesi kullanılarak yapılan mod I delaminasyon testidir. Kayma ve kesme modlarında test standardı oluşturma çabaları, çeşitli organizyonlar arasında işbirliği ile sürdürülmektedir. Özellikle mod II için pek çok numune bulunmaktadır, ancak test metodunda fikir birliğine varılamamaktadır.

Bu tez çalışmasının konusu tek yönlü karbon / epoksi kompozitlerde mod II delaminasyonudur. Standart için önerilen numuneler arasından sondan yüklemeli ayrık numune kullanılarak, önerilen prosedüre uygun biçimde deneyler gerçekleştirilmiştir. Elde üretilmiş bir karbon / epoksi kompozit malzemenin mod II delaminasyon dayanımı, bu test protokolüne uygun biçimde ölçülmüştür.

Deney numunesinin geometrisi, sonlu elemanlar yazılımı kapsamında ideal olarak modellenmiştir. Üretilen malzemenin mekanik özellikleri, kompozit malzemelerin mikromekanik analizine dayanan denklemlerle yaklaşık olarak bulunmuş, numunenin malzeme modelinde kullanılmıştır. Delaminasyon davranışının simülasyonu için hasar mekaniği tabanlı yaklaşım kullanılmıştır. Simüle edilen deney koşullarıyla beraber sonlu elemanlar analizi gerçekleştirilmiştir.

Deneysel çalışmanın sonuçları ile sonlu elemanlar analizinin sonuçları karşılaştırılmıştır. Delaminasyon davranışı iki çalışmada farklılık göstermekte, sonlu elemanlar sonuçlarından elde edilen malzeme yumuşamasının simülasyonu deneysel sonuçlarla uyum göstermektedir.

Sonuçlar tartışılmış ve çalışmaya eklenebilecek olası gelişmeler saptanmıştır.

1. INTRODUCTION

Composite materials are being increasingly used in a wide range of industrial applications where high strength to weight ratio is in need. With an extensive variety of constituent materials and being adjustable to fit the need, composites are preferable in many areas.

Fibre reinforced polymers, which are commonly referred to as FRPs, are considered the new base material in a number of industries such as automotive, aerospace, construction and marine. These materials are commonly accepted as modern composites.

Although FRP composites provide better mechanical properties, their behavior and failure mechanisms are not fully understood yet. In order to compensate the lack of knowledge and experience, safety margins are being increased leading to additional weight and cost.

Delamination is one of the failure modes that require consideration while designing a laminated composite. Physical phenomenon of delamination can be simply described as the separation of adjacent layers in a laminated composite material. It can occur due to various reasons that can take place during manufacturing, maintenance or service and it may reduce the load bearing capacity and service life of a FRP structure severely. Resistance of a FRP composite to delamination initiation or propagation, also known as delamination toughness, is expressed with the quantity of critical energy release rate which is a concept based on fracture mechanics. Delamination toughness is becoming widely accepted as a material property and it can be calculated or measured via mathematical models and standardized tests.

1.1 Background

As a result of understanding the majority of the subject, delamination failure in composites received a great deal of research attention within the past decades.

Mathematical and numerical models were developed for delamination modeling within the framework of fracture mechanics and damage mechanics. In fracture mechanics; delamination in composites was defined in accordance to the concepts of fracture mechanics as a problem [1, 2]. Then the problem is solved by means of calculating strain energy release rates with various techniques. One of the most widely adopted techniques is Virtual Crack Closure Technique (VCCT) originating from crack closure concept developed by George R. Irwin in 1957 [3-5]. This technique is mostly employed in interface elements for finite element codes in either original [6-11] or enhanced forms [12, 13]. Implementation of VCCT into finite element code was discussed by Matthews and Hitchings [14]. A well-known interface element was developed by Xie and Biggers [15, 16] for calculating strain energy release rates during delamination growth by using stationary meshes. This element was implemented into Abaqus FEA [17]. Another interface element by Xie and Biggers [18] based on Modified Crack Closure Integral (MCCI) proposed by Rybicki and Kanninen [19] in 1977; was designed for 2D progressive crack growth problems and applicable for simulation of delamination in composites. J-integral is also a fracture mechanical method for calculating strain energy release rate developed by Genady P. Cherepanov in 1967 [20] and by James R. Rice in 1968, independently [21]. This technique is utilized frequently to calculate strain energy release rates in delamination models, mostly for analytical solutions to complex problems [22-27]. Another approach for simulating delamination is damage mechanics based cohesive zone model [28]. With certain advantages it provides over fracture mechanics based approach, cohesive zone model is extensively used in analytical and numerical solutions [29-34].

Standardization of delamination test methods has also a long history. The purpose of these efforts is to develop reliable test methods to obtain delamination toughness of a material experimentally. A number of test specimens have been proposed for all pure modes (I, II and III) and mixed modes (I/II, I/III and II/III) which were evaluated with an international collaboration between many organizations. Some test method

proposals became standardized such as mode I [35, 36] and mixed mode I/II [37] while most test methods are still in proposal stage [38].

For mode II delamination test methods, several number of test specimens were proposed. Some of these specimens are ENF [39], SENF [40], 4ENF [41] and ELS [42] specimens. However, the idea of whether it is possible to provide pure shear stress for delamination, remains controversial [43].

1.2 Purpose of the Study

Aim of this study is to investigate delamination toughness property of a hand-manufactured unidirectional carbon reinforced epoxy composite through experimental and finite element methods.

Experimental study is based on a protocol for mode II tests using ELS specimen [44]. Unidirectional carbon/epoxy composite material to be tested in experiments is hand-manufactured and implemented with an initial defect. These specimens were tested under bending loading in order to induce and observe the propagation of mode II delamination.

For the finite element model and analysis, SAMCEF finite element software was utilized. Specimen and loading conditions are ideally modeled and delamination behavior was simulated with cohesive zone model.

Results are presented; accuracy of experimental results for measuring delamination resistance and finite element analysis results for simulating delamination behavior are discussed.

2. DELAMINATION IN COMPOSITES

2.1 Causes of Delamination

Delamination initiation or propagation occurs under high interlaminar stress conditions. Residual stresses which originate from manufacturing process, change in temperature and humidity conditions or geometrical configuration are generally permanent high interlaminar stress sources and their effects on material arise in long term. Mechanical loads on the other hand, such as low velocity impact or machining of the structure, introduce momentary increase in interlaminar stress and their effects can be detected immediately. These causes which lead to delamination initiation or propagation are explained below.

2.1.1 Manufacturing

Manufacturing process of FRP composites generally requires resin curing. In order to provide the conditions for a curing reaction, component is heated to high temperatures and then cooled down to room temperature. This process applies 200-300°C of temperature difference on laminate, which leads to residual stress in laminate arising from different thermal expansion coefficients of laminae. Due to orthotropic nature of the material, laminae with different orientations display mismatching thermal expansions. Therefore, laminate consisting of laminae with varying lay-up angles undergoes residual stress and becomes less resilient to delamination [45].

2.1.2 Environmental effects

Temperature and humidity are two main environmental effects influencing mechanical properties of FRP composites. Change in humidity conditions, as well as thermal effects, cause residual stress within laminate due to moisture absorption followed by anisotropic differing in material properties and therefore decrease material's resistance to delamination [45].

2.1.3 Drilling

When building a composite structure, drilling holes into composite parts may be necessary for fastening, cabling or weight saving. However, this operation induces high interlaminar stress and frequently causes delamination in area surrounding the hole.

Top layers are forced upwards and bottom layers downwards during the entrance and exit of the drill bit, respectively. After penetration, back surface of the material and nearby plies are usually observed to be more damaged than the front surface (Figure 2.1).

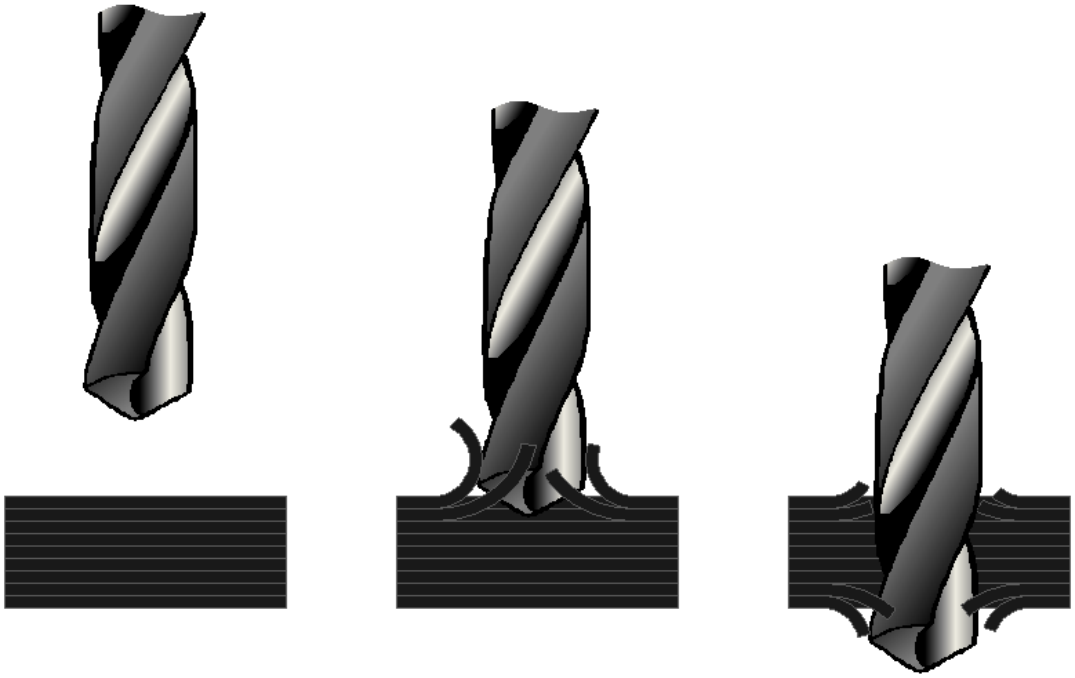

Figure 2.1 : Delamination caused by drilling

Resultant delamination may propagate to become critical for the structure under further loading. For avoiding structural failure and minimizing interlaminar damage, better knowledge on damage mechanisms of drilling and investigation on special drills are necessary [46, 47].

2.1.4 Geometrical configuration

Main reasons to geometry-dependent delamination are discontinuities in material and configurations leading to singularities in interlaminar stress. Several geometrical cases leading to delamination are given below [48].

Taper: Internal or external ply drops cause critical stress intensities under tension and bending loads.

Inclusions: Bolts, holes and notches are critical for causing stress singularity at the area near inclusion. Structures with inclusion are prone to delamination particularly under bearing conditions.

Skin-stringer debonding: Joining techniques applied during curing stage of FRPs are commonly used instead of traditional methods. Some of the joining elements utilized in these processes, such as stringers, may cause delamination when debonding from the laminate under several loading scenarios.

Free-edge: One of the most common causes of delamination is known as free-edge effect. This effect arises from differences in lamina properties stacked together. These differences cause high interlaminar stress at the edge of the component, leading to delamination under long term loading.

2.1.5 Low velocity impact

Low velocity impacts may occur during manufacturing, maintenance or service life by means of dropped objects, runway debris, etc. Impacts taken on composite shell structures over a certain velocity or kinetic energy limit result in matrix cracks inducing delamination. This limit depends on properties of the laminate. After impact, delamination effect may be observed right away or on the long term loading, depending on the velocity of the impact [49, 50].

2.2 Delamination Modeling

Delamination occurrence is a potentially dangerous phenomenon; however it is not completely intolerable. Not every delamination in a laminated structure necessarily leads to catastrophic failure. To ensure the structural resistance or tolerance to this kind of damage, gaining comprehensive knowledge on delamination behavior and boundaries of acceptability is vital. Therefore, developing tools to predict delamination initiation and propagation is in need for designing more reliable and stable structures with lower cost. With the improvement of these tools including analytical models, numerical methods and standardized tests, FRP composites can be utilized more safely and widely.

There are two main approaches for delamination modeling in FRP composites: Fracture mechanics based models and damage mechanics based models.

2.2.1 Fracture mechanics based models

As a physical phenomenon, delamination in a FRP composite can be considered as an interlaminar crack formed in anisotropic media. Therefore, most analytical and numerical models utilized to predict delamination behavior of a composite material are extended from fracture mechanics concepts applying to isotropic materials.

2.2.1.1 Fracture modes

In fracture mechanics, any deformation or crack propagation can be defined as a combination of three the modes of fracture (Figure 2.2). Mode I or opening mode expresses the deformation caused by normal stresses applied in normal direction to the plane of crack. Sliding mode, denoted by mode II originates from in-plane shear stress inducing crack propagation perpendicular to the leading edge. Mode III, which is tearing mode, refers to the deformation parallel to leading edge, caused by out-of-plane shear stress [51].

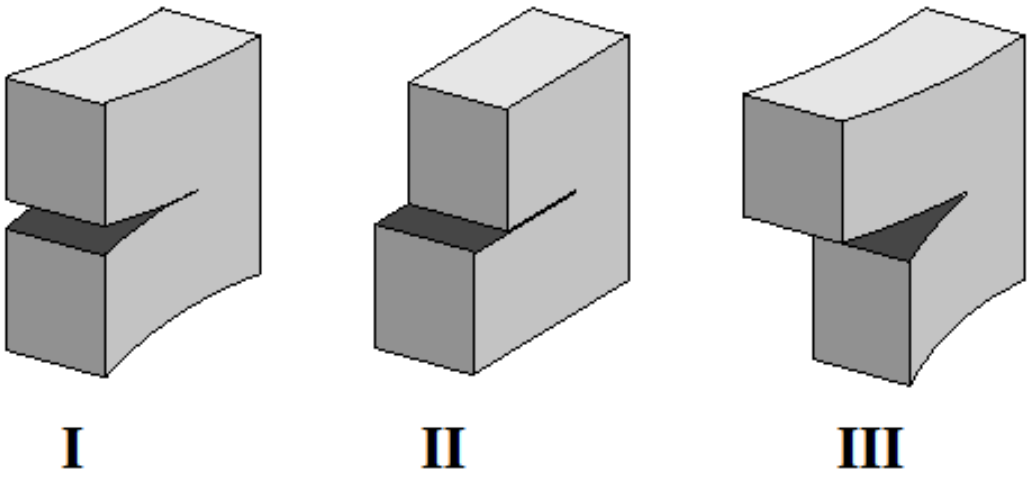

Figure 2.2 : Three fracture modes

2.2.1.2 Stress and deformation fields

Elastic stress field near a crack tip was first characterized by George R. Irwin (1907-1998) in late 1950s [52]. Irwin introduced the “stress intensity factor” concept to fracture mechanics, which facilitated the calculation of crack-tip stress and strain

fields subjected to tensile and shear loads [53]. Up to the present day, the elastic stress field near a crack tip has been a subject to a number of studies [1, 54].

According to this concept, a crack is defined as a line of discontinuity with zero thickness and $2a$ length in a homogeneous isotropic linear elastic infinite plate (Figure 2.3).

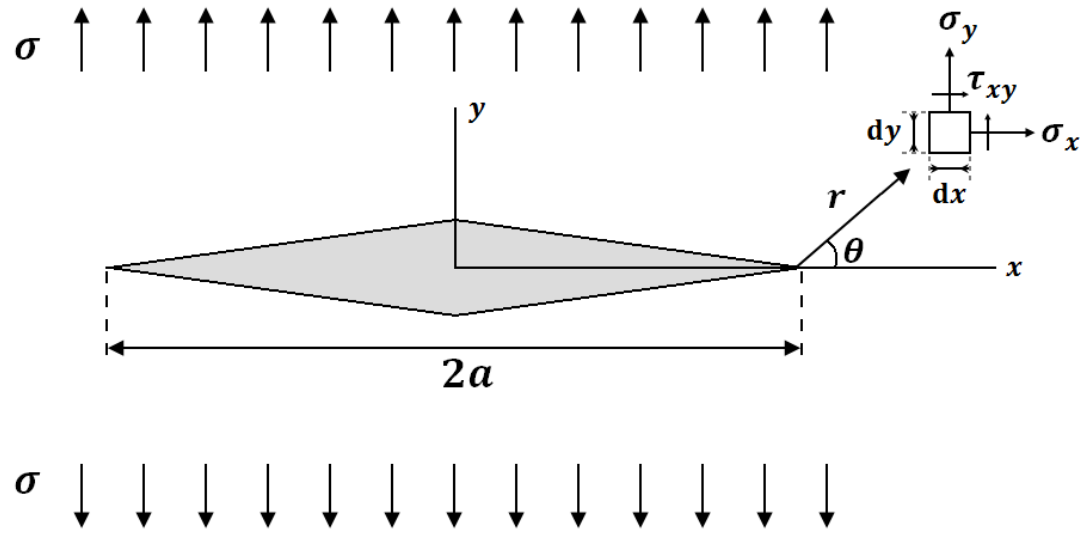

Figure 2.3 : Crack in a homogeneous isotropic linear elastic infinite plate

Assuming that a tensile stress σ is applied to the crack at infinity, stresses of an element dxdy at distance r and angle θ to the crack tip are evaluated for mode I as following:

$$\sigma_x = \sigma\sqrt{\frac{a}{2r}}\cos\left(\frac{\theta}{2}\right)\left[1 - \sin\left(\frac{\theta}{2}\right)\sin\left(\frac{3\theta}{2}\right)\right]$$

$$\sigma_y = \sigma\sqrt{\frac{a}{2r}}\cos\left(\frac{\theta}{2}\right)\left[1 + \sin\left(\frac{\theta}{2}\right)\sin\left(\frac{3\theta}{2}\right)\right]$$

$$\tau_{xy} = \sigma\sqrt{\frac{a}{2r}}\cos\left(\frac{\theta}{2}\right)\sin\left(\frac{\theta}{2}\right)\cos\left(\frac{3\theta}{2}\right)$$

$\sigma_z = 0$ for plane stress,

$\sigma_z = \nu(\sigma_x + \sigma_y)$ for plane strain. **(2.1)**

Generalized form can be written as

$$\sigma_{ij} = \frac{K_I}{\sqrt{2\pi r}} f_{ij}(\theta)$$

where $K_I = \sigma\sqrt{\pi a}$ **(2.2)**

Equation 2.1 and 2.2 shows the evaluation of K_{I}, which is the stress intensity factor for mode I. This factor is also evaluated for mode II and mode III, allowing the stress field around a crack tip to be characterized as following:

$$\sigma_x = \frac{K_{\mathrm{I}}}{\sqrt{2\pi r}}\cos\left(\frac{\theta}{2}\right)\left[1-\sin\left(\frac{\theta}{2}\right)\sin\left(\frac{3\theta}{2}\right)\right] - \frac{K_{\mathrm{II}}}{\sqrt{2\pi r}}\sin\left(\frac{\theta}{2}\right)\left[2+\cos\left(\frac{\theta}{2}\right)\cos\left(\frac{3\theta}{2}\right)\right]$$

$$\sigma_y = \frac{K_{\mathrm{I}}}{\sqrt{2\pi r}}\cos\left(\frac{\theta}{2}\right)\left[1+\sin\left(\frac{\theta}{2}\right)\sin\left(\frac{3\theta}{2}\right)\right] + \frac{K_{\mathrm{II}}}{\sqrt{2\pi r}}\sin\left(\frac{\theta}{2}\right)\cos\left(\frac{\theta}{2}\right)\cos\left(\frac{3\theta}{2}\right)$$

$$\tau_{xy} = \frac{K_{\mathrm{I}}}{\sqrt{2\pi r}}\cos\left(\frac{\theta}{2}\right)\sin\left(\frac{\theta}{2}\right)\cos\left(\frac{3\theta}{2}\right) + \frac{K_{\mathrm{II}}}{\sqrt{2\pi r}}\cos\left(\frac{\theta}{2}\right)\left[1-\sin\left(\frac{\theta}{2}\right)\sin\left(\frac{3\theta}{2}\right)\right]$$

$$\tau_{yz} = \frac{K_{\mathrm{III}}}{\sqrt{2\pi r}}\cos\left(\frac{\theta}{2}\right)$$

$$\tau_{zx} = -\frac{K_{\mathrm{III}}}{\sqrt{2\pi r}}\sin\left(\frac{\theta}{2}\right)$$

$\sigma_z = 0$ for plane stress,

$\sigma_z = \nu(\sigma_x + \sigma_y)$ for plane strain. **(2.3)**

Also, deformations can be written as:

$$u = \frac{K_{\mathrm{I}}}{2\mu}\sqrt{\frac{r}{2\pi}}\cos\left(\frac{\theta}{2}\right)\left[\kappa-1+2\sin^2\left(\frac{\theta}{2}\right)\right] + \frac{K_{\mathrm{II}}}{2\mu}\sqrt{\frac{r}{2\pi}}\sin\left(\frac{\theta}{2}\right)\left[\kappa+1+2\cos^2\left(\frac{\theta}{2}\right)\right]$$

$$v = \frac{K_{\mathrm{I}}}{2\mu}\sqrt{\frac{r}{2\pi}}\sin\left(\frac{\theta}{2}\right)\left[\kappa+1-2\cos^2\left(\frac{\theta}{2}\right)\right] - \frac{K_{\mathrm{II}}}{2\mu}\sqrt{\frac{r}{2\pi}}\cos\left(\frac{\theta}{2}\right)\left[\kappa-1-2\sin^2\left(\frac{\theta}{2}\right)\right]$$

$$w = \frac{2K_{\mathrm{III}}}{\mu}\sqrt{\frac{r}{2\pi}}\sin\left(\frac{\theta}{2}\right)$$

$\kappa = \frac{3-\nu}{1+\nu}$ for plane stress,

$\kappa = 3-4\nu$ for plane strain **(2.4)**

where μ is shear modulus and ν is Poisson's ratio.

2.2.1.3 Irwin's crack closure concept and strain energy release rate

According to Irwin's crack closure concept, the work done on a brittle material is spent for creating new crack surfaces, since very little energy is used for plastic deformation. Therefore, extending a crack's length from a to $a+\Delta a$ requires the same amount of work to close the crack from $a+\Delta a$ to a [3]. Using stress and deformation field equations, the work required to close a crack from length $a+\Delta a$ to a is written as:

$$W = \frac{1}{2}\int_0^{\Delta a} \sigma_y(\Delta a - r)\, v(r)\, \mathrm{d}r \quad \textbf{(2.5)}$$

And strain energy release rate G is obtained as:

$$G = \lim_{\Delta a \to 0} \frac{W}{\Delta a} = \lim_{\Delta a \to 0} \frac{1}{2\Delta a}\int_0^{\Delta a} \sigma_y(\Delta a - r)\, v(r)\, \mathrm{d}r \quad \textbf{(2.6)}$$

Substituting G in stress and deformation field equations and integrating:

$$G = G_{\mathrm{I}} + G_{\mathrm{II}} + G_{\mathrm{III}} = \frac{K_{\mathrm{I}}^2}{E'} + \frac{K_{\mathrm{II}}^2}{E'} + (1+\nu)\frac{K_{\mathrm{III}}^2}{E} \quad \textbf{(2.7)}$$

G is total strain energy release rate and G_{I} , G_{II} and G_{III} are mode I, mode II and mode III energy release rates, respectively. Likewise; K_{I} , K_{II} and K_{III} are mode I, mode II and mode III stress intensity factors, respectively.

$E' = E$ for plane stress

$E' = E/(1-\nu^2)$ for plane strain, **(2.8)**

where E is the Young's modulus and ν is the Poisson's ratio of the material.

Strain energy release rate is one of the most fundamental concepts in fracture mechanics. This quantity expresses the released energy per unit area of the newly formed surface of progressed crack. Strain energy release rate is used as a failure criterion for predicting delamination initiation or propagation. According to this criterion, crack extension occurs when this quantity reaches a critic value, G_c. This value is called critical energy release rate, and varies for all three modes. Predicting delamination initiation or propagation via critic strain energy release rate value is called the Virtual Crack Closure Technique (VCCT) [4, 5] and is implemented widely in finite element programs such as Abaqus FEA and MSC Nastran [17, 55].

2.2.2 Damage mechanics based models

Another approach to delamination failure is developed within the framework of damage mechanics. These are cohesive zone or interface models. Advantage of these models over fracture mechanics based models arise mostly in finite element models, where tracking the growth of delamination easier since remeshing is not needed for representation of material softening. Another major advantage is discarding the need for an initial crack and therefore enabling the prediction of delamination initiation as well as propagation [56].

According to this model, a cohesive or interface layer is assumed to exist between delamination surfaces. This layer is used for modeling the material softening, and it may have linear or nonlinear responses under normal and shear stress conditions. The core of the model is traction-displacement curve. Damage initiation occurs when traction τ reaches the interfacial strength or maximum traction τ° (Figure 2.4). When area under the curve is equal to interlaminar fracture toughness G_c, traction reaches zero. This means that the fracture energy is released and the crack formation is complete. After a new crack is created, the delaminated area is represented by a traction-free geometrical discontinuity [28].

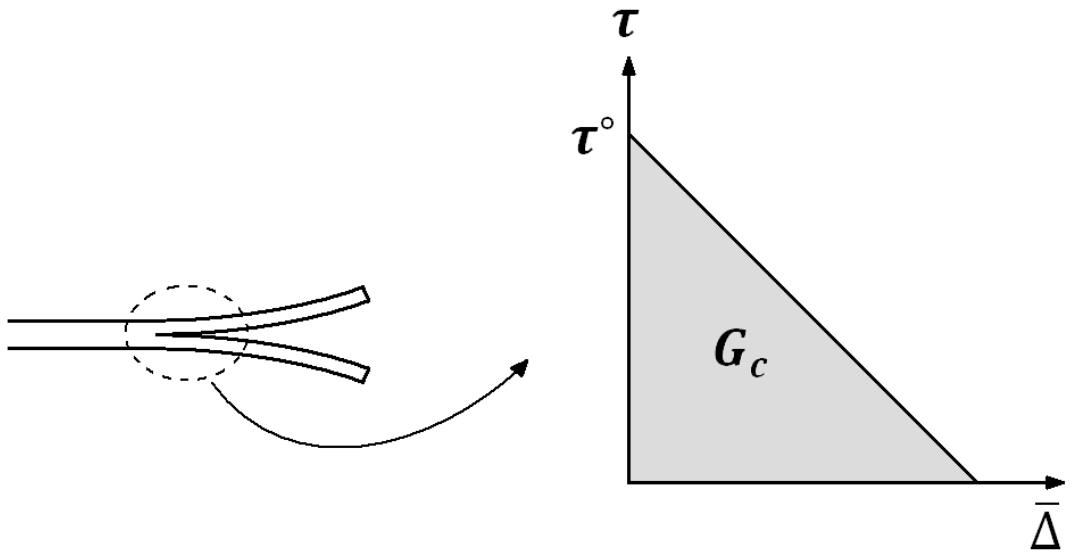

Figure 2.4 : Traction-displacement curve for the tip of the delamination

2.2.2.1 Pure mode loading criterion

Criteria for delamination initiation and propagation are simple for pure mode loading. Delamination initiation is predicted when traction of mode I (τ_1), mode II (τ_2) or mode III (τ_3) reaches interfacial strength or maximum traction in mode I (τ_1°), II (τ_2°) or mode III (τ_3°), respectively. Therefore initiation criterion for pure mode loading expressed in generalized form is:

$$\tau_i = \tau_i^{\circ} \qquad \textbf{(2.9)}$$

Similarly, when energy release rate calculated as area under traction-displacement curve of mode I (G_{I}), mode II (G_{II}) or mode III (G_{III}) reaches interfacial strength or maximum traction of mode I (G_{I_c}), II (G_{II_c}) or mode III (G_{III_c}), respectively, delamination propagates.

2.2.2.2 Mixed-mode loading criterion

Mixed-mode loading criterions on the other hand, are more complicated due to coupling effects between modes. Cohesive models for predicting delamination initiation, taking interaction of modes into account, are usually based on Ye's criterion [57]:

$$\mathrm{f}_{initiation} = \mathrm{f}(\tau_i) - 1 = \left(\frac{\langle \tau_3 \rangle}{\tau_3^\circ}\right)^2 + \left(\frac{\tau_2}{\tau_2^\circ}\right)^2 + \left(\frac{\tau_1}{\tau_1^\circ}\right)^2 - 1 = 0 \qquad \textbf{(2.10)}$$

where $\mathrm{f}_{initiation}$ is the failure criterion, $\mathrm{f}(\tau_i)$ is the norm of tractions and $\langle . \rangle$ is the MacAuley bracket defined as

$$\langle x \rangle = \frac{1}{2}(x + |x|) \qquad \textbf{(2.11)}$$

One of the commonly used failure criterions for predicting delamination propagation is the power law expression [58]:

$$\mathrm{f}_{propagation} = \mathrm{f}(G_i) - 1 = \left(\frac{G_\mathrm{I}}{G_{\mathrm{I}_c}}\right)^\alpha + \left(\frac{G_\mathrm{II}}{G_{\mathrm{II}_c}}\right)^\beta + \left(\frac{G_\mathrm{III}}{G_{\mathrm{III}_c}}\right)^\gamma - 1 = 0 \qquad \textbf{(2.12)}$$

where α, β and γ are determined via experimental study. When experimental data is not available, these variables are chosen as $\alpha = \beta = \gamma = 1$ for linear, and $\alpha = \beta = \gamma = 2$ for quadratic failure criteria.

2.3 Standardization of Delamination Testing

As a result of rapidly developing knowledge of composite materials, delamination damage is today known to be a threat to FRP structures. Understanding the loading conditions leading to this mode of failure is the first step to eliminate this threat. After that, the structures can be built to undergo these loading conditions safely. To achieve this goal, interlaminar strength of the material must be known accurately. Therefore, standard testing methods are necessary to measure interlaminar fracture toughness of FRP composites, for both quality assurance and safety issues.

2.3.1 Historical development

Fracture testing methods of composite materials are not a recent research subject. First testing methods were based on studies of other materials, such as mica in 1930s, metal crystals in 1950s, and timber in 1970s. Efforts to develop standard testing methods for measuring delamination resistance of composites have a long history,

starting from early 1980s. First delamination test procedure was proposed within a NASA document published in 1982 [59], describing a mode I delamination test based on DCB (Double Cantilever Beam) specimen. A methodology to measure G_{I_c} was defined in the document, which was later used by resin and composite suppliers to develop new resin systems [60].

Most of the test methods for pure and mixed fracture modes are still in standardization progress and are being developed with the contributions of ASTM (American Society for Testing and Materials), ESIS (European Structural Integrity Society) and JIS (Japanese Industrial Standards) organizations.

Delamination testing methods for mode I and mode II are shortly described below. Mode III and mixed modes are not mentioned in this study.

2.3.2 Mode I delamination testing

After years of collaboration between ASTM, ESIS and JIS, mode I testing method using DCB specimen (Figure 2.5) passed as an ASTM standard in 1994 and then an ISO (International Standards Organization) standard in 2001.

To perform mode I delamination test, DCB specimen is pulled both sides from the tip of the delaminated area with a constant displacement rate. Delamination propagation is observed and recorded along with the load-displacement curve, as the crack extends from the tip of the initial delamination. After the test, mode I interlaminar fracture toughness G_{I_c} is determined using various data analysis techniques and delamination resistance of the material is obtained [35, 36].

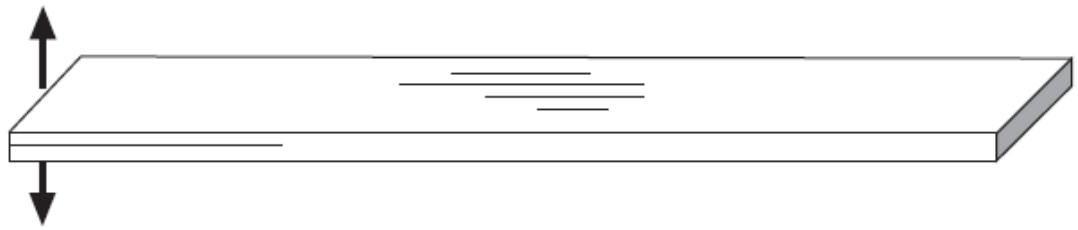

Figure 2.5 : DCB specimen [61]

2.3.3 Mode II delamination testing

There are many specimen proposals for mode II delamination test method, but none of them are internationally agreed on. Most favored four specimens proposed for standardization are described.

2.3.3.1 ENF (end notch flexure) specimen

This specimen (Figure 2.6) was proposed in 1982 by Russell and Street [39]. Despite its simplicity, one major disadvantage of ENF is unstable propagation for specimens with crack length over free length ratio (a/L) under 0,7.

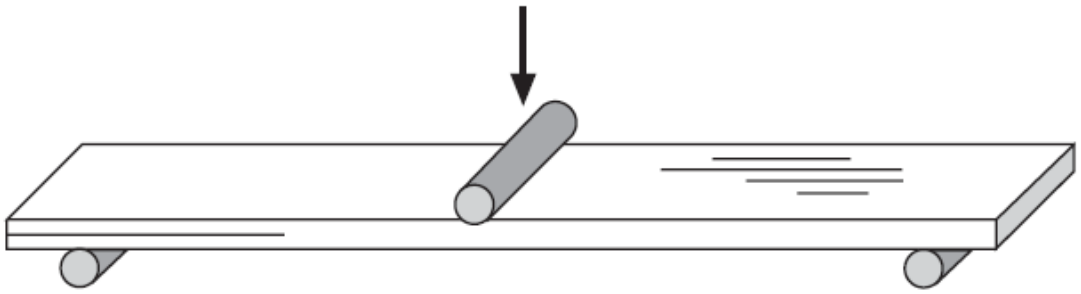

Figure 2.6 : ENF specimen [61]

2.3.3.2 SENF (stabilized end notch flexure) specimen

This specimen (Figure 2.7) was proposed in 1991 [40], as an improved version of ENF specimen which uses the crack extension as a control loop to stabilize the delamination propagation. This method is relatively complicated and requires advanced equipment.

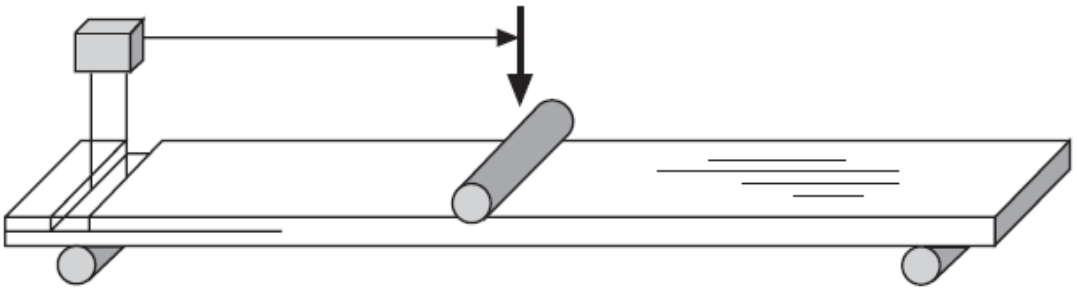

Figure 2.7 : SENF specimen [61]

2.3.3.3 4ENF (four point bend end notch flexure) specimen

This specimen (Figure 2.8) was proposed in 1997 [41], as another improved version of ENF specimen loaded in four points, allowing better propagation between the central points.

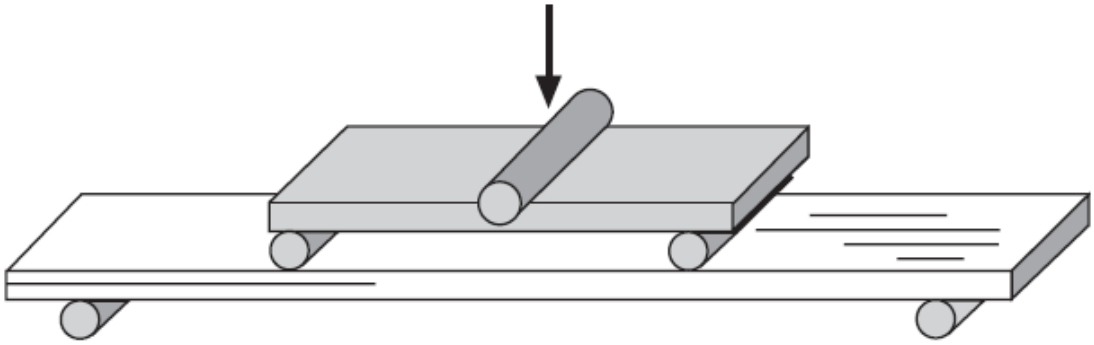

Figure 2.8 : 4ENF specimen [61]

2.3.3.4 ELS (end loaded split) specimen

This specimen (Figure 2.9) was proposed in 1987 [42], as a testing approach mostly researched by ESIS group. It provides stable propagation for specimens with crack length over free length ratio (a/L) over 0,55. Clamping of the fixture introduces some complications; however they can be partially fixed with a recently-proposed method [62].

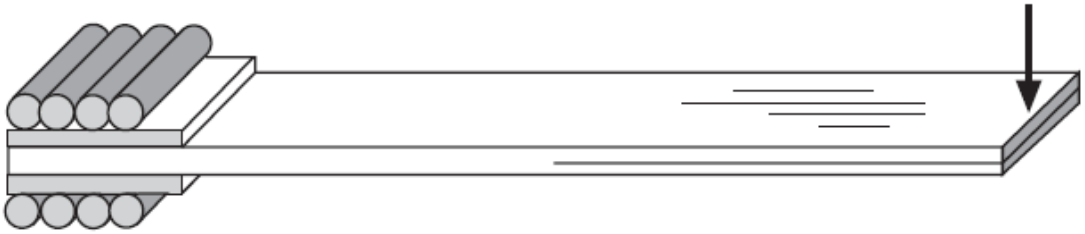

Figure 2.9 : ELS specimen [61]

3. EXPERIMENTAL STUDY

In this section, experimental study aiming to measure the mode II delamination resistance of a unidirectional carbon reinforced epoxy composite material is presented. These experiments were performed in accordance to the Mode II ELS protocol established by ESIS Technical Committee 4 in 1999 [44]. Additionally, a review of the protocol presenting some corrections and adjustments [62] was utilized for assistance and clarification of some points in ESIS protocol.

3.1 Summary of the Test

Mode II ELS protocol by ESIS TC 4 describes determination of mode II delamination resistance of unidirectional fibre reinforced laminates using ELS specimen. According to this protocol, mode II delamination resistance is calculated from the data acquired by observing and recording the growth of delamination in an ELS specimen. For stable delamination propagation, specimen is manufactured with an initial delamination which is obtained from an inserted non-adhesive starter film or a precrack. Shear load to extend this initial crack is provided from a test machine, introducing bending force though the pin inserted into the load-block glued to the end of specimen. While upper crosshead of the machine forces specimen edge to vertical deflection with a constant rate, load block is free to rotate around the pin, allowing rotation at the specimen end. Geometry of the ELS specimen which will be tested under these described conditions is shown in Figure 3.1.

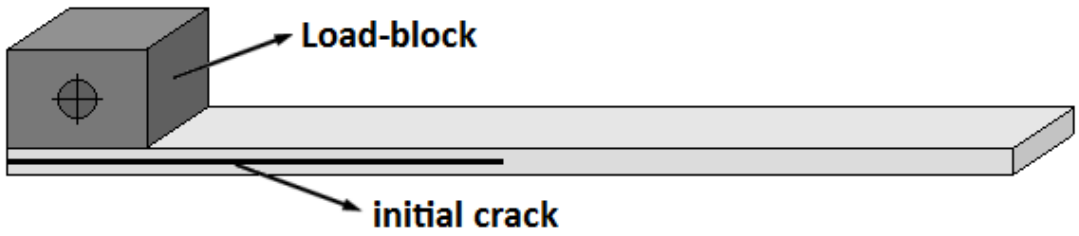

Figure 3.1 : Simple geometry of ELS specimen

There are two options for the test fixture included in protocol. In first fixture, loaded end of the specimen is horizontally fixed and in second fixture clamped end of the specimen is horizontally fixed (Figure 3.2). Due to the large vertical displacement applied on specimen during the experiment, one of the two ends of specimen should be free to slide horizontally in order to discard axial stress.

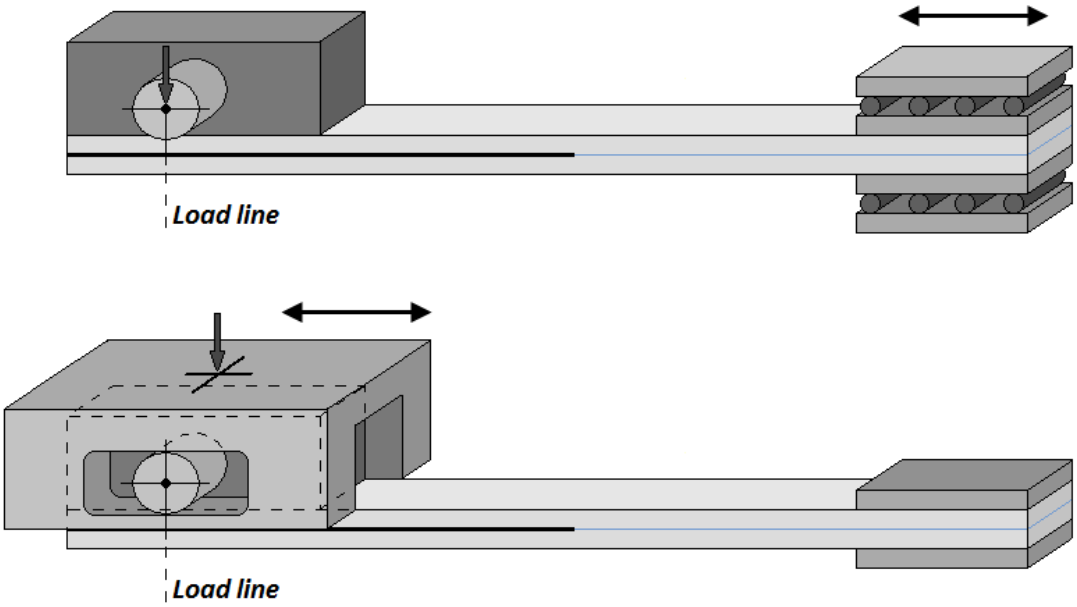

Figure 3.2 : Test fixture options

3.2 Specimen Design

3.2.1 Specimen geometry

Geometric parameters of the ELS specimen are given in Figure 3.3.

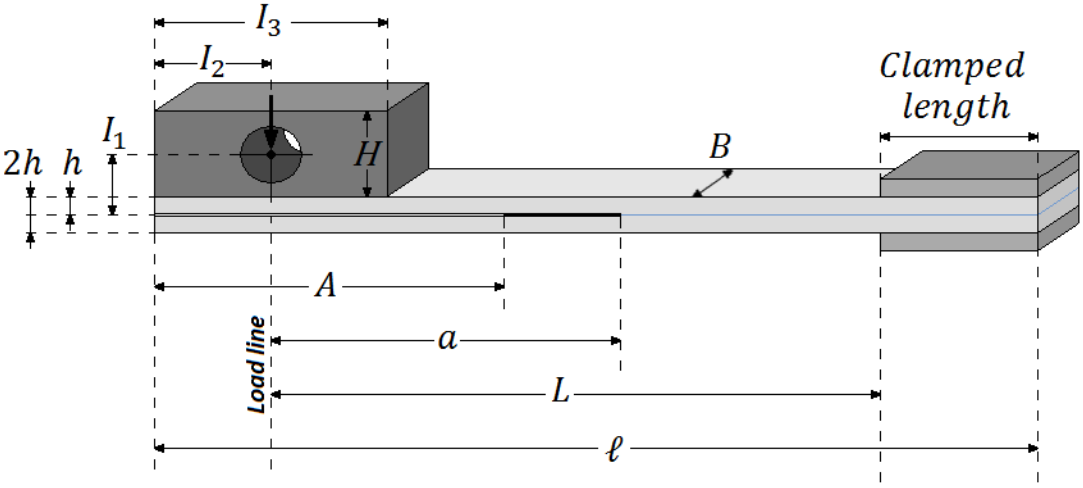

Figure 3.3 : Geometric parameters of ELS specimen

Definitions of these parameters are as following:

ℓ Total length of the specimen

L Free length of the specimen, distance between load line and clamp

a Initial delamination length, distance between the load line and the tip of the initial delamination

A Starter film length, distance between the specimen end and the tip of the starter film

B Width of the specimen

h Half-thickness of the specimen

$2h$ Total thickness of the specimen

I_1 Distance between the center of the pin and the mid-thickness line of the specimen

I_2 Half length of the load-block

I_3 Length of the load-block

H Height of the load-block

There are certain limitations and recommendations for the specimen geometry included in the protocol; however none of these parameters are specified with absolute certainty. These limitations can be listed as following:

- Initial delamination to free length ratio must be at least 0,55 for a stable crack propagation.
- Total specimen length cannot be smaller than initial delamination length plus 110 mm.
- Total specimen length should not be shorter than 170 mm.
- Tip of the initial delamination must reach at least 50 mm beyond the load line.
- Initial delamination should allow at least 30 mm of delamination propagation before reaching within 10 mm near the clamped end.
- Specimen width must be between 15 and 30 mm.

These limitations are formulated in following equations:

$a/L \geq 0{,}55$ **(3.1)**

$\ell \geq a + 110$ mm **(3.2)**

$\ell \geq 170$ mm **(3.3)**

$a \geq 50$ mm **(3.4)**

$a + 40 \text{ mm} \leq L$ **(3.5)**

$30 \text{ mm} > B > 15 \text{ mm}$ **(3.6)**

Additionally, recommended values for some of the parameters acquired from ESIS protocol and review are given in Table 3.1.

Table 3.1 : Recommendations for geometric properties of ELS specimen [44, 62]

Parameter	Symbol	ESIS protocol	Review	Unit
Total specimen length	ℓ	170	190	mm
Initial delamination	a	60	55	
Free length	L	100	105	
Clamped length of the specimen	-	-	75	
Half length of the load-block	I_2	-	10	
Width of the specimen	B	20	20	

Finally, taking specified limitations and recommendations into account and considering the feasibility factor, some of the geometric properties of specimen are chosen as shown in Table 3.2. The rest of the parameters are chosen through following steps of the study due to their dependence on other factors.

Table 3.2 : Geometric properties chosen for test specimens

Parameter	Symbol	Value	Unit
Total length of the specimen	ℓ	220	mm
Free length of the specimen	L	135	
Initial delamination length	a	80	
Half length of the load-block	I_2	10	
Clamped length of the specimen	-	75	
Width of the specimen	B	20	

3.2.2 Initial defect

As mentioned before, all specimens must be manufactured with an initial delamination to extend from while undergoing shear load. There are three types of

initial defects which are starter film insert, mode I precrack and mode II precrack. At least two types of initial defect must be separately used in tests in order to compare the results and eliminate the influence of initial defect type.

3.2.2.1. Starter film

A starter film inserted into the mid-thickness of laminate provides the initial delamination. Specimen can be tested directly after manufacturing, no additional intervention to specimen is necessary. Therefore, length of the starter film must be equal to aimed initial delamination plus the distance before load line to specimen end. This necessity is formulated in Equation 3.7.

$$A = a + I_2 \quad \textbf{(3.7)}$$

As the material of starter film, recommended options in protocol are PTFE (polytetrafluorethylene) for epoxy matrix composites cured at temperatures below 180°C and polyimide for composites cured at temperatures above 180°C. The thickness of the film must be less than 15 μm and it must be coated with a release agent during manufacturing.

3.2.2.2 Mode I precrack

Mode I precrack is an initial delamination obtained by pulling specimen's two faces apart from each other. This procedure can be performed with hand or by performing mode I delamination test using machinery. For proper separation of surfaces, opening can be performed by extending the crack from a starter film inserted into the mid-thickness of laminate during manufacturing process.

The procedure of obtaining mode I precrack by opening the specimen via hand tools is called wedge opening. The steps of this procedure are described as following in the protocol:

- If precrack is obtained by extending from a starter film, the specimen must be clamped 5 mm from the tip of the film. If precrack is obtained without a starter film, clamp must be placed maximum 60 mm from the specimen end.
- The wedge must be at least as wide as the specimen and opening angle of the wedge must be as small as possible.

- The wedge must be driven into the specimen by tapping on the side or utilizing a fixture. The tip of the wedge should not touch the tip of the delamination while being driven. If precrack is obtained without a starter film, specimen may be clamped at short distances from the tip of the delamination and then clamped again after wedge opening is complete up to that distance.
- Wedge opening must be sustained until the tip of the delamination reaches the clamp. The precrack may extend a few mm into the clamp.

According to these steps, when extending precrack from a starter film via wedge opening, the tip of the delamination reaches about 1 cm beyond the starter film (5 mm for the clamping distance at the beginning and a few mm for the extension of delamination into the clamp). Therefore, using the method of mode I precrack by wedge opening extended from a starter film, requires a geometrical condition formulated as

$$A + 1 \text{ cm} = a + I_2 \quad \textbf{(3.8)}$$

3.2.2.3 Mode II precrack

This initial defect can only be obtained by applying mode II delamination test protocol to a specimen with a starter film and performing the test until the tip of the delamination reaches the aimed length of the initial delamination.

3.2.2.4 Initial defect selection

Due to the simplicity and feasibility of the procedures, two initial defects are chosen as starter film insert and mode I precrack obtained by wedge opening using a starter film. The material to be used for non-adhesive starter is chosen as PTFE, since available composite material for manufacturing of specimens is cured at temperatures below 180°C.

With the selection of these parameters added to the previous geometrical properties, two types of specimen are selected to be used in mode II delamination experiments. ELS specimens used in experiments were implemented with starter film insert and mode I precrack initial defects (Figure 3.4).

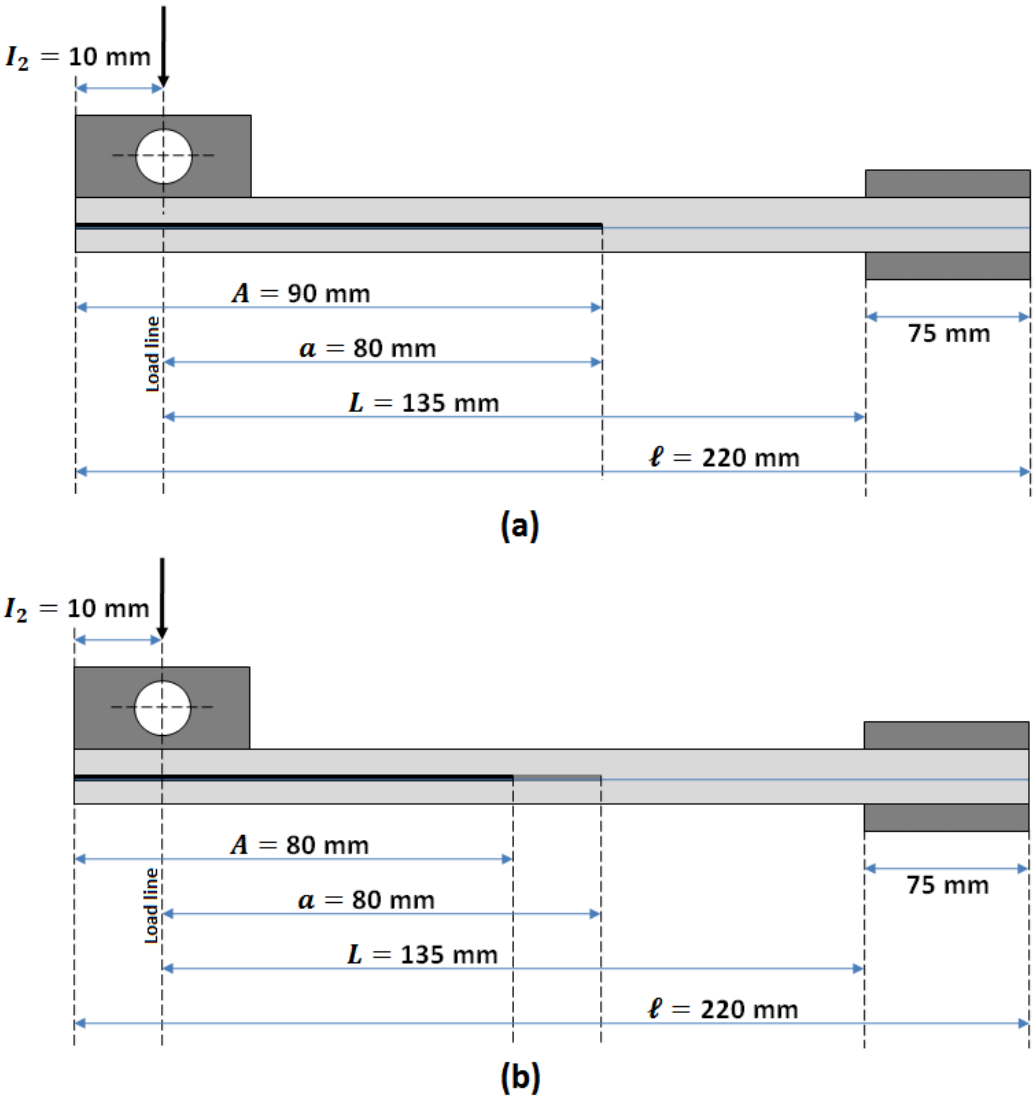

Figure 3.4 : Properties of ELS specimens with a. starter film insert, b. mode I precrack initial defects

3.3 Specimen Manufacturing and Preparation

3.3.1 Plate design

In order to obtain better geometrical quality, specimens were manufactured within plates and extracted from plates afterwards. For the design of these plates, following necessities were taken into account:

- According to protocol, 5 specimens each for a type of initial defect must be tested in a set of experiments.
- Due to the lack of experience in these experiments, number of specimens must be more than the specified number.

- Width of each specimen (B) is 20 mm and the width of the carbon fibre tow is 50 cm.
- Recommended specimen thickness ($2h$) is 3 mm for carbon reinforced composite with 60% fibre volume ratio in ESIS protocol and at least 4 mm for carbon/epoxy composites in review.
- The thickness of carbon fabric material which was available for the study is roughly 0,3 mm.
- Number of layers must be an even number since starter film must be placed at the mid-thickness.
- Used area of the plate must be in a certain distance from the sides of the plate in order to obtain proper edges and reduce the thickness variation due to edge effect.
- Width of the starter film must be larger than the width of the plate to be able to track the sideline of the film after curing.

Parameters of the plates designed according to these considerations are given in Table 3.3 and drawings of these plates (for both initial defect types) are given in Appendix A.

Table 3.3 : Plate properties

Initial defect type	Starter film insert	Mode I precrack
Number of specimens in each plate	10	
Number of layers	14	
Dimensions of the used area of the plate	22 cm x 20 cm	
Dimension of the total area of the plate	24 cm x 25 cm	
Dimensions of the used area of the starter film	9 cm x 20 cm	8 cm x 20 cm
Dimensions of the total area of the starter film	10 cm x 30 cm	9 cm x 30 cm

3.3.2 Materials

This test protocol is suitable for measuring mode II delamination resistance of unidirectional fibre reinforced composites. Since carbon prepregs were not available for the study, unidirectional carbon fabric and epoxy materials were the only option for manufacturing of specimens. Additionally a small amount of PTFE film was required.

3.3.2.1 Carbon fibre

Unidirectional carbon fabric material is fabricated with 12K carbon fibres and has an areal density of 300 g/m^2. Some mechanical and physical properties of this material, which are taken directly from the supplier, are given in Table 3.4. These properties are necessary for finite element modeling which will take place in following sections of the study.

Table 3.4 : Properties of carbon fibre material [63]

Material property	Value
Density	1,8 g/cm^3
Filament diameter	7 μm
Modulus of elasticity	230 GPa
Tensile strength	4900 MPa
Elongation at break	2,1 %

3.3.2.2 Epoxy

For the matrix phase of composite, lamination epoxy system MGS® L285 was selected. This system composes of a specified volume ratio or weight ratio of MGS® L285 laminating resin and one of the MGS® 285, 286, 287 hardeners. In this study, MGS® 287 hardener was combined with laminating resin (Table 3.5). Some of the known properties of resultant epoxy system are given in Table 3.6.

Table 3.5 : Properties of laminating resin and hardener [64]

	Laminating resin L285	Hardener 287	Unit
Density	1,18 – 1,23	0,93 – 0,96	g/cm^3
Viscosity	600 - 900	80 - 120	mPas

Table 3.6 : Properties of the epoxy [64]

Material property	Value
Density	1,18 - 1,20 g/cm^3
Modulus of elasticity	3,0 - 3,3 GPa
Flexural strength	110 - 120 MPa
Tensile strength	70 - 80 MPa
Compressive strength	120 - 140 MPa
Elongation at break	5,0 -6,5 %

3.3.2.3 PTFE

Since the required amount of PTFE film was too small to purchase from large companies, neither the purity nor the slimness of the material could be obtained.

However, a small amount (about 1 m^2) of non-adhesive PTFE film with a thickness of 0,15 mm [65] was donated to the study by Oras Polimer Plastik.

3.3.3 Manufacturing process

Manufacturing process of the specimens to be used in experiments is performed through the following steps:

- Material preparation
- Composite lay-up
- Curing
- Cutting
- Marking
- Measuring

3.3.3.1 Material preparation

As the first step of production, carbon fabric material (Figure 3.5) must be measured and cut from the tow in prescribed dimensions. Each plate is planned to compose of 14 layers of carbon fabric and 1 layer for each plate is also needed for spare. In total, 30 layers are cut from the carbon fibre tow. Since the width of the tow is 50 cm and the dimensions of layers are 25 cm x 24 cm, total length of carbon fabric used from the tow for this study is 3,6 m.

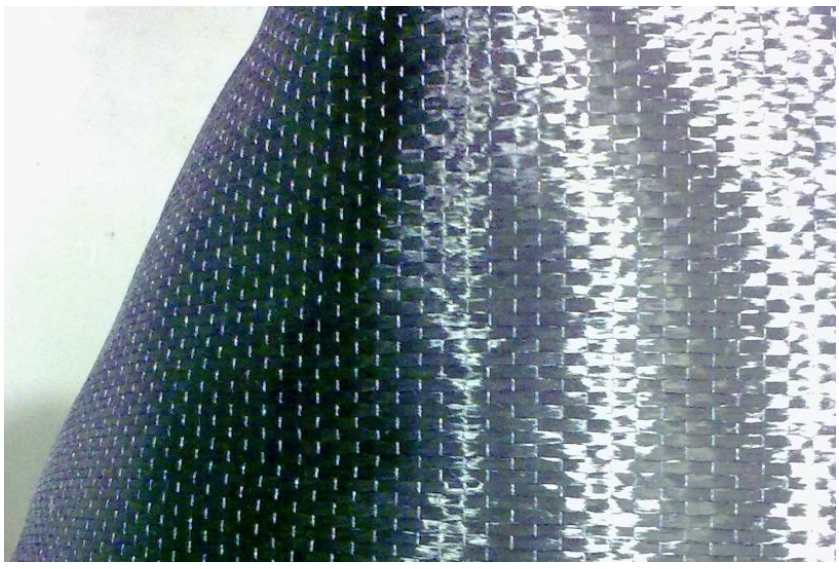

Figure 3.5 : Unidirectional carbon fabric material

For the measurement and cutting of carbon fabric, some equipment is required and a special procedure is followed. First, lines defining the borders should be roughly located on fabric using a ruler. Paper tape should be driven along the fabric aligning the borderlines roughly with the centerline of the tape. Then, borderlines should be drawn on paper tape with precise measurements. Finally, fabric should be cut from drawn borderlines, using a manual or electric scissor specially designed for composites. During this procedure, extreme caution is advised to keep the direction of carbon fibres proper for the quality of resultant composite material.

After carbon fabric layers are cut from the tow, they must be weighed on scale in order to calculate the epoxy amount needed. According to the standard procedure based on experience, weight ratio of carbon and epoxy must be roughly 1:1. The weight of 28 layers carbon fabric is measured as 550 g including the paper band at the edges, which is neglected.

Mixing ratios according to product information of epoxy laminating resin and hardener products and necessary amount of laminating resin and hardener calculated according to these ratios are given in Table 3.7. In these calculations, density of the mixed epoxy is taken as 1,20 g/cm^3 and the total weight 550 g. Laminating resin and hardener components should be weighed on scale, joined in a container and mixed carefully. Mixing is complete when no clouding is visible in container.

Epoxy mixture was prepared according to given ratios and instructions. For the equal distribution of epoxy amount used in two plates and better mixture quality, mixture was prepared in two separate pots each containing the half of material.

Table 3.7 : Mixing ratios and amounts of epoxy components [64]

	Weight ratio	Volume ratio	Weight	Volume
Laminating resin	5/7	2/3	392,86 g	305,55 ml
Hardener	2/7	1/3	157,14 g	152,78 ml
Epoxy	1	1	550 g	458,33 ml

3.3.3.2 Composite lay-up

For the preparation of lay-up surface, two metal plates with 70 cm x 70 cm dimensions were covered with plastic film sheets in order to provide smooth surface to both sides of the plates. Paper tapes at the edge of fabric layers were removed. It should be noted that removal of the tape may pull the fibres of a unidirectional fabric

apart and cause serious deformation; therefore the tape should be very carefully removed or should not be removed at all.

Afterwards, bottom layers of both plates were placed on the lower metal plate and next layers were stacked on top them after wetting the fabric with epoxy mixture via a brush. Each layer was wetted with epoxy before placing the next one (Figure 3.6). Again, movements of the brush should not cause disruption to the directions of the fibres while wetting the fabric.

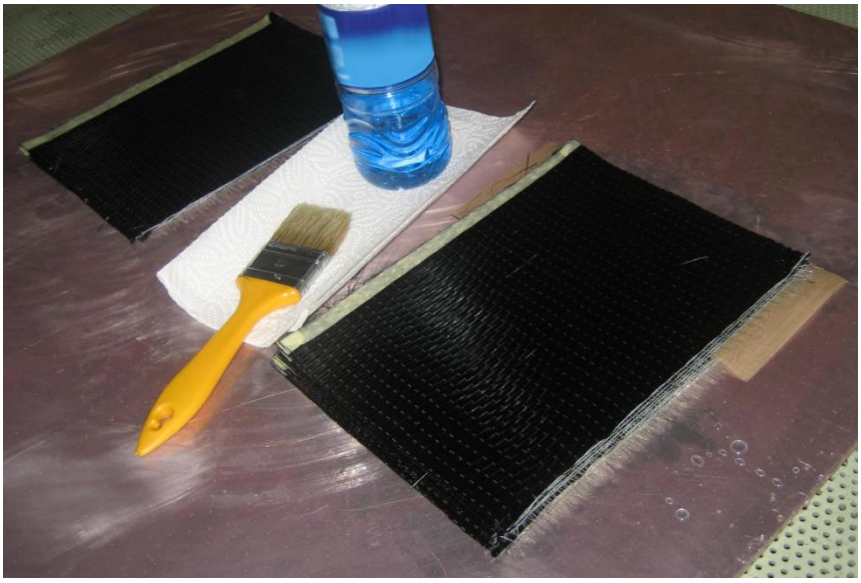

Figure 3.6 : Lay-up procedure

This procedure was repeated until the half-thickness was reached, which was seven fabric layers for each plate. On top of the seventh layers, starter films were placed according to their defined positions. Afterwards, seven more layers were stacked together with the same procedure.

Lay-up procedure should be applied as quickly as possible due to the gel time of epoxy which starts once the mixture is prepared. Epoxy was applied to plates simultaneously from two separate containers, in order to avoid any variations epoxy may show with progressing time. Gel times given for different temperatures (Table 3.8) and temperature development of the epoxy with gel time are presented in (Figure 3.7).

Table 3.8 : Gel time of epoxy at different temperatures [64]

Temperature	Gel time
20 - 25 °C	5-6 hours
40 - 45 °C	80-120 minutes

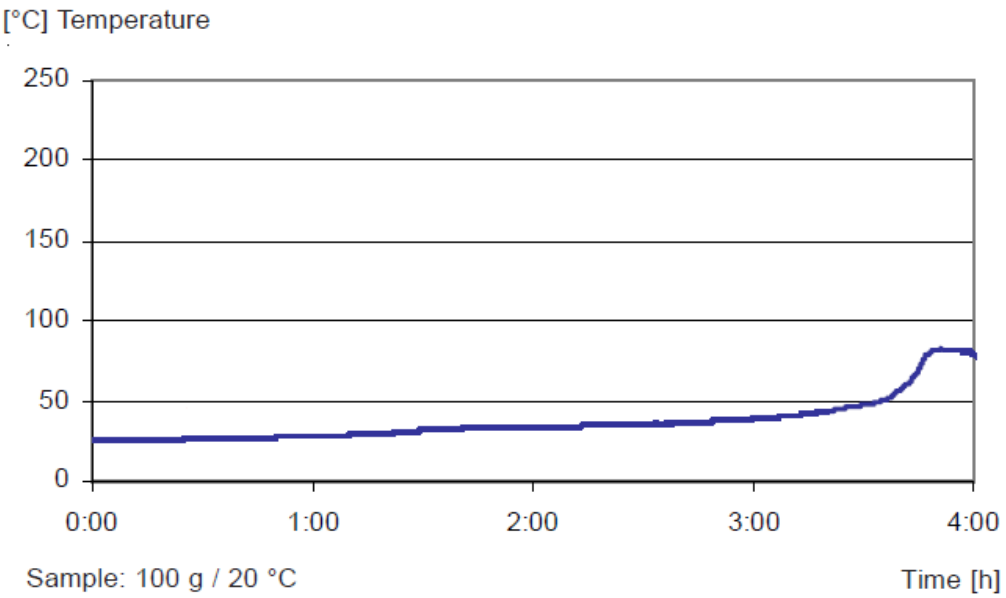

Figure 3.7 : Temperature development of epoxy during gel time [64]

3.3.3.3 Curing

After the completion of composite lay-up, upper metal plate was closed onto wet fabrics and the composite plates were prepared for curing process.

According to the instructions given for epoxy, curing process composes of two stages. First, the composite component should be left in room temperature (23 °C) for 24 hours. This provides initial curing. Secondly, the component should be placed into a controlled oven for heat treatment at temperatures between 50 - 80 °C for 15 hours. Necessary heat treatment temperatures for different operational temperatures of the composite component are given in Table 3.9.

Table 3.9 : Required heat treatments for different operational temperatures [64]

Operational temperature	Heat treatment temperature
-60 °C to 54 °C	50 - 55 °C
-60°C to +72 °C	80 °C

Composite plates were left in room temperature for a day. Afterwards, complete set-up including metal plates on top and the bottom were placed into the heated vacuum curing table (Figure 3.8), which provides vacuum for moulding and controlled heating for the curing process of the composite. Heat treatment in 56 °C was applied to composite plates for 15 hours. Temperature of the epoxy during curing process for different heat treatment temperatures is given in Figure 3.9.

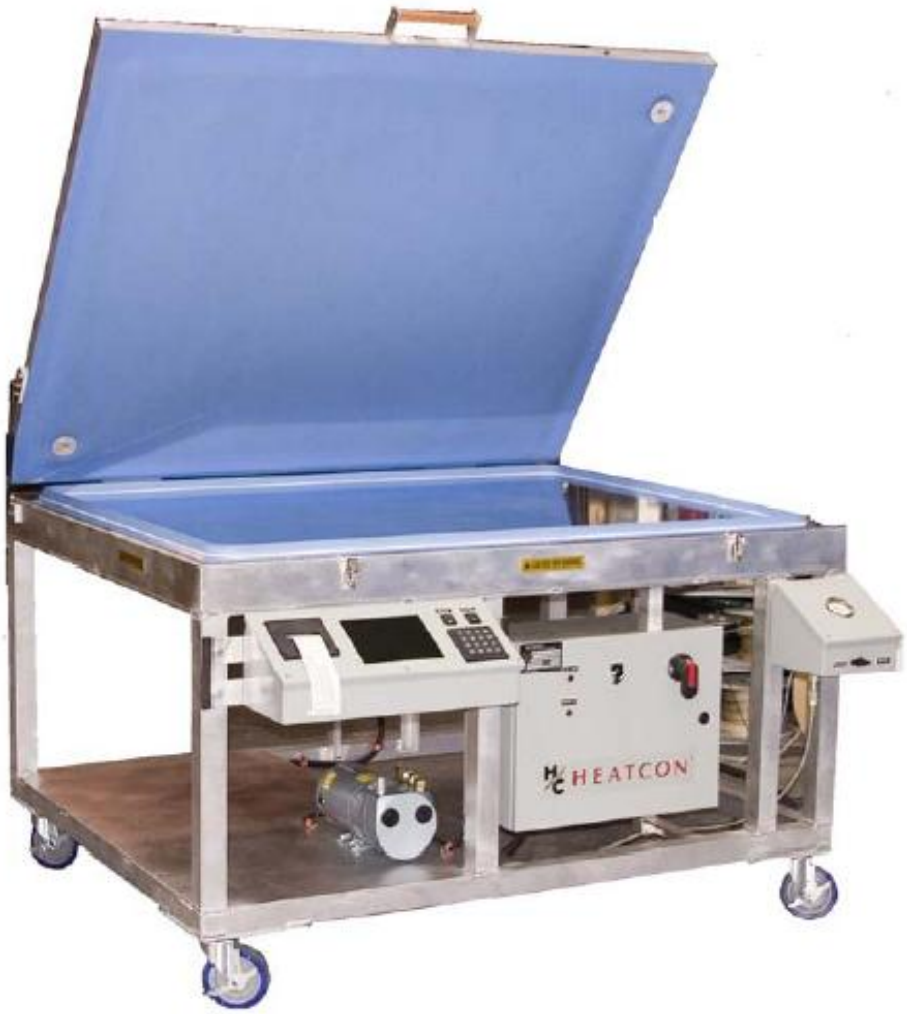

Figure 3.8 : Heated vacuum curing table [66]

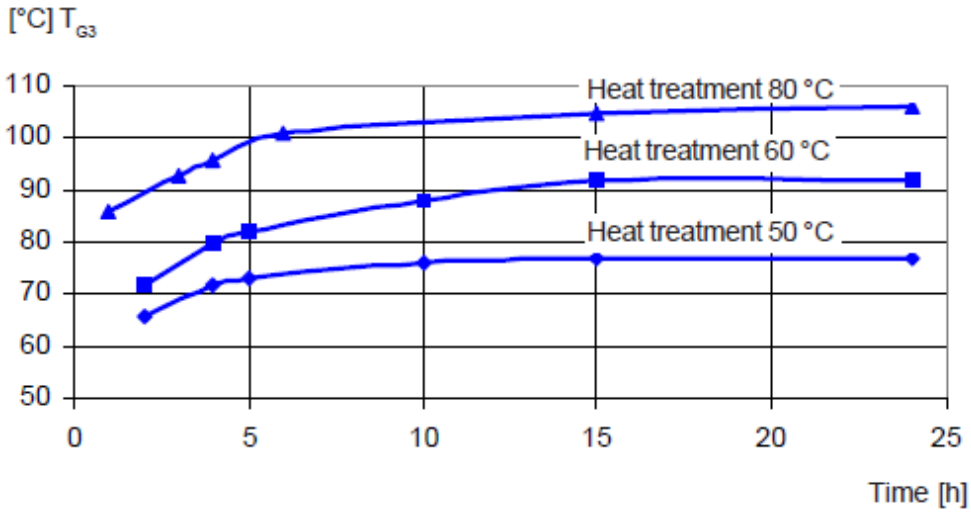

Figure 3.9 : Curing process temperatures [64]

When curing process is complete, composite material meets its final mechanical properties as a laminate. These properties are calculated in following sections, using measurements made after specimen manufacturing.

3.3.3.4 Cutting

After 15 hours of heat treatment, manufacturing process of the plates was complete. Plates were removed from the curing table, separated from the metal plates and placed on a clean surface (Figure 3.10). It can be seen that the extra epoxy used in manufacturing has leaked into the space between plates under the pressure of vacuum and cured as a bulk material (Figure 3.11). Extra epoxy is trimmed from the edges manually by breaking or cutting with a composite scissor. When plates became easier to work on (Figure 3.12), the sideline of PTFE film was tracked from the free edges and marked on the plates with a white ink permanent marker pen.

Since the rest of the marking was performed using this pen, it should be noted that the ink line of the pen was too thick for accurate marking. To solve this problem, all the procedures taking these markings as reference, were performed by taking the centerline of the ink lines as reference. Additionally, a black pen with a thin ink line was utilized occasionally, marking on the white ink.

Using this line and the direction of fibres, borderlines of specimens were marked on plates. Considering the cutting line, specimens were marked 1 mm wider than prescribed dimensions. Then specimens on each plate were numbered from 1 to 10 and marked letters denoting their initial defect type (Figure 3.13).

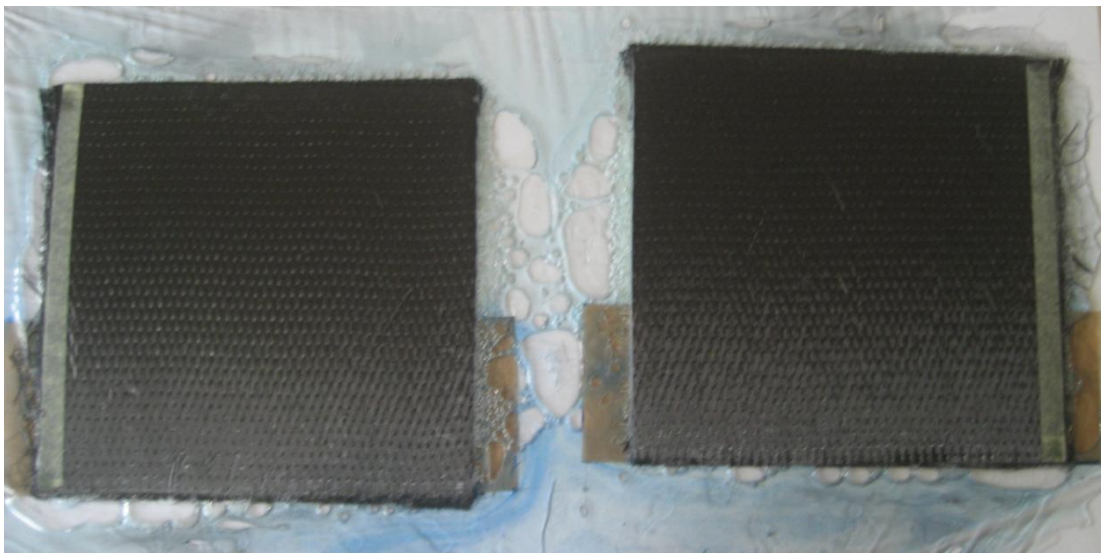

Figure 3.10 : Plates after manufacturing

Figure 3.11 : Extra epoxy from plates

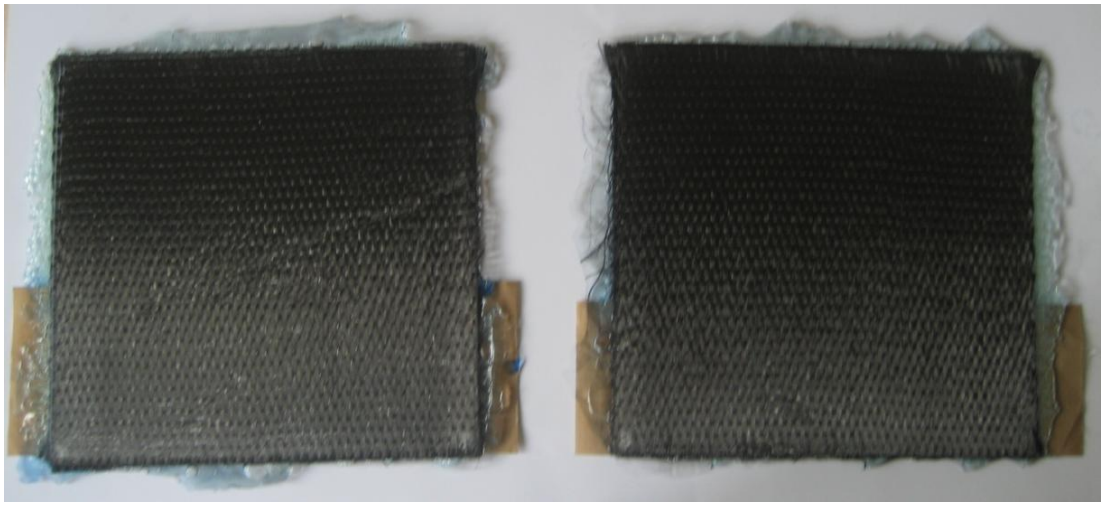

Figure 3.12 : Plates after trimming

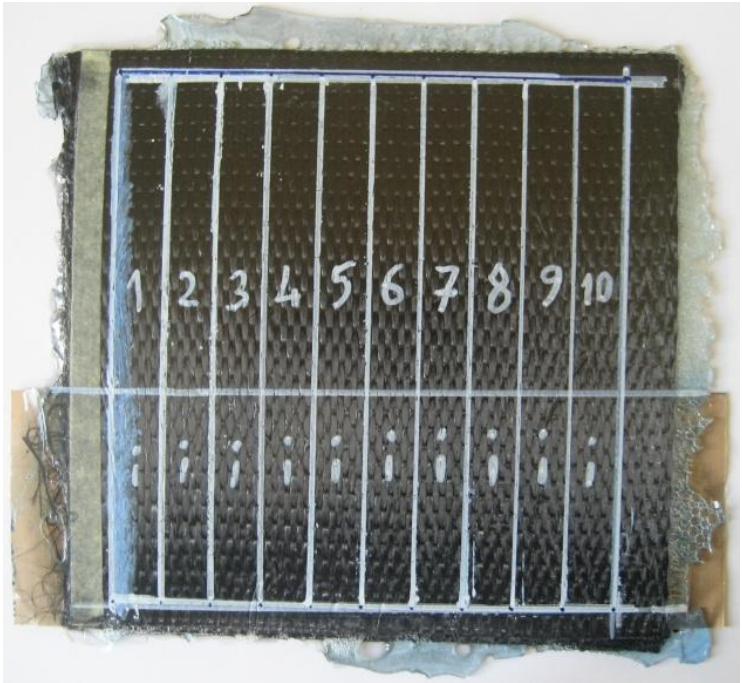

Figure 3.13 : Marked plate

After these steps, plates were ready for cutting. This operation was performed using a hand held power tool with a maximum speed of 27000 rpm [67] turning a circular saw blade with a thickness of 0,5 mm (Figure 3.14).

Figure 3.14 : Hand held power tool used for cutting plates

3.3.4 Test preparation

3.3.4.1 Marking

According to protocol, both lateral areas of specimens should be painted with white ink between the points where the delamination propagation will take place. These points are the tip of the initial crack and 10 mm before the clamp. Taking defined specimen geometry into consideration, these points are calculated as 90 mm and 135 mm from free end of the specimen, respectively.

A ruler to measure the distance and white ink permanent marker pen to paint the lateral areas of specimens were utilized. Since the sensitivity of white ink pen was too low due to the thickness of ink line, another pen with dark ink was utilized as mentioned before. First, the points were established roughly via ruler and roughly marked with white pen. After the area between points was painted intensely with white ink, points were more sensitively established and the white ink outside the propagation area was covered with dark pen.

Specimens after these procedures are shown in Figure 3.15, where i and p letters denote starter film insert and mode I precrack initial defects, respectively. This representation was utilized through the rest of the study. Specimens were abridgely named as i-specimens and p-specimens as specimen groups and recognized with specimen codes ($i1$, $i2$, $i3$, $i4$, $i5$, $i6$, $i7$, $i8$, $i9$, $i10$ and $p1$, $p2$, $p3$, $p4$, $p5$, $p6$, $p7$,

$p8$, $p9$, $p10$) separately. Likewise, for referring of plates containing these specimens, i-plate and p-plate abridgements were found suitable.

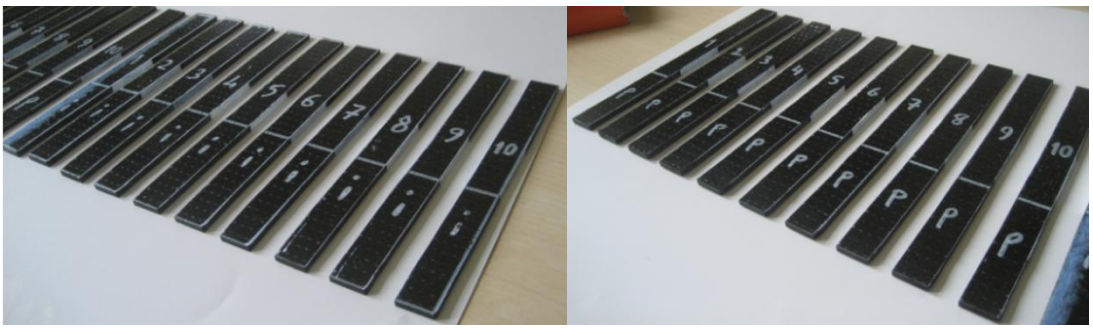

Figure 3.15 : Specimens after cutting and marking

3.3.4.2 Measurement

All specimens were measured and weighed on scale after these preparations. Measurements made in accordance with the ESIS protocol and additional measurements considered necessary are listed below:

- Mass of the specimen
- Length of the specimen, to the nearest mm
- Starter film lengths from both lateral sides of the specimen
- Thickness of the specimen at seven locations (specimen end, 10 mm from specimen end, quarter length, half length, three quarter length, 10 mm from other end, other end), to the nearest 0,01 mm
- Width of the specimen at seven locations (same locations) to the nearest 0,02 mm

Complete measurements are presented in Appendix B. Average values for both specimen types are given in Table 3.10.

Table 3.10 : Average parameter values of specimens

Parameters	Average value				
	Mass	Length	Width	Thickness	Starter film length
i-specimens	27,6	219,4	20,1657	4,1317	89,2
p-specimens	27,2	218,9	20,0094	4,1399	79,45
Unit	g			Mm	

3.3.4.3 Wedge opening

As mentioned in previous sections, two initial defect types selected for the study are starter film insert and mode I precrack obtained by wedge opening using a starter

film. Specimens with mode I precrack (p-specimens) were obtained with this procedure.

Specimens were clamped 90 mm from the end, which is the starting point of planned delamination propagation area painted with white ink. The edge of the specimen was notched with a knife from where the edge of starter film was visible. All specimens opened easily. Knife was driven to a few mm before the end of starter film. After that, knife was tapped with a hammer until the observed delamination line reaches the start point of white ink area (Figure 3.16).

Figure 3.16 : Wedge opening

Sometimes the starter film in specimens may introduce problems. For being pushed in with a knife, starter films cluster between the faces of specimen and separate from rest of the film when pulled out, leaving a piece which prevents the faces from closing. Two specimens, $p4$ and $p9$ were scrapped due to this condition (Figure 3.17). In other cases, starter film fell out of specimen or stayed in exact position before wedge opening. In both cases, specimens were considered proper for testing.

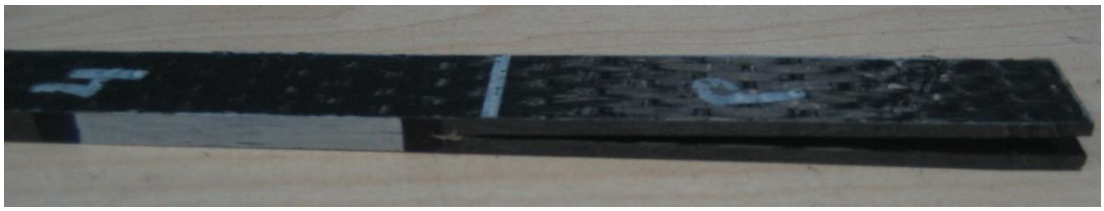

Figure 3.17 : Scrapped specimen

3.4 Testing

These experiments were performed in accordance to ESIS protocol using MTS 322 as test machine, Samsung Focus™ Windows Smartphone as camera and an additional made-to-order fixture.

3.4.1 Equipment

3.4.1.1 Requirements

According to ESIS protocol, test machine to be used in this experimental study is required to have these qualities:

- Qualified to ISO 5893 [68]
- Capable of producing a controlled deflection rate between 1 and 5 mm/min
- Capable of recording load and displacement data during test procedure with an accuracy of ±1%.
- Load cell with an accuracy within ±1% of the load range

Other than these requirements, either test machine itself or an additional test fixture should be available to provide the loading and clamping arrangements specified in protocol. These requirements are being capable of introducing the load through a pin inserted into the load-block and having either an upper crosshead or a clamping arrangement free to slide horizontally.

3.4.1.2 Test machine

Some basic specifications of the machine are given in Table 3.11 and major components of the load unit are presented in Appendix C. To perform the experiments using this machine, 5 kN load cell was utilized.

Table 3.11 : Basic specifications of MTS 322 test machine [69]

Features	MTS 322 property
Actuator number	3
Maximum axial load	100 kN
Maximum side load	25 kN
Temperature interval of the chamber	-110 °C - 310 °C
Software	Model 793.10 MultiPurpose TestWare

3.4.1.3 Additional test fixture

Since the upper crosshead of the test machine is not capable of sliding horizontally, using a sliding clamp arrangement became the only available option for test fixture. Therefore, an additional test fixture specifically designed for these series of experiments was utilized. Geometry of this additional test fixture is given in Figure 3.18.

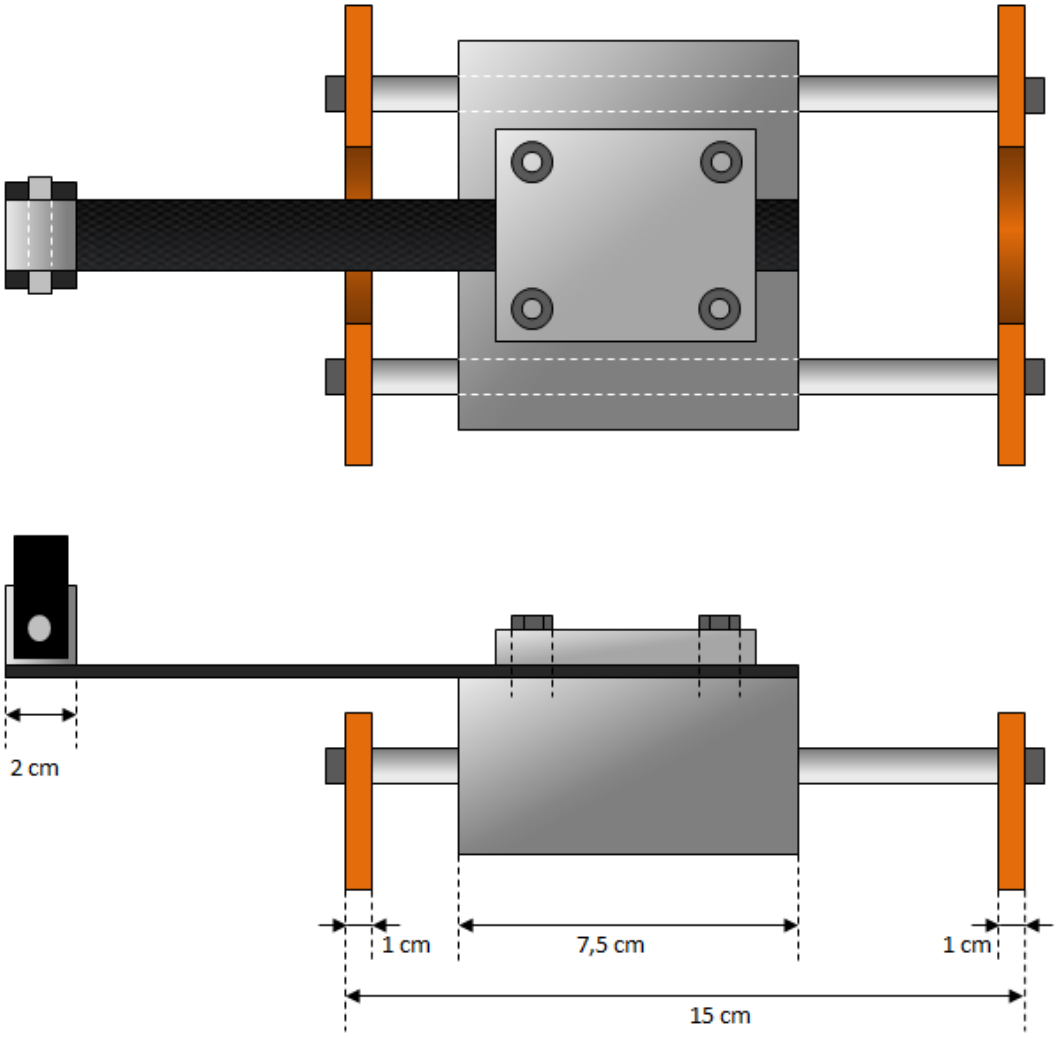

Figure 3.18 : Geometry of the additional test fixture

This fixture composes of 3 components:

- Load transfer unit
- Sliding clamp unit
- Riser block

Load transfer unit (Figure 3.19) transfers the bending load from upper crosshead of test machine to specimen edge via a pin inserted into the load block. This mechanism allows the specimen end to rotate freely during loading.

Sliding clamp unit (Figure 3.20) allows the other end of the specimen to move horizontally when bending load is applied. Load range in this experiment is relatively small (200-300 N), therefore this component was designed to have a high sensitivity.

In order to clamp the specimen with this mechanism, plate at the top is fastened to the sliding block at the bottom using 4xM10 bolts.

Figure 3.19 : Load transfer unit

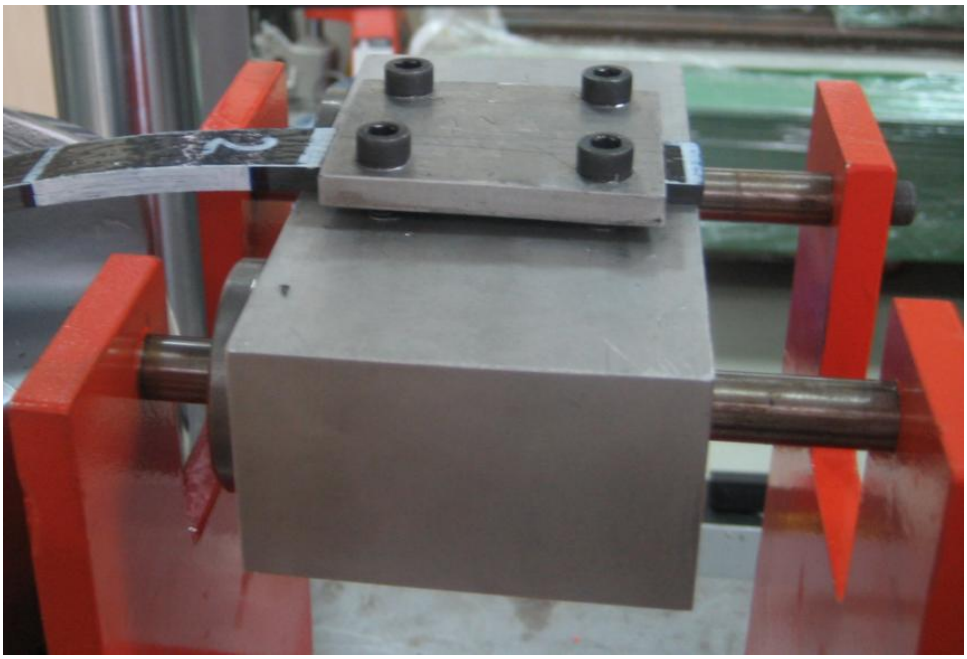

Figure 3.20 : Sliding clamp unit

Since the test procedure requires only upper crosshead and the specimen should be placed horizontally, a riser block was necessary for elevating the sliding clamp unit to the level of upper crosshead. This block was placed under the sliding clamp unit.

3.4.2 Final specimen geometry

Before explaining the test procedure in detail, final geometric details of the specimen are presented in Figure 3.21 and Table 3.12, including values and parameters determined after manufacturing and the arrival of test fixture.

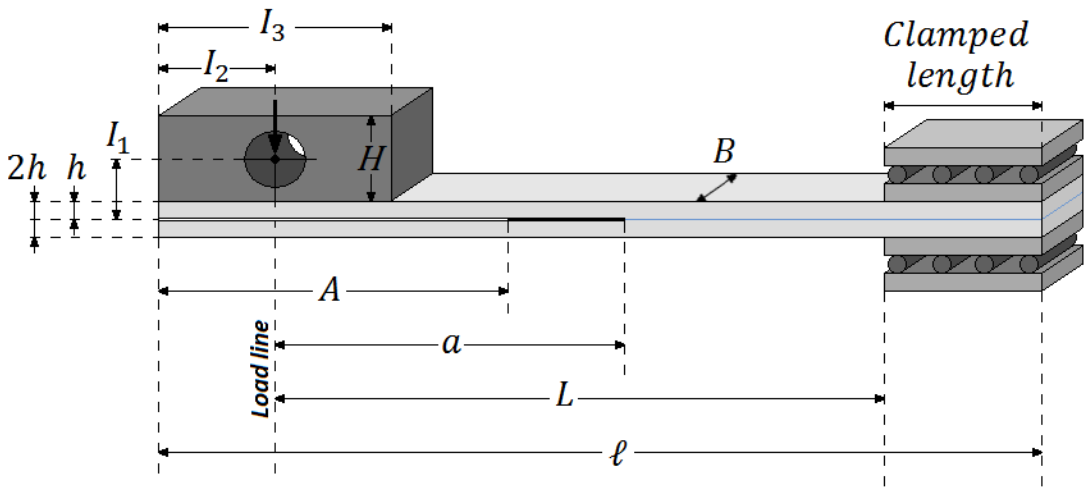

Figure 3.21 : Geometric parameters of the test specimen

Table 3.12 : Final geometric details of the specimens

Parameter	Symbol	Value		Unit
		i-specimens	p-specimens	
Total length of the specimen	ℓ	220		
Free length of the specimen	L	135		
Initial delamination length	a	80		
Starter film length	A	90	80	
Clamped length of the specimen	-	75		
Width of the specimen	B	20		
Mid-thickness of the specimen	h	2,0659	2,0700	mm
Total thickness of the specimen	$2h$	4,1317	4,1399	
Distance between the center of the pin and the mid-thickness of the specimen	I_1	17,07		
Half length of the load-block	I_2	10		
Length of the load-block	I_3	20		
Height of the load-block	H	30		

3.4.3 Test procedure

3.4.3.1 Requirements

Conditions and application of the test procedure included in protocol can be summarized as following:

Environmental conditions: Test should be performed under temperature and humidity conditions in accordance with ISO 291 [70] which is 23 ±2 °C temperatures and 50 ± 5% humidity.

Load-block preparation: For gluing load-block to the specimen, both surfaces should be lightly abraded and cleaned with a solvent first. Since the loads introduced in the test are quite low, a cyanoacrylate adhesive known as the Super Glue® has been found adequate in experience.

Crosshead rate: Loading of the specimen should be performed with a constant rate between 1-5 mm/min. When crack growth reaches prescribed point at the end of white ink area, loading should be stopped. Unloading of the specimen may be performed with a rate up to 25 mm/min.

Data recording: Load (P) and displacement (δ) values (Figure 3.22) should be recorded during the test. These values may be recorded automatically by the software of test machine. Delamination propagation should be observed and recorded with or without using a device such as travelling microscope. Recording the point of delamination onset, both in time and location on specimen, is essential for data analysis. For reliability and facilitation of propagation tracking, specimen edges should be marked showing certain distances in delamination propagation.

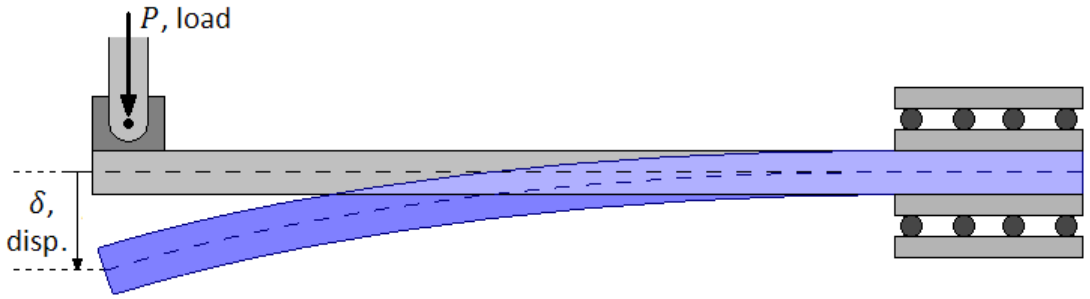

Figure 3.22 : Load and displacement parameters

According to the protocol; every 1 mm from the tip of the initial crack for at least 5 mm, every 5 mm after that and every 1 mm after 25 mm at least up to 30 mm should be marked (Figure 3.23). Maximum horizontal displacement of the sliding clamp, d_{max} should be noted by recording the positions before and after loading.

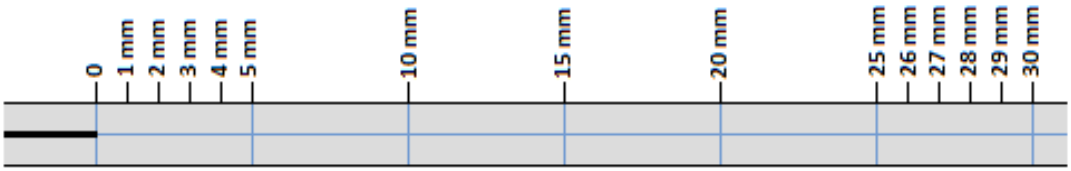

Figure 3.23 : Delamination propagation marking

3.4.3.2 Test set-up

Taking these requirements into consideration, fixture conditions of the test protocol were provided by following these steps:

- Load-block is glued to specimen from prescribed area using specified adhesive.
- Load transfer component is placed into the upper crosshead and fixed using test machine controls.
- Specimen is placed between clamp plate and sliding block and aligned to be at equal distances to the bolts at both sides. If specimen lies angled, load transfer component should be slightly rotated to fix the misalignment (Figure 3.24).
- Upper crosshead is moved up or down with a high sensitivity using computer control, for the alignment of specimen which should be on a horizontal line.
- Sliding block is moved to the location where its back surface aligns with back surface of the specimen of its clamped end. This alignment is necessary to fulfill the clamping distance condition.
- When specimen is properly set up without misalignments, four bolts are driven into the clamp plate and tightened to fix the specimen end in sliding clamp unit.
- For the observation and recording of delamination propagation, camera was fixed next to the fixture and directed to the white ink area from a close distance (Figure 3.25).

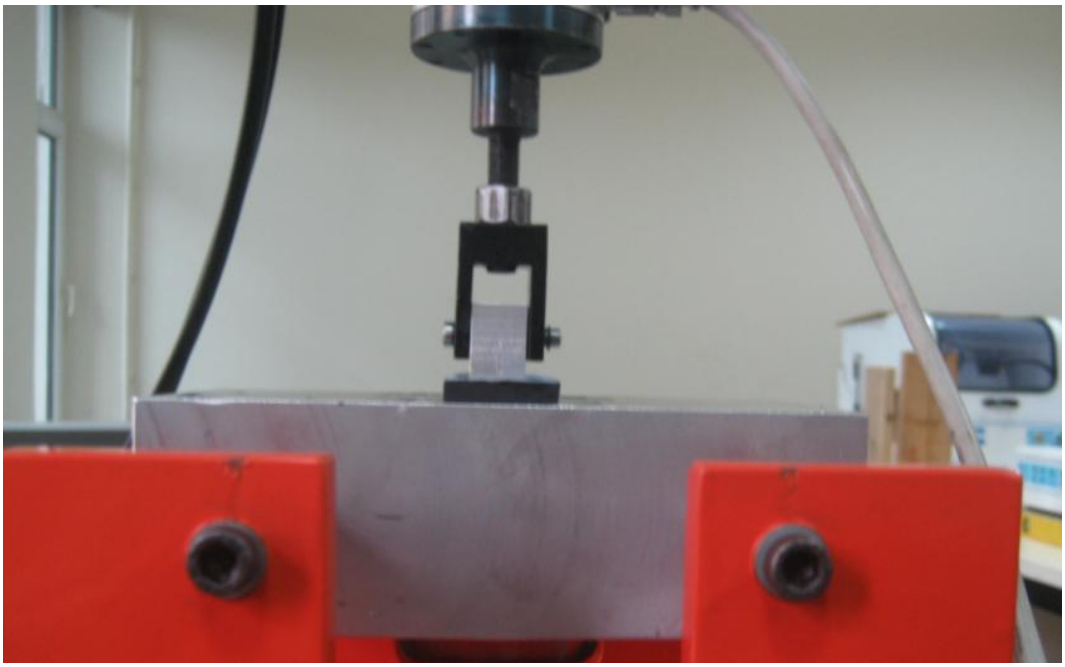

Figure 3.24 : Specimen alignment

Figure 3.25 : Camera set-up

3.4.3.3 Loading-unloading

First loading process was performed with a constant crosshead rate which was randomly chosen between 1 - 5 mm/min. The purpose of this trial was to observe the delamination propagation and record the deflection of the crosshead when crack growth reached the end of white ink area. This occurred approximately at 40 mm deflection. Therefore, loading and unloading procedures were planned as given in Table 3.13.

Table 3.13 : Loading-unloading procedure

Process #	Action	Target deflection (mm)	Time (s)	Crosshead rate (mm/min)
1	Loading	-40	1000	2,4
2	Hold	-	60	-
3	Unloading	0	200	12

Following the completion of design steps, manufacturing and test set-up; experiments of 20 specimens were performed in two work days. Steps of test procedure, which were followed while testing each specimen, are described below.

- With specimen placed into the fixture, deflection value is set to zero with offset command from the computer.
- Position of the sliding clamp is measured and recorded.
- Video recording with camera is initiated.
- Loading procedure is started with computer control.
- Crosshead applies deflection to the edge of specimen with a rate of 2,4 mm/min until deflection is 40 mm (Figure 3.26).
- After loading is complete, position of the sliding clamp is measured and recorded while the machine holds position for 60 seconds.
- Unloading is performed with a rate of 12 mm/min until the deflection is back to start point (Figure 3.27).
- Video recording is stopped.
- Position of the sliding clamp is measured and recorded again.
- Load-block glued to the specimen is pulled apart and its surface is prepared for the next specimen.
- Tested specimen (Figure 3.28) and data of the experiment is properly stored.

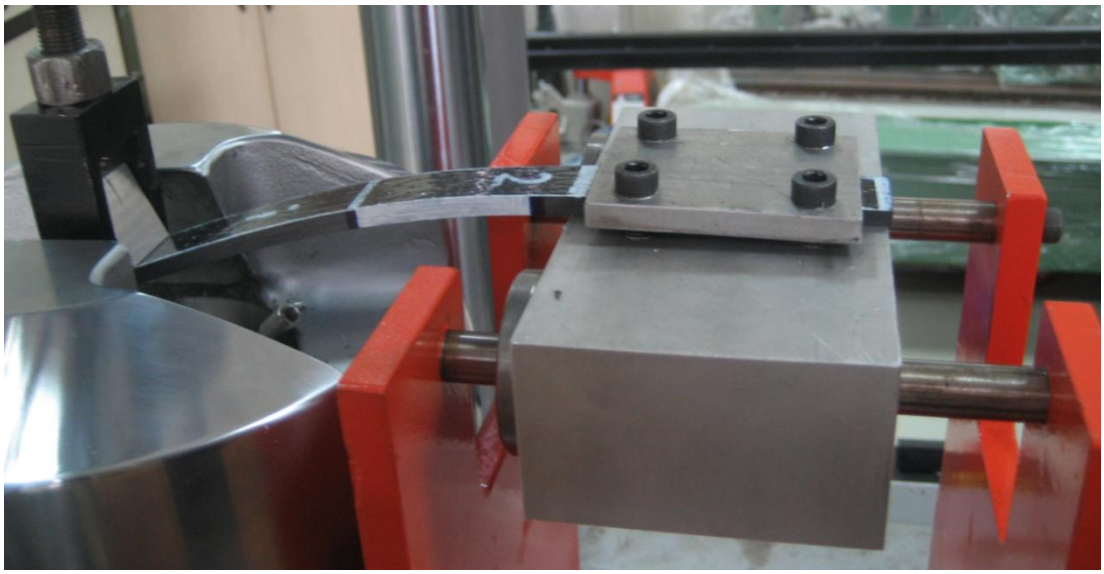

Figure 3.26 : Loading procedure

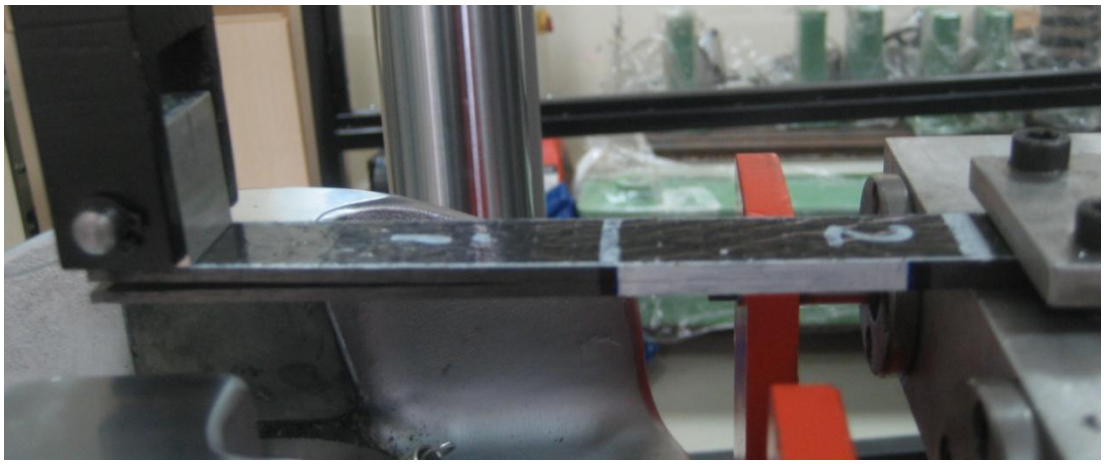

Figure 3.27 : Specimen after unloading procedure

Figure 3.28 : Tested specimen

4. FINITE ELEMENT MODELING

As mentioned in previous sections, delamination in FRP composites can be modeled with two approaches: fracture mechanics based approach and damage mechanics based approach. In this study, cohesive zone model is utilized for the simulation of mode II delamination within the framework of damage mechanics. This simulation was performed via SAMCEF Field V8.1 (student release 2011) finite element software as an implicit non-linear analysis. Steps of this analysis are explained in this section.

4.1 Geometry Modeling

For the sake of simplicity, some portions of the specimen were not included in model. Loading was assumed to be applied from a single point instead of through an adherent area between the load-block and specimen. This point was located on load line and the edge portion of specimen before load line was excluded from the model. Area of specimen that remains in sliding clamp was also excluded from the model and constraints representing sliding clamp system were applied to this edge.

As can be seen in Figure 4.1, remaining portion of the specimen has a length of 135 mm and 80 mm of this length is initially delaminated. Rest of the length is free for delamination propagation. Each portion was modeled with two rectangular boxes, representing upper and lower half-laminates.

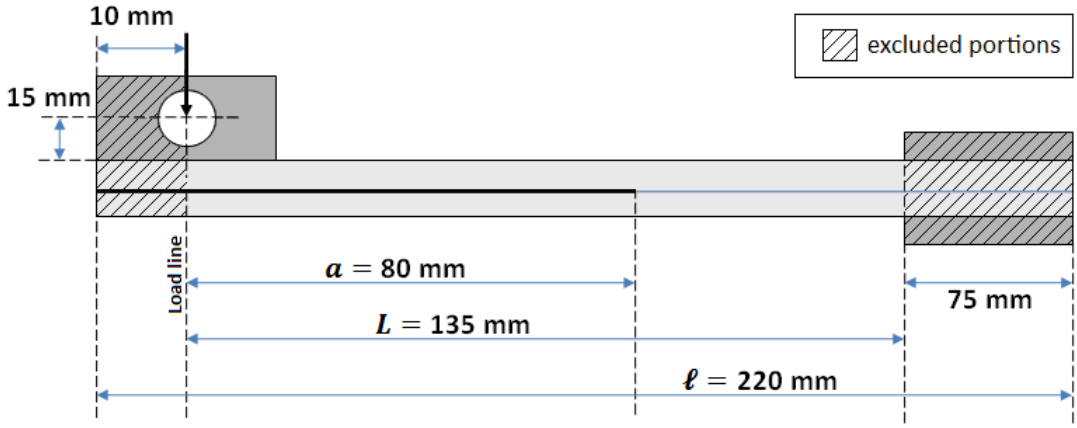

Figure 4.1 : Dimensions and geometry of specimen for finite element modeling

In *MODELER* module, boxes were defined within *create box* dialogs and loading point was defined as a *vertex*. Location chosen for this point was 15 mm above upper surface which was the location of the center of the pin inserted into load-block during the experimental study. With these definitions, model geometry was created as seen in Figure 4.2. Darker colored boxes represent the region with initial delamination.

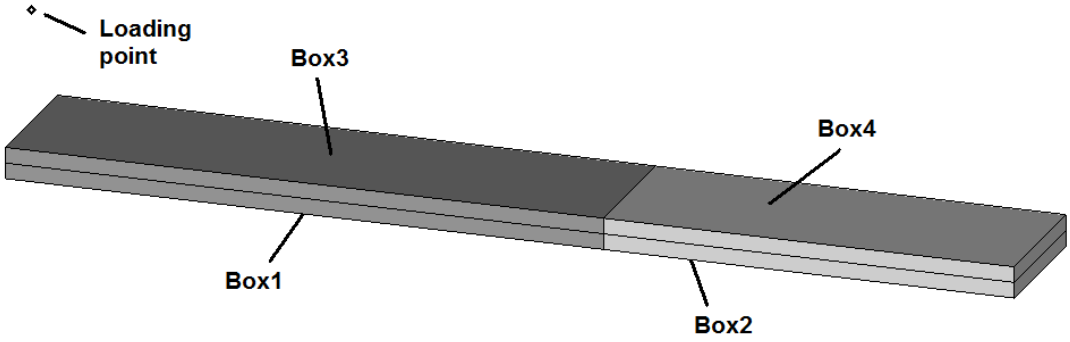

Figure 4.2 : Basic specimen geometry

4.2 Materials

Two materials were defined within *material* dialog of *ANALYSIS DATA* module. These are carbon/epoxy composite and interface material.

4.2.1 Composite material

Properties of unidirectional carbon/epoxy laminate are evaluated approximately by theoretical approach. Details of this process are described in following sections. Material was defined as elastic and orthotropic within the *material* dialog and the properties were entered as shown in Table 4.1.

Table 4.1 : Composite material properties for finite element model

	1	2	3	Unit
Young's modulus	138860	6380	6380	MPa
Poisson's ratio	0,3	0,33	0,3	-
Shear modulus	2990	2400	2990	MPa
Mass density		1565		kg/m^3

4.2.2 Interface material

Interface material defines the character of cohesive zone. Delamination behavior of propagation area is simulated via interface material. Therefore, values entered for this material can be considered the core of analysis.

Interface material was defined by selecting *Smith-Ferrante* from the list in *material* dialog. As explained in Smith-Ferrante material theory [71], there are three parameters to be entered for this material: maximum cohesive stress (σ_{max}), energy release rate per thickness length (G_c) and weighting coefficient (β). As can be seen in Smith-Ferrante cohesive law demonstrated in graph (Figure 4.3); when tractions reach maximum cohesive stress during loading delamination occurs and tractions decrease with a curve which the area under is equal to G_c. This effect is irreversible and if structure is unloaded and loaded again, loading follows the straight line in the middle of graph.

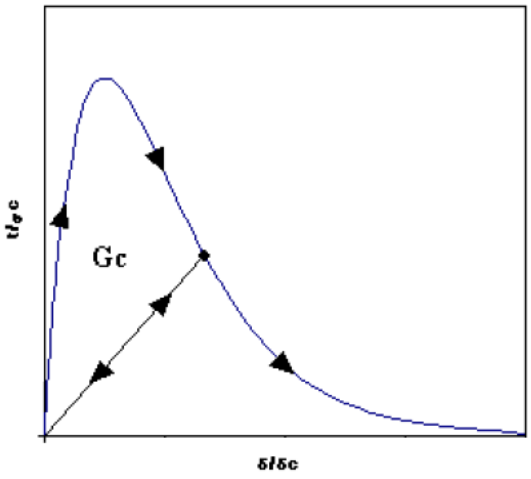

Figure 4.3 : Smith-Ferrante cohesive law [71]

First of the entered parameters, maximum cohesive stress (σ_{max}) was assumed equal to the transverse tensile strength in accordance with transversely isotropic material assumption. Second parameter, energy release rate (G_c) was taken from the experimental results. This value is to be entered per unit thickness, which is the

current solver unit for length. Therefore the value was divided by 1 mm. Last of the parameters, weighting coefficient (β), was taken as the reference value given in software tutorials for delamination [71]. Entered values for Smith-Ferrante interface material are given in Table 4.2.

Table 4.2 : Smith-Ferrante interface material properties

Parameter	Symbol	Entered value	Unit
Maximum cohesive stress	σ_{max}	38,6	MPa
Energy release rate	G_c	2E+6	J/m3
Weighting coefficient	β	0,05	-

4.3 Behavior

Structural behavior was defined by assigning material properties to structure and describing relationships between boxes.

4.3.1 Composite volume

To assign material properties and stacking sequence information to composite laminate; *composite volume* was selected from behavior list and laminate was selected as layer type in *behavior* dialog. Afterwards, stacking sequence of the laminate was described via *composite viewer* interface.

To be able simulate delamination in mid-thickness, only half of the laminate was defined. Another concern was to separate the one ply closest to the mid-thickness from the rest of the plies while meshing. This provides simplicity when examining results of delamination between two plies. To ensure having mesh points separating one ply closest to the mid-thickness from others, a *break* was inserted between plies using *insert break* button.

There are 7 plies in each half of laminate. Thickness of a single ply is 0,3 mm. For the desired stacking sequence, one ply was defined having the thickness of 6 plies, a *break* was inserted and another ply was defined. Defined stacking sequence for half laminate is presented in Table 4.3.

Table 4.3 : Half laminate stacking sequence

#	Name	Material	Thickness (mm)	Angle (°)
1	6 plies	Carbon/epoxy composite	1,8	0
2	break	-	0	-
3	single ply	Carbon/epoxy composite	0,3	0

After half laminate was defined as carbon/epoxy composite volume, it was assigned to boxes symmetrically with respect to mid-thickness line, using *behavior* dialog.

4.3.2 Assembly

In this stage, boxes do not share any common surfaces or edges and are not connected in any way. Relationships between 4 boxes were defined using *assembly* dialog.

Firstly, Box1 was connected to Box2 and Box3 was connected to Box4 via *connection between mesh nodes* assembly. With this connection, lower boxes (Box1 and Box2) were defined to behave as a single box and likewise for upper boxes (Box3 and Box4). Then, in order to define the behavior of propagation area, Box2 and Box4 were assembled with *Smith-Ferrante* interface material defined previously. Finally, to model the delaminated portion of the specimen, Box1 and Box3 were defined with *contact* assembly condition. This contact was described as flexible on both surfaces and without friction. Connections defined between boxes are shown in Figure 4.4.

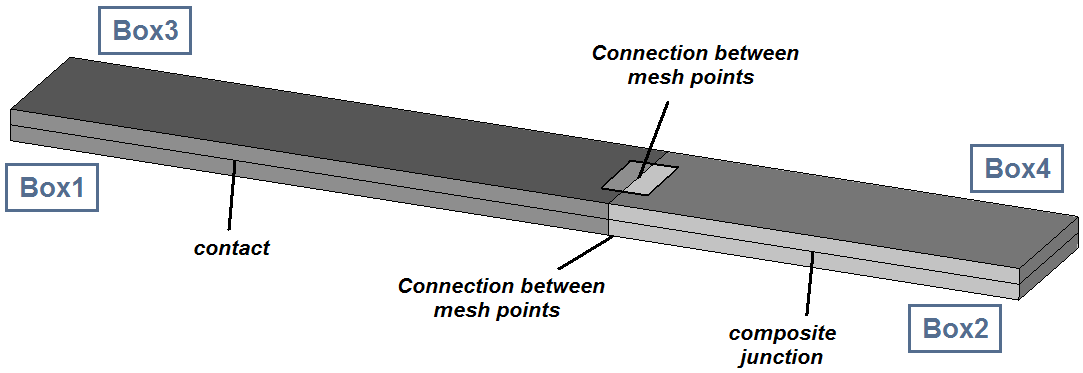

Figure 4.4 : Connections between boxes

4.4 Loading

For the simulation of loading, two conditions should be provided: effect of load-block and the crosshead rate.

For load-block effect, delaminated edge of the specimen (upper edge of Box3) was connected with loading point via *fixed* assembly condition. This condition provides a rigidity which results in zero displacement of connected elements relative to each other.

As explained in experimental study steps, specimens were subjected to a deflection-controlled bending which can be expressed with a displacement function moving from $\delta = 0$ at $t = 0$ point to $\delta = 40$ at $t = 1000$ point, where δ is displacement in mm and t is time in s units. Therefore the crosshead rate was 0,04 mm/s for the loading phase of the experiments. It should be noted that unloading phase is not simulated in this analysis since the resultant values does not have a role in calculations.

For the definition of crosshead rate, *prescribed displacement* was assigned to loading point within the *constraint* dialog. Displacement value was defined as linear function starting from $\mathrm{f}(u) = 0$ at $u = 0$ point to $\mathrm{f}(u) = 40$ at $u = 1000$. Direction was selected as z-axis in reverse direction.

4.5 Constraints

For the simulation of sliding clamp system, rotation about all axes and translations along y and z axes at the constrained edge of specimen (back surfaces of Box2 and Box4) were locked within the *constraint* dialog. However, this system was later proved to be insufficient. Nodes at these surfaces were observed to move away from each other along x axis, disrupting the integrity of the specimen edge. For a better simulation of experiment; back surface of the constrained edge of specimen should remain flat and vertical at the end of experiment, similar to the cross section of actual specimen at the border of constraint and unconstrained portions. Therefore, aside from rotation and translation locks, all four edges at the constrained back surface of specimen (back surfaces of Box2 and Box4) were rigidly connected via *fixed* assembly condition, reducing the relative movement of nodes to zero.

4.6 Meshing

Before meshing of the model within the *MESH* module, mesh constraints were defined. All edges of the model along length and width directions were divided into lines of 2,5 mm length. No mesh constraints were assigned along the thickness direction, since it was already defined in half-laminate composite volume.

The mesh was generated afterwards. Meshing of the model is shown in Figure 4.5. Detailed look of the mesh along thickness is also given in Figure 4.6.

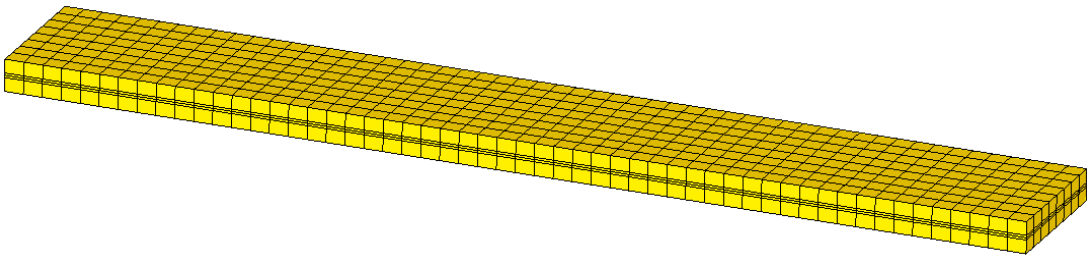

Figure 4.5 : Mesh of the model

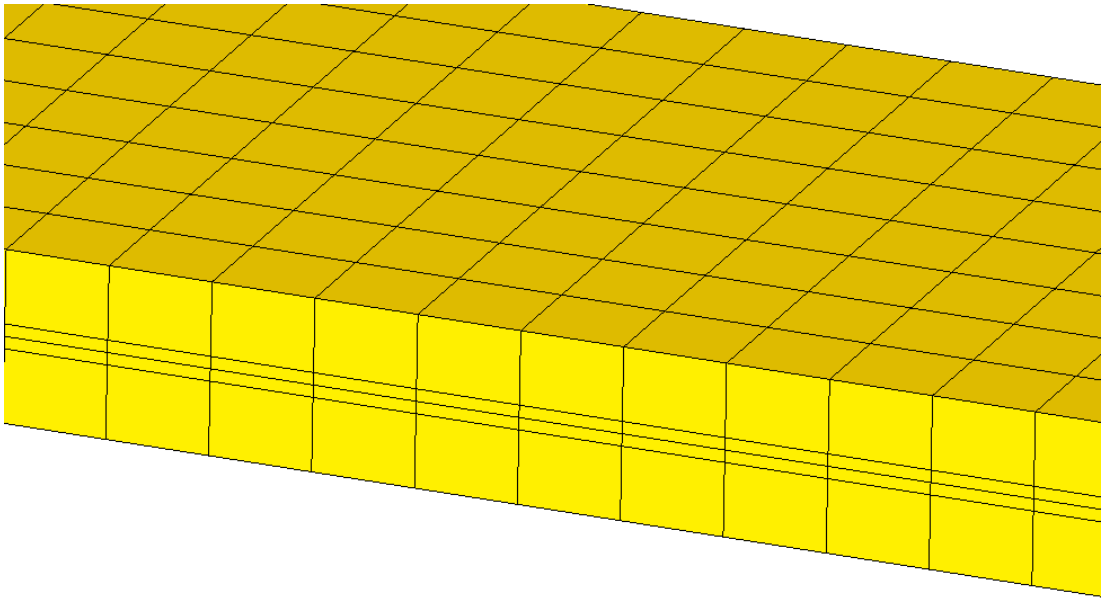

Figure 4.6 : Detailed look of the mesh along thickness

4.7 Solution

Before the solution stage of this implicit non-linear analysis, several settings were applied within the settings dialog of *SOLVER* module. Time interval of the experiment was set from $t = 0$ to $t = 1000$ s and *imposed time step* was chosen as 10 s. This gives 101 sets of generated results calculated at every 10 s of the simulation from 0 to 1000 s. *Response type* was selected as *static*. Threshold values for energy and force parameters were entered to provide an easier convergence process. Finally, resultant force on loading point was required as solution output from the *output* dialog.

After these settings were applied, model was checked for data incoherence using *check* button. When model was found clean from any incoherence in data, solution was performed using *convert and launch* dialog.

5. RESULTS

5.1 Material Properties

In certain sections of this study, mechanical properties of the composite material are needed. Since performing additional experimental study on prepared composite laminate was unavailable as an option, mechanical properties of the material were obtained through analytical equations based on micromechanical analysis of lamina [72].

There are 9 variables to obtain in order to model the characteristics of composite laminate since material is orthotropic. These properties are E_1, E_2, E_3 elastic moduli, ν_{12}, ν_{13}, ν_{23} Poisson's ratios and G_{12}, G_{13}, G_{23} shear moduli.

Additionally, transverse tensile strength of the material is needed for the interface material properties of finite element model.

5.1.1 Approach

To evaluate the elastic properties of composite using properties of fibre and matrix materials, strength of materials approach was utilized. This approach is based on modeling the characteristics of a unidirectional lamina via volume elements consisting of rectangular blocks. Stacked blocks having the same height, same length and different width represent fibre and matrix components of the material (Figure 5.1).

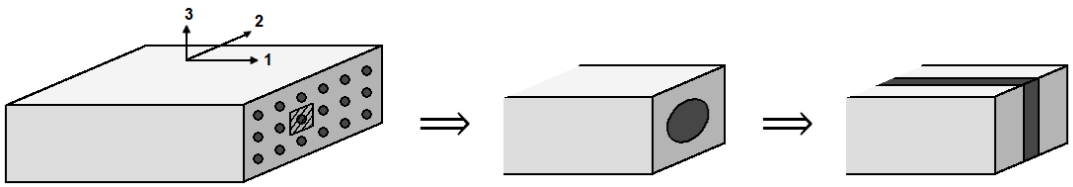

Figure 5.1 : Strength of materials approach

Additionally, as an assumption to reduce the number of unknown properties, laminate was assumed to be transversely isotropic. This assumption claims that if the distances between fibres are same in two directions in a plane for every section of the

material, elastic behavior of the material does not vary through that plane and the material is transversely isotropic. That plane is known as the plane of isotropy. Longitudinal direction is 1 and transverse directions are 2 and 3 for this study (Figure 5.2). Assuming transversely isotropic material case, equations that apply to elastic properties of material reduce the independent unknown elastic properties to E_1, E_2 elastic moduli, ν_{12}, ν_{23} Poisson's ratios and G_{12} shear modulus.

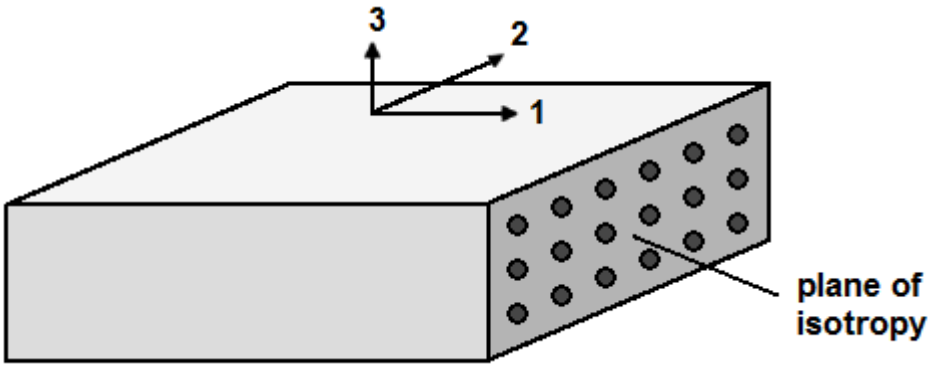

Figure 5.2 : Transversely isotropic material

For the evaluation of transverse tensile strength, ratio of the fibre diameter to fibre spacing (d/s) is necessary. In plane of isotropy of a transversely isotropic material; fibres are arranged in a square array, allowing the approximate determination of d/s ratio as a function of fibre volume ratio.

5.1.2 Calculation steps

Using known dimensions and post-manufacture measurements of plates (Table 5.1) and material properties of carbon, epoxy and PTFE taken from suppliers (Table 5.2); strength of materials approach and transversely isotropic material assumption are applied through several steps to obtain approximate elastic properties. These steps are applied for used area of plates and performed separately for i-plate and p-plate.

Table 5.1 : Known and measured properties of plates

	Symbol	i-plate	p-plate	Unit
Plate mass	w_c	0,272		kg
Number of plies	n	14		-
Plate area	A	0,044		m^2
PTFE area	A_{PTFE}	0,018	0,016	

Table 5.2 : Material properties of carbon, epoxy and PTFE

Parameter	Material						Unit
	Carbon (fibre)		Epoxy (matrix)		PTFE		
	Symbol	Value	Symbol	Value	Symbol	Value	
Areal density	$\rho_{f,A}$	0,3	-		$\rho_{PTFE,A}$	0,291	kg/m^2
Density	ρ_f	1800	ρ_m	1200	-		kg/m^3
Long. elastic modulus	E_{f_1}	230	E_m	3,1	-		GPa
Trans. elastic modulus	E_{f_2}	22			-		
Shear modulus	G_f	22	G_m	1,308	-		
In-plane Poisson's ratio	$\nu_{f_{12}}$	0,3	ν_m	0,3	-		-
Out-of-plane Poisson's ratio	$\nu_{f_{23}}$	0,35			-		
Ultimate tensile strength	$(\sigma_f^T)_{ult}$	4900	$(\sigma_m^T)_{ult}$	75	-		MPa
Ultimate compressive strength	$(\sigma_f^C)_{ult}$	-	$(\sigma_m^C)_{ult}$	130	-		

Elastic properties of the composite laminate were approximately obtained through following steps:

- Carbon fibre mass w_f is determined by

$$w_f = n \cdot A \cdot \rho_{f,A} \quad \textbf{(5.1)}$$

where n is number of plies used in plate, A is the area of the plate and $\rho_{f,A}$ is the areal density of carbon fabric.

- Carbon fibre volume v_f is determined by

$$v_f = w_f/\rho_f \quad \textbf{(5.2)}$$

where w_f is the mass and ρ_f is the density of carbon fibre.

- Epoxy mass w_m is determined by

$$w_m = w_c - w_f - \rho_{PTFE,A} \cdot A_{PTFE} \quad \textbf{(5.3)}$$

where w_c is the mass of composite plate, w_f is the mass of carbon fibre, $\rho_{PTFE,A}$ is the areal density of PTFE and A_{PTFE} is the area of PTFE remaining in plate.

- Epoxy volume v_m is determined by

$$v_m = w_m/\rho_m \quad \textbf{(5.4)}$$

where w_m is the mass and ρ_m is the density of epoxy.

- Composite volume v_c is determined by

$$v_c = v_m + v_f \quad \textbf{(5.5)}$$

where v_m is matrix volume and v_f is fibre volume.

- Fibre volume ratio V_f is determined by

$$V_f = v_f / v_c \quad \textbf{(5.6)}$$

and matrix volume ratio V_m is determined by

$$V_m = v_m / v_c \quad \textbf{(5.7)}$$

where v_f, v_m and v_c are fibre, matrix and composite volumes, respectively.

- Longitudinal elastic modulus E_1 is determined by

$$E_1 = E_{f_1} V_f + E_m V_m \quad \textbf{(5.8)}$$

where E_{f_1} is carbon fibre's longitudinal elastic modulus, E_m is epoxy's elastic modulus, V_f and V_m are fibre and matrix volume ratios, respectively.

- Transverse elastic modulus E_2 is determined by

$$\frac{1}{E_2} = \frac{V_f}{E_{f_2}} + \frac{V_m}{E_m} \quad \textbf{(5.9)}$$

where E_{f_2} is carbon fibre's transverse elastic modulus, E_m is epoxy's elastic modulus, V_f and V_m are fibre and matrix volume ratios, respectively.

- In-plane shear modulus G_{12} is determined by

$$\frac{1}{G_{12}} = \frac{V_f}{G_f} + \frac{V_m}{G_m} \quad \textbf{(5.10)}$$

where G_f is carbon fibre's shear modulus, G_m is epoxy's shear modulus, V_f and V_m are fibre and matrix volume ratios, respectively.

- In-plane Poisson's ratio ν_{12} is determined by

$$\nu_{12} = \nu_{f_{12}} V_f + \nu_m V_m \quad \textbf{(5.11)}$$

where $\nu_{f_{12}}$ is carbon fibre's in-plane Poisson's ratio, ν_m is epoxy's Poisson's ratio, V_f and V_m are fibre and matrix volume ratios, respectively.

- Out-of-plane Poisson's ratio ν_{23} is determined by

$$\nu_{23} = \nu_{f_{23}} V_f + \nu_m V_m \quad \textbf{(5.12)}$$

where $\nu_{f_{23}}$ is carbon fibre's out-of-plane Poisson's ratio, ν_m is epoxy's Poisson's ratio, V_f and V_m are fibre and matrix volume ratios, respectively.

- Assuming transversely isotropic material:

$$E_2 = E_3$$

$$\nu_{12} = \nu_{13}$$

$$G_{12} = G_{13} \quad \textbf{(5.13)}$$

- According to transversely isotropic assumption, out-of-plane shear modulus G_{23} is determined by

$$G_{23} = \frac{E_2}{2(1+\nu_{23})} \quad \textbf{(5.14)}$$

where E_2 is transverse elastic modulus and ν_{23} is out-of-plane Poisson's ratio of the composite.

- Fibre diameter to fibre spacing ratio d/s is determined by

$$\frac{d}{s} = \sqrt{\frac{4\,V_f}{\pi}} \quad \textbf{(5.15)}$$

where V_f is the fibre volume ratio.

- Ultimate transverse tensile strength $(\sigma_2^T)_{ult}$ is determined by

$$(\sigma_2^T)_{ult} = E_2 \left[\frac{d}{s}\,\frac{E_m}{E_{f_2}} + \left(1 - \frac{d}{s}\right)\right] \frac{(\sigma_m^T)_{ult}}{E_m} \quad \textbf{(5.16)}$$

where d/s is fibre diameter to fibre spacing ratio, E_2 is transverse elastic modulus of the composite, E_m is epoxy's elastic modulus, E_{f_2} is carbon fibre's transverse elastic modulus and $(\sigma_m^T)_{ult}$ is epoxy's ultimate tensile strength.

Elastic material properties (Table 5.3) and the ultimate transverse tensile strength (Table 5.4) evaluated for both plates are presented.

Table 5.3 : Approximate elastic material properties of carbon/epoxy unidirectional laminate

Elastic property	Symbol	Value		Unit
		i-plate	p-plate	
Longitudinal elastic modulus	E_1	139,05	138,67	GPa
Through the width elastic modulus	E_2	6,39	6,37	
Through the thickness elastic modulus	E_3	6,39	6,37	
In-plane shear modulus	G_{12}	3,00	2,99	
	G_{13}	3,00	2,99	
Out-of-plane shear modulus	G_{23}	2,40	2,39	
In-plane Poisson's ratio	ν_{12}	0,30		-
	ν_{13}	0,30		
Out-of-plane Poisson's ratio	ν_{23}	0,33		

Table 5.4 : Ultimate transverse tensile strength

Parameter	Symbol	Value		Unit
		i-plate	p-plate	
Fibre volume ratio	V_f	0,5991	0,5975	-
Fibre diameter to fibre spacing ratio	d/s	0,8734	0,8722	-
Ultimate transverse tensile strength	$(\sigma_2^T)_{ult}$	38,58	38,63	MPa

5.2 Experimental Results

Mode II delamination resistance of a FRP composite laminate is defined by critical energy release rate, G_{II_c}. This value can be accepted as a material property and is derived separately for two occasions: delamination initiation and propagation. In this section, results of the experimental study performed to evaluate these values are presented and the calculation steps are explained.

5.2.1 Specimen selection

In this experimental study, 20 specimens were manufactured with 2 types of initial defects. These defects are starter film insert and mode I precrack, denoted with i and p letters, respectively. Since there are 10 specimens with each type of defect, it was found suitable to denote starter film insert defected specimens with $i1$, $i2$, $i3$, $i4$, $i5$, $i6$, $i7$, $i8$, $i9$, $i10$ and mode I precrack defected specimens with $p1$, $p2$, $p3$, $p4$, $p5$, $p6$, $p7$, $p8$, $p9$, $p10$ specimen codes.

7 specimens from starter film insert group and 8 specimens from mode I precrack group were tested properly. These specimens are $i2$, $i3$, $i4$, $i5$, $i6$, $i7$, $i8$ and $p1$, $p2$, $p3$, $p5$, $p6$, $p7$, $p8$, $p10$. After data of these experiments were examined, 3 specimens from each group were selected for data analysis. These specimens are $i4$, $i6$, $i7$ and $p1$, $p3$, $p8$.

5.2.2 Data parameters

For the calculation of critical energy release rate; time, displacement, load data and delamination propagation values are required. These are the raw data of experimental study and all other parameter values are calculated using these. At any point in loading or unloading process;

- time parameter (t) indicates the duration since the beginning of experiment,
- load (P) is the bending force applied by upper crosshead to the specimen edge,
- displacement (δ) is the deflection of specimen edge.

Propagation variables are time (t) and delamination length (a). These parameters are measured when delamination propagation occurs. At any point in experiment where crack propagation occurs;

- time (t) is duration since the beginning of experiment to the occurrence of propagation,
- delamination length (a) is the distance from load line to the tip of newly propagated crack.

5.2.3 Data acquirement

Time, load and displacement values were recorded as data points with a frequency of 102,4 Hz during experiments. This gives 102400 data points in loading phase and 20480 data points in unloading phase for a single specimen; each containing time, load and displacement information. Since this amount of data is too much to be processed, it was reduced to have one data point in every 10^{-1} s. This resulted in 10000 data points in loading phase and 2000 data points in unloading phase for each specimen.

Propagation variables, time (t) and delamination length (a) were measured manually from recorded videos. For each specimen, a video was recorded with a camera fixed

to the white ink area. These videos were scanned by eye to record time information and video frame each time delamination was observed to propagate. When all images were listed, horizontal distances from the load line to the tip of delamination were measured on screen. These values were converted to distances on a curved beam and scaled to actual length units using known reference distances (Figure 5.3).

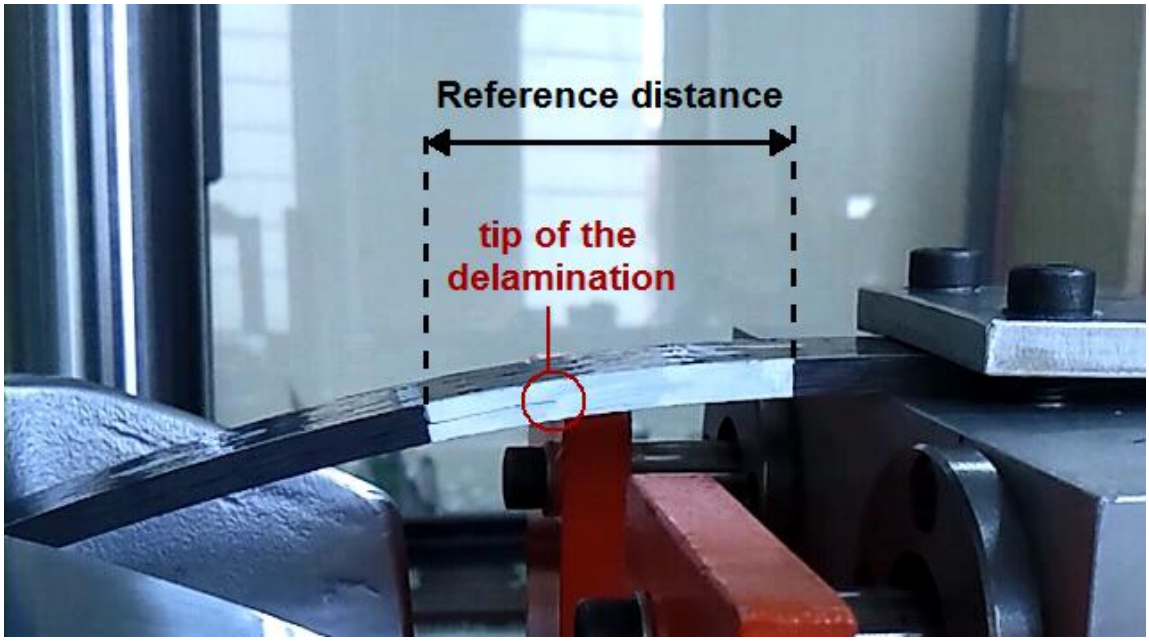

Figure 5.3 : Obtaining delamination length from video recordings

5.2.4 Load-displacement curves

When the reducement of time, displacement and load data to a processable amount was complete, load values were graphed with respect to displacement values for every tested specimen. These graphs, load-displacement curves, are the core of data analysis for this test method. Load-displacement curves for selected specimens are given in Figure 5.4 and load-displacement curves for all tested specimens are given in Appendix D.

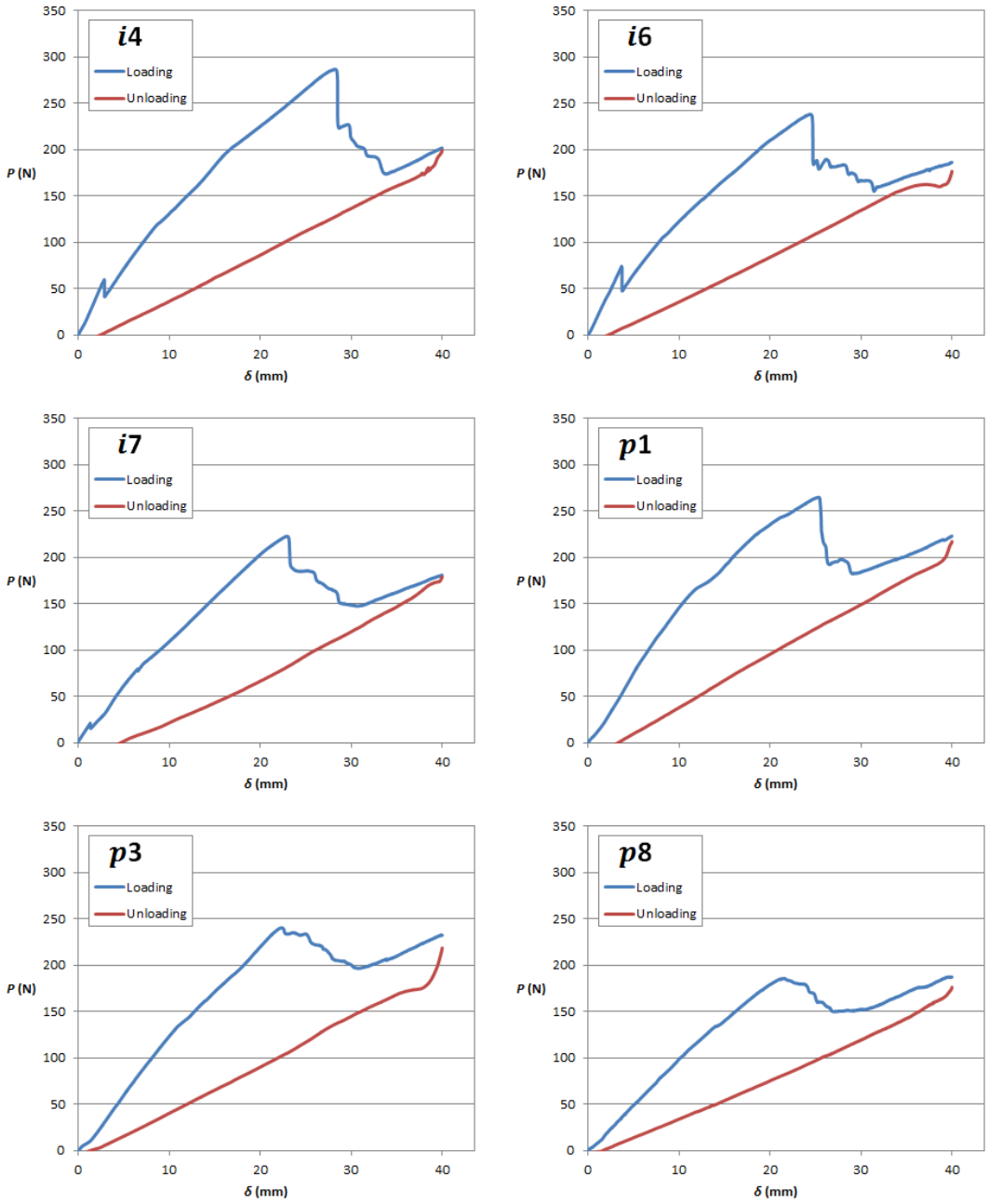

Figure 5.4 : Load-displacement curves of selected specimens

5.2.5 Critical points

According to protocol, there are several types of critical points that should be determined and marked on load-displacement curve for each experiment in order to analyze the data. These are called initiation and propagation points and they can be defined as following:

- Propagation point, denoted by $PROP$, are points where a delamination propagation is visually detected on experiment video. In order to obtain the location of propagation points on load-displacement curves, time information of

propagation were matched with time values of experimental data. Delamination length (a) was also measured for every propagation point; however these values were not marked on load-displacement curves.

- Deviation from linearity, initiation point denoted by NL, is the point in loading phase where non-linearity in bending behavior is first detected. Method to determine the location of NL point is not very specific. In this study, NL points were obtained via linear regression approach applied to portions of data starting from origin.
- Visual observation, initiation point denoted by VIS, is the point in loading phase where delamination movement from the tip of initial delamination is first detected visually. VIS points were determined with same method as propagation points. Video recordings were scanned by eye and the time of delamination growth into the white ink area was recorded to find the corresponding load and deformation values in data points.
- Maximum load point, initiation point denoted by MAX, is the point in loading data where the maximum value of load is reached. This point is simply obtained by examining data points in loading phase.
- 5% increase of compliance point, initiation point denoted by C_0 + 5%, is the point in loading data where compliance is calculated as 5% higher than its initial value, C_0. To obtain this point, initial compliance should be calculated first. A straight line is drawn from origin to fit the linear region of load-displacement curve. Initial compliance C_0 is inverse of the slope of this line. Afterwards, another line with compliance value of C_0 + 5% is drawn and the intersection of this line with the curve is obtained. However, C_0 + 5% points were not calculated in this study due to high scatter ratio of data points in small scale.

An example of load-displacement curve marked with initiation points is presented in protocol (Figure 5.5). When load-displacements curves from this study are compared to example, it can be observed that last portions, where load values start rising for the second time, are unnecessary for data analysis. Increments of load values observed in these regions results from the completion of crack propagation and the continuation of loading phase although the bending stiffness of the specimen is fixed. Therefore, it was found suitable to remove these points from the data. This procedure was applied

to all selected specimens automatically via scanning data points following MAX point for minimum load value and deleting the subsequent data portion.

Load-displacement graphs of selected specimens containing initiation points and trimmed data are given in Figure 5.6.

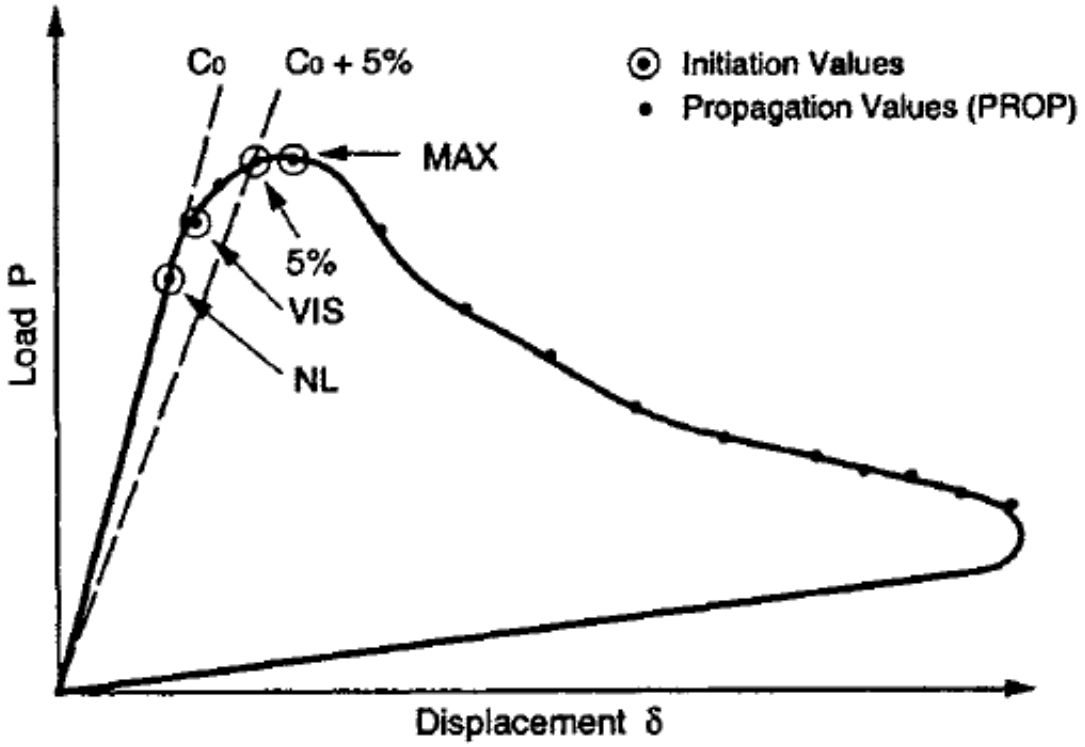

Figure 5.5 : An example of load-displacement curve [44]

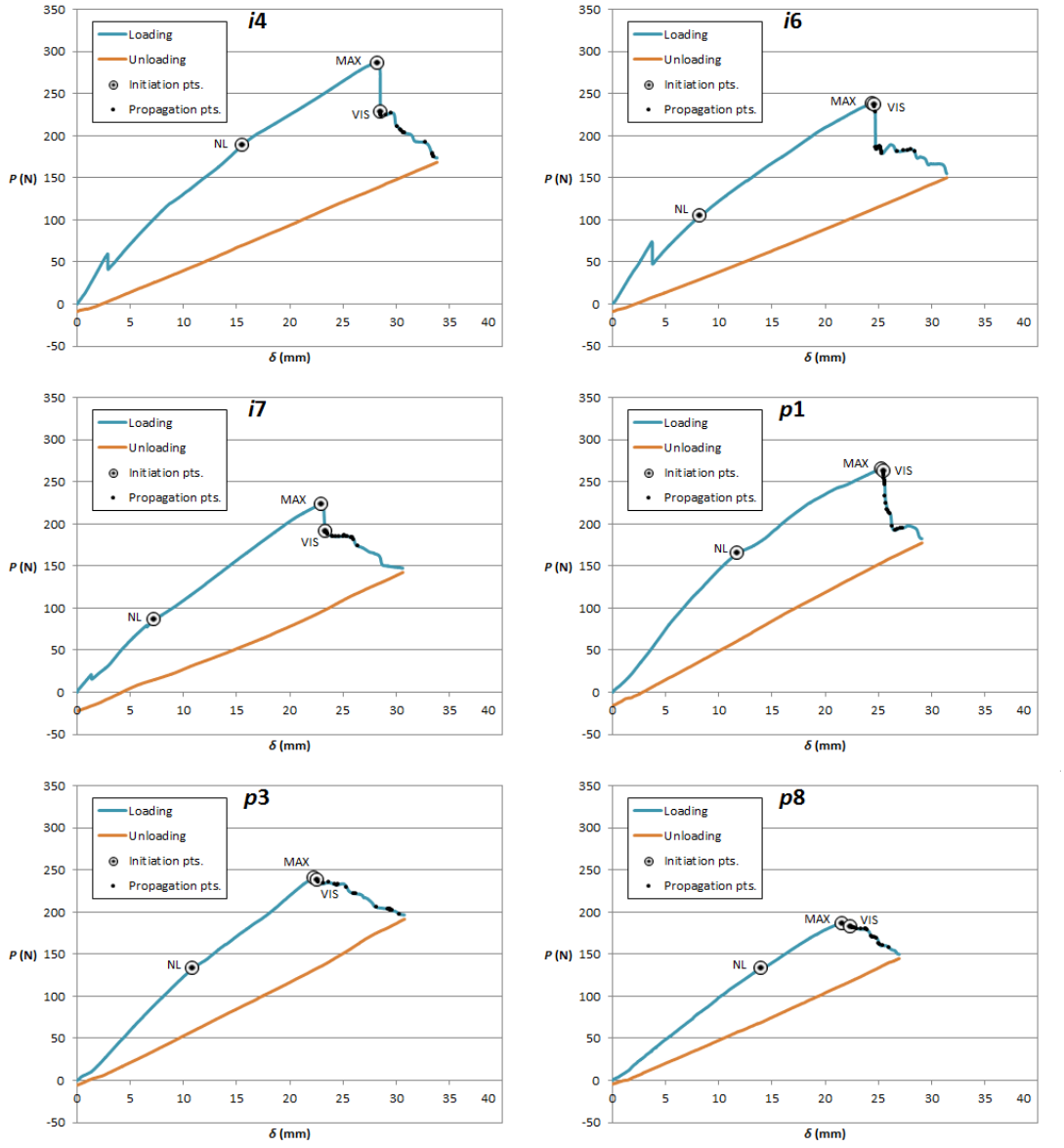

Figure 5.6 : Trimmed load-displacement curves of selected specimens with initiation and propagation points

5.2.6 Calculation methods

Two methods are included in protocol regarding to the calculation of critical energy release rate values. These are Corrected Beam Theory (CBT) and Experimental Compliance Method (ECM). Additionally, values obtained using both methods should be corrected due to large displacements and load-block effect. Critical energy release rate values were derived for all initiation and propagation points using both methods.

5.2.6.1 Corrected Beam Theory

This method is based on a simple beam theory approximation which includes a correction due to the rotation at the delamination tip. Using this method, critical energy release rate is given by

$$G_{\mathrm{II}_c} = \frac{9P^2(a+\Delta_{\mathrm{II}})^2}{4B^2Eh^3} \quad \textbf{(5.17)}$$

where Δ_{II} is the correction term for rotation at the tip of delamination. This term can be approximately calculated as

$$\Delta_{\mathrm{II}} = 0{,}42\ \Delta_{\mathrm{I}} \quad \textbf{(5.18)}$$

where Δ_{I} is delamination length correction obtained from mode I delamination test. If this test was not performed, this value should be taken as 0. Therefore, Equation 5.18 can be rewritten for our case ($\Delta_{\mathrm{I}} = 0$):

$$G_{\mathrm{II}_{c(CBT)}} = \frac{9P^2a^2}{4B^2Eh^3} \quad \textbf{(5.19)}$$

where P is load, a is delamination length, B is specimen width, E is flexural modulus and h is mid-thickness of the specimen.

Flexural modulus of the material is required to be determined via three-point bending test performed in accordance with ISO 14’125 test standard [73]. However, this test could not be performed and flexural modulus of the material was calculated via equations based on mechanics of composite materials. Theory and calculations were described in previous sections.

5.2.6.2 Experimental Compliance Method

This method is based on compliance parameter, C. This parameter is calculated for every initiation and propagation point using this equation:

$$C = \frac{\Delta\delta}{\Delta P} = \frac{\delta-\delta_0}{P-P_0} \quad \textbf{(5.20)}$$

where δ_0 and P_0 are the first deformation and load values recorded at the beginning of the experiment.

Determined compliance values for $PROP$ and VIS points are plotted versus the cube of delamination length, a^3. Slope of the linear regression line which fits into these

points is denoted with m. This value is calculated once for every specimen. After value of m is obtained, critical energy release rate is given by:

$$G_{\mathrm{II}_c(ECM)} = \frac{3P^2ma^2}{2B} \quad \textbf{(5.21)}$$

where P is load, a is delamination length and B is specimen width.

5.2.6.3 Large displacement and load-block correction

This correction is applied to critical energy release rate values determined via both methods to cancel the effects of large displacements and load-block. Correction factors θ_1 and θ_2 are given by:

$$\theta_1 = \frac{3}{20}\frac{\left[15+50\left({}^{a}/_{L}\right)^2+63\left({}^{a}/_{L}\right)^4\right]}{\left[1+3\left({}^{a}/_{L}\right)^3\right]^2} \quad \textbf{(5.22)}$$

$$\theta_2 = -3\left({}^{L}/_{a}\right)\frac{\left[1+3\left({}^{a}/_{L}\right)^2\right]}{\left[1+3\left({}^{a}/_{L}\right)^3\right]} \quad \textbf{(5.23)}$$

where a is delamination length and L is the free length of the specimen.

Using corrections factors θ_1 and θ_2, corrected critical energy release rate value is calculated as following:

$$G_{\mathrm{II}_c(corrected)} = G_{\mathrm{II}_c}\left[1-\theta_1\left({}^{\delta}/_{L}\right)^2-\theta_2\left({}^{\delta\, I_1}/_{L}\right)\right] \quad \textbf{(5.24)}$$

where G_{II_c} is critical energy release rate value obtained from either one of methods, δ is deformation, L is free length of the specimen and I_1 is the distance between center of the pin inserted into the load-block and mid-thickness of the specimen.

5.2.7 Calculation process

Evaluation of critical energy release rate value was performed in several steps which were repeated for every specimen. These steps are described in detail as following and values of all variables used in calculation process are given in Appendix E.

- Data points for loading phase containing time (t), deformation (δ) and load (P) information were listed and sorted in ascending order with respect to time parameter.

- Initiation (NL, MAX, VIS) and propagation ($PROP$) points containing propagation time (t) and delamination length (a) were determined.
- Initiation and propagation points were matched to the closest data points using time as a common parameter.
- Matched data points were listed and sorted in ascending order with respect to time and marked on load-displacement curve.
- Specimen width (B) and mid-thickness (h) parameters were taken as average of values from specimens' detailed measurements (Table B1, Table B2).
- Flexural modulus (E) values were taken from Table 5.3.
- Critical energy release rates were calculated according to Corrected Beam Theory for NL, MAX, VIS and $PROP$ points ($G_{\mathrm{II}_{c(CBT)}}$ values).
- Compliance values (C) were calculated for VIS and $PROP$ points and they were plotted with respect to cube of delamination length (a^3).
- Slope of C versus a^3 curve (m) is determined using a linear regression line.
- Critical energy release rates were calculated according to Experimental Compliance Method for NL, MAX, VIS and $PROP$ points ($G_{\mathrm{II}_{c(ECM)}}$ values).
- Distance between the center of the pin and the mid-thickness line of the specimen (I_1) was calculated via

  $$I_1 = \frac{H}{2} + h \qquad \textbf{(5.25)}$$

  formula where h is the half thickness of the specimen and H is the height of the load-block which is 30 mm.
- Large displacement and load-block correction factors θ_1 and θ_2 were calculated for NL, MAX, VIS and $PROP$ points.
- Both critical energy release rate results ($G_{\mathrm{II}_{c(CBT)}}$ and $G_{\mathrm{II}_{c(ECM)}}$ values) were corrected for large displacements and load-block effect.

5.2.8 Results

With the application of described data analysis steps using both calculation methods (Corrected Beam Theory and Experimental Compliance Method), critical energy

release rate values were evaluated at initiation and propagation points for $i4$, $i6$, $i7$ and $p1$, $p3$, $p8$ specimens. Critical energy release rate values calculated via Corrected Beam Theory are given in Figure 5.7, Figure 5.8 and values calculated via Experimental Compliance Method are given in Figure 5.9 and Figure 5.10.

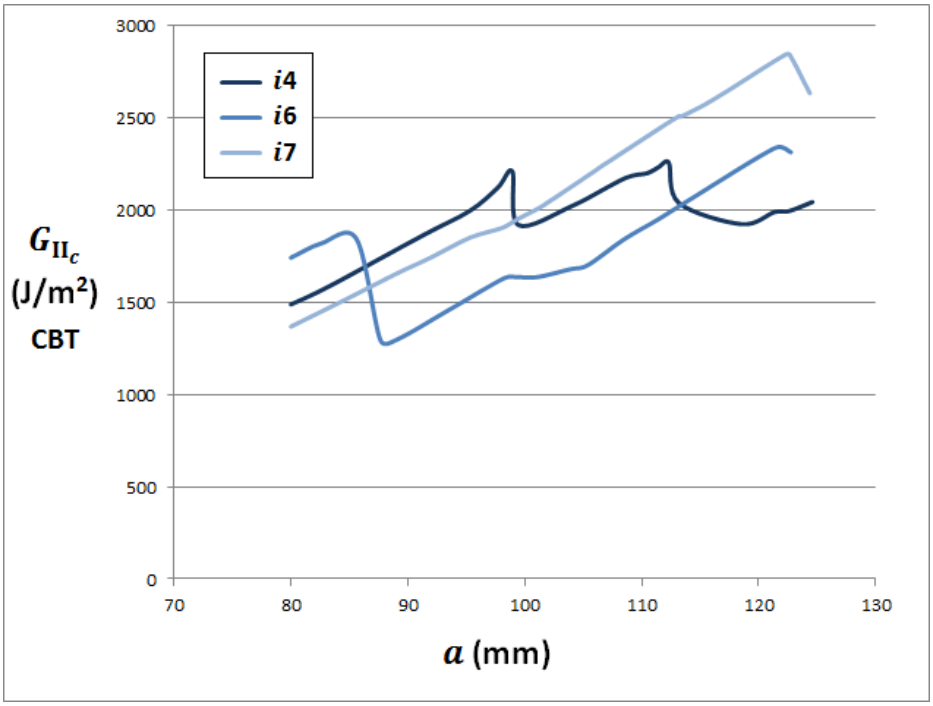

Figure 5.7 : Critical energy release rates calculated for i-specimens via Corrected Beam Theory

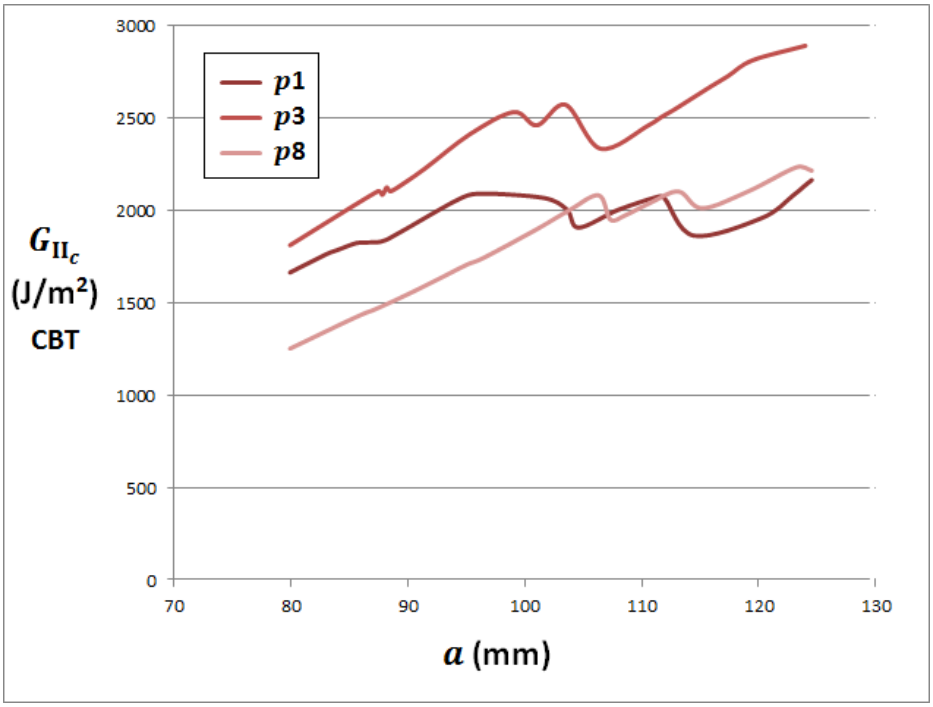

Figure 5.8 : Critical energy release rates calculated for p-specimens via Corrected Beam Theory

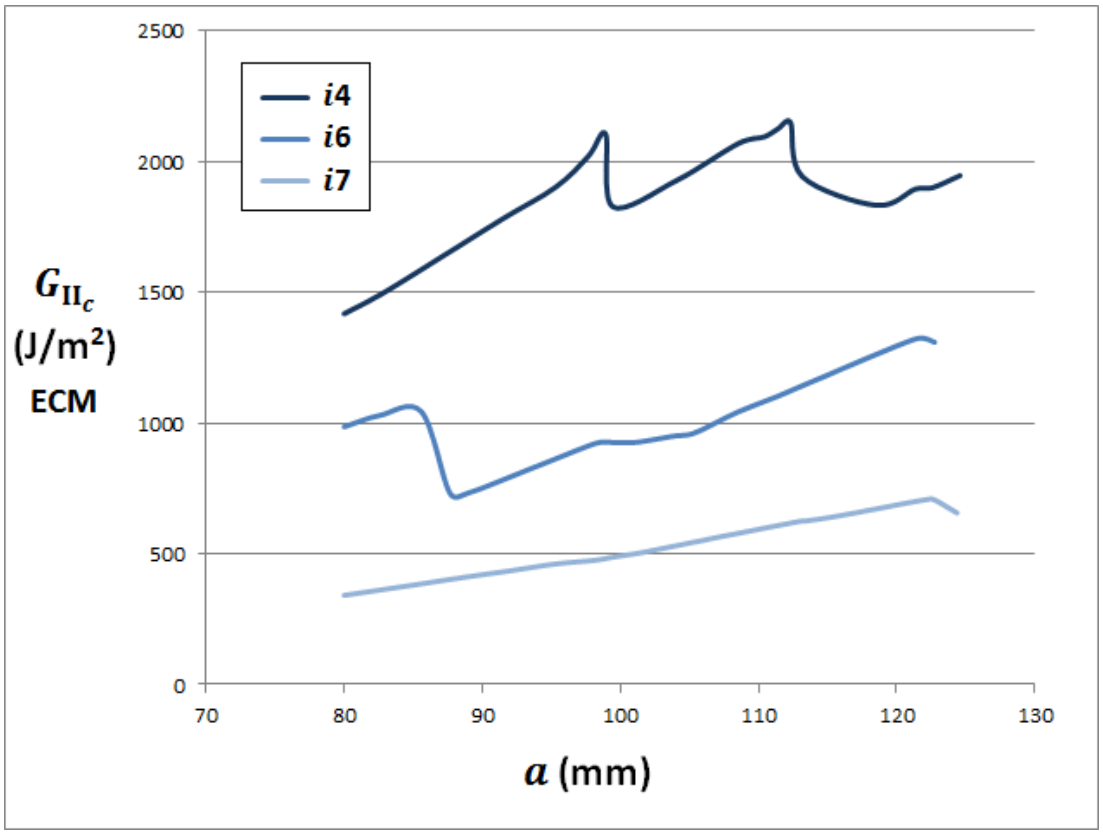

Figure 5.9 : Critical energy release rates calculated for *i*-specimens via Experimental Compliance Method

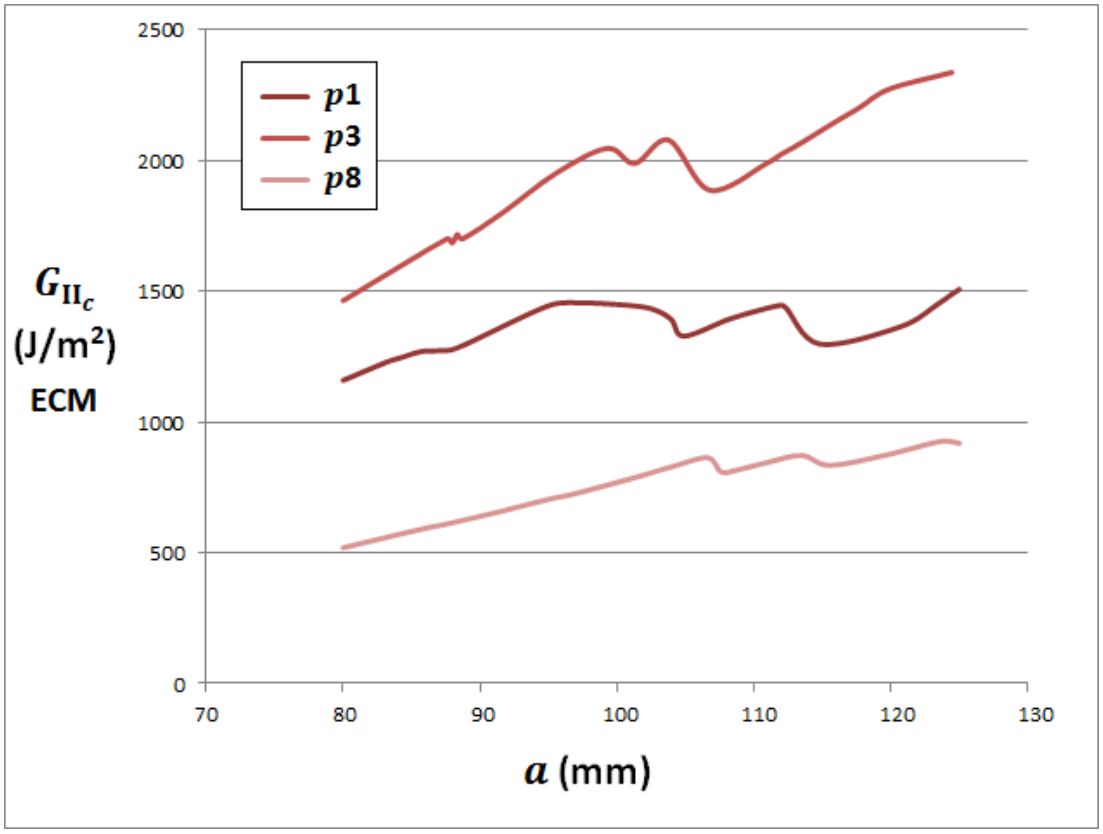

Figure 5.10 : Critical energy release rates calculated for *p*-specimens via Experimental Compliance Method

It can be seen that variance of $G_{\mathrm{II}_c(ECM)}$ values is unreasonably high comparing to $G_{\mathrm{II}_c(CBT)}$ values. Regardless of the cause of this situation, it is clear that $G_{\mathrm{II}_c(CBT)}$ results are more accurate. Therefore, $G_{\mathrm{II}_c(CBT)}$ values were taken as reference when calculating final G_{II_c} values.

Critical energy release rate quantity is measured for two situations: initiation and propagation of delamination. These quantities express composite laminate's resistance to delamination onset and growth, respectively. Evaluation of these properties are explained in following steps, which were applied for both starter film insert defected and mode I precrack defected specimens.

To evaluate the critical energy release rate for initiation, G_{II_c} values for initiation points (NL, VIS, MAX and C_0 + 5%) should be listed for all selected specimens. Average and standard deviation must be calculated for each initiation point. Lowest average G_{II_c} value among initiation points gives critical energy release rate for delamination initiation.

To evaluate the critical energy release rate for propagation, G_{II_c} and delamination length (a) values of all selected specimens' propagation points ($PROP$) should be listed and sorted in ascending order with respect to parameter a. 50% of these $PROP$ points must be selected for the calculation of average and standard deviation of G_{II_c} values. The average value gives critical energy release rate for delamination propagation.

Obtained G_{II_c} values are given in Table 5.5. In accordance with protocol, average G_{II_c} values of initiation points and 50% of $PROP$ points' G_{II_c} values are plotted versus delamination length a in Figure 5.11.

Table 5.5 : Final critical energy release rate values

Critical energy release rate G_{II_c} (J/m^2)	Initial defect type	
	starter film insert	mode I precrack
For initiation	542	620
For propagation	1978	2061

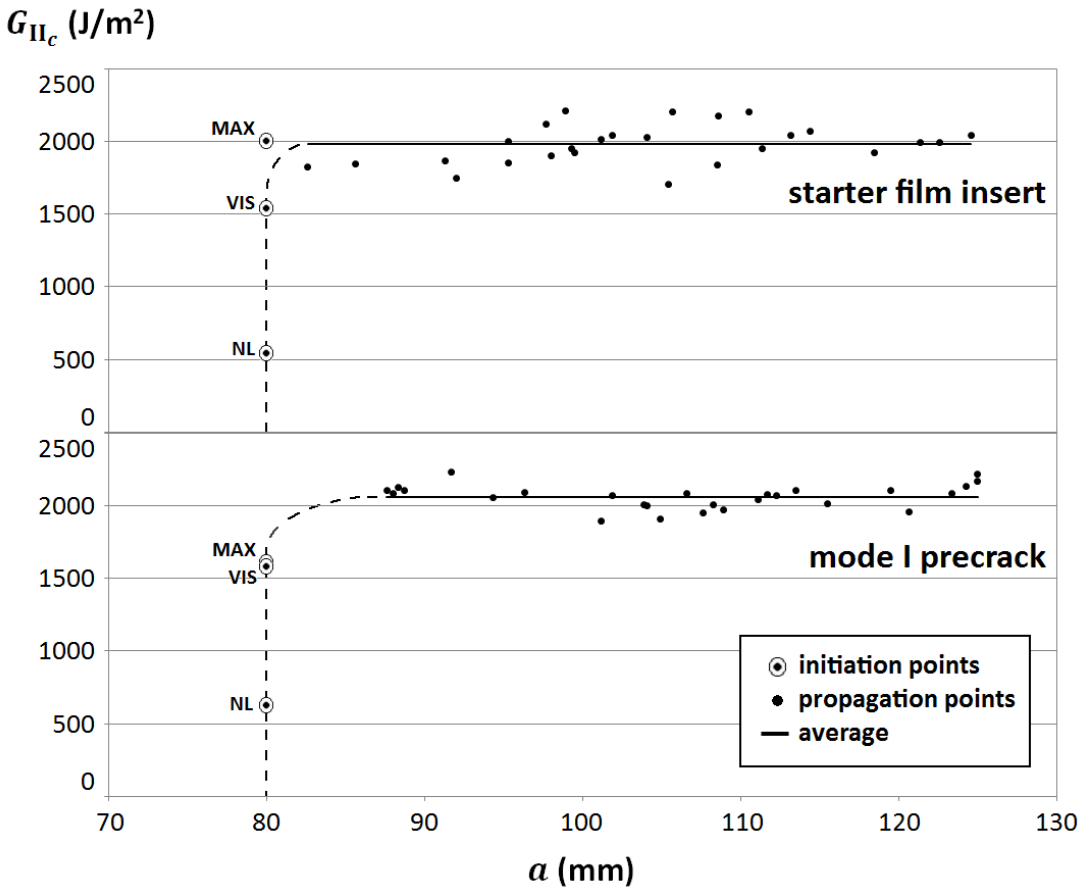

Figure 5.11 : Final critical energy release rate values

5.3 Finite Element Analysis Results

5.3.1 Resultant force

Resultant force measured on loading point was specifically required as an output in solution settings stage of the analysis. After analysis was complete, resultant force on loading point was given as components in x, y and z directions. Loading point resultant force component in z direction gives the equivalent of bending load P in experimental study. Plot of this variable with respect to simulation time (t) from 0 to 1000 s is given in Figure 5.12. Maximum value of the variable is given as 261,1169 N at $t = 1000$ in listed analysis results, which is close to the average maximum value of P calculated from experimental study.

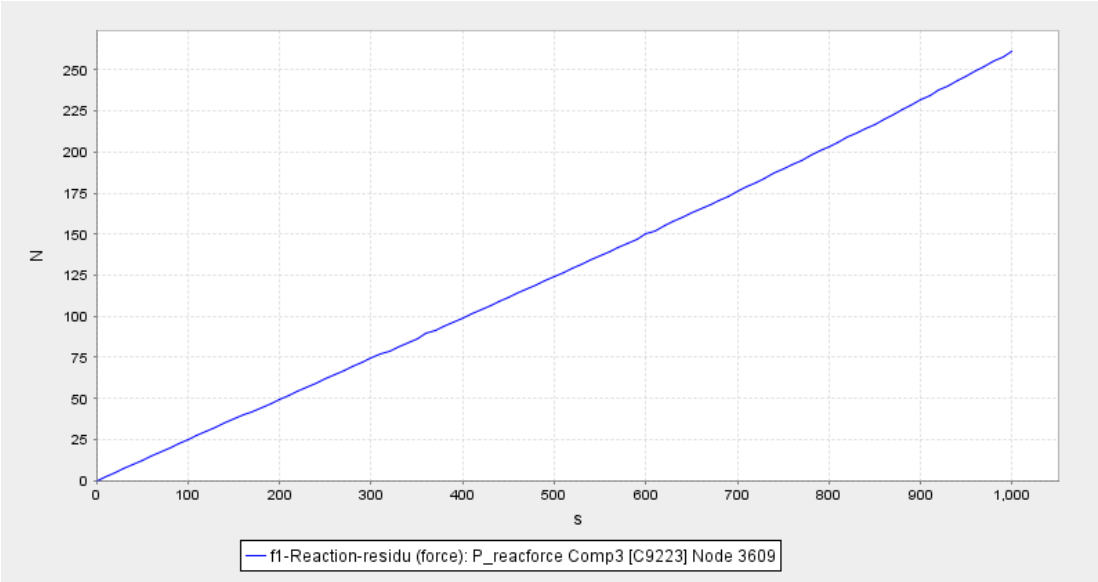

Figure 5.12 : Plot of the resultant force on loading point, component in z direction

5.3.2 Nodal displacements

Nodal displacements of the model were given as a time-dependent variable set in results of the analysis. Plots of nodal displacements for the last frame of simulation ($t = 1000$ s) are presented in Figure 5.13 as side view and Figure 5.14 as oblique view.

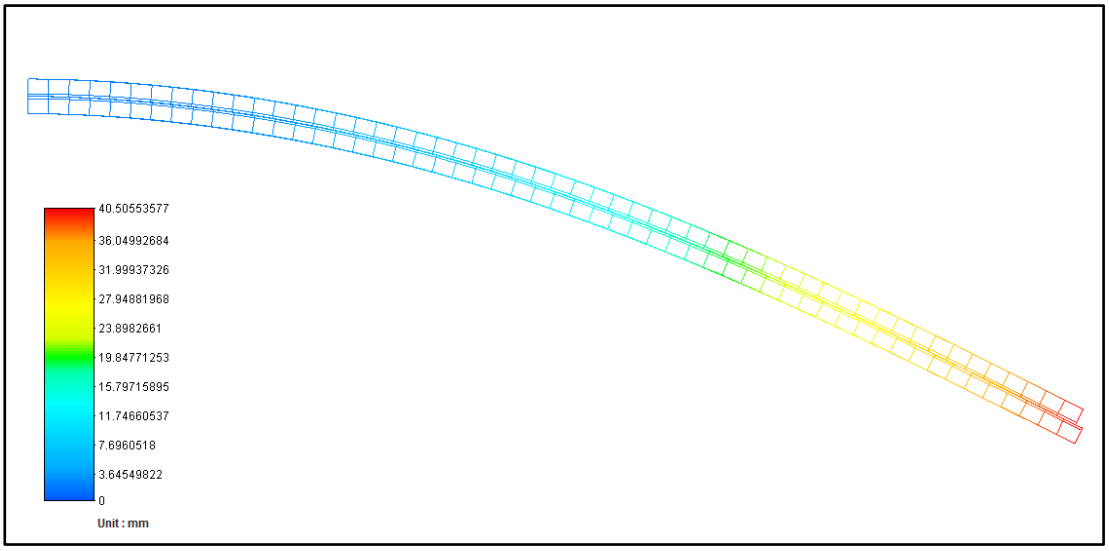

Figure 5.13 : Nodal displacements at the end of experiment (side view)

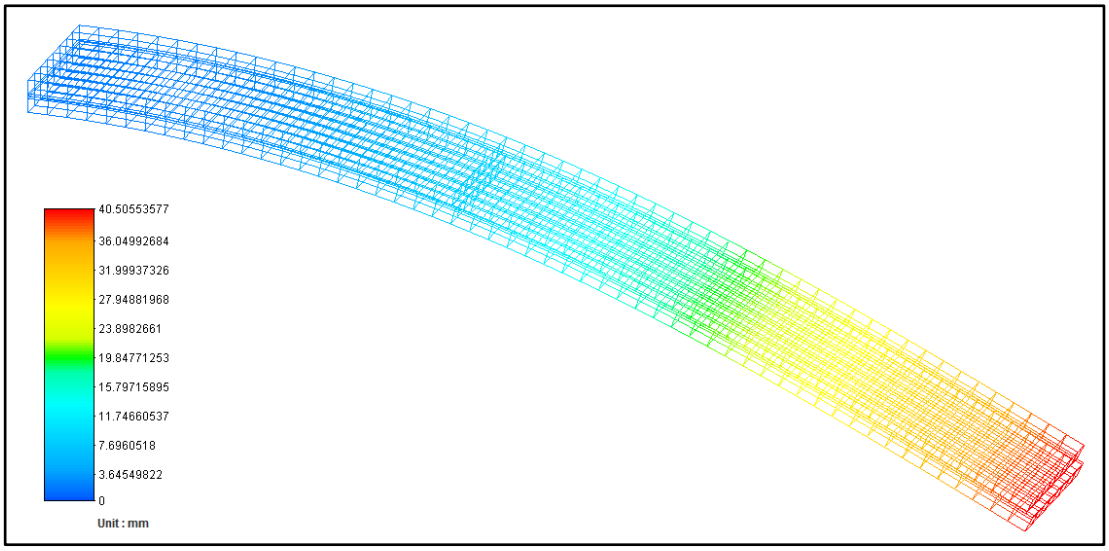

Figure 5.14: Nodal displacements at the end of experiment (oblique view)

5.3.3 Delamination length

Since delamination length is not a default or optional result parameter of the software, it was manually calculated using listed results of nodal displacement parameter for all 101 time steps of the simulation.

First step for evaluating delamination length values was to list time-dependent deformation values of all 101 time steps for two sets of nodes. First set of nodes are located on the mid-width line of top surface of lower rectangular box (Box 2, Figure 5.15) and the second set of nodes are located on the mid-width line of the bottom surface of upper rectangular box (Box 4, Figure 5.16), both located in crack propagation area.

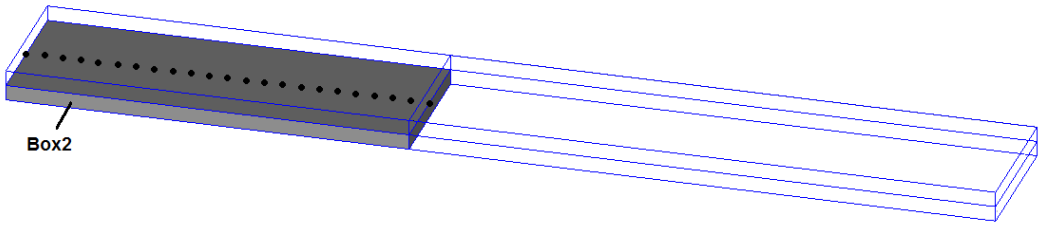

Figure 5.15 : First set of nodes

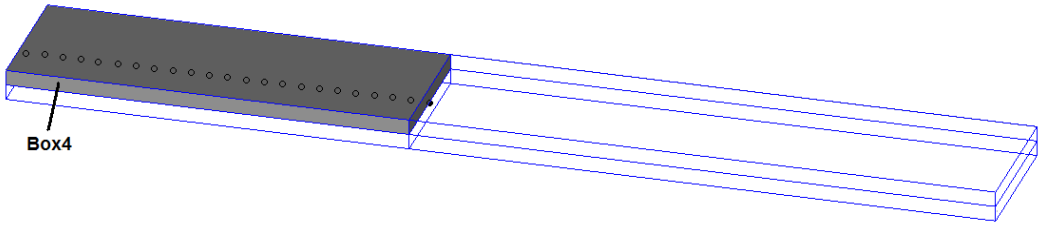

Figure 5.16 : Second set of nodes

These sets are coincidental before loading starts ($t = 0$). As the specimen is loaded, crack propagation occurs and corresponding nodes or coupled nodes move away from each other. To derive the crack propagation values, opening length of coupled nodes were calculated using x and z components of time-dependent nodal displacement data (y components were neglected since the deformation is very small at mid-width line). Denoting the number of node couples with i, node sets with u and l (upper and lower) and nodal displacements along x and z directions with Δx and Δz; opening length of coupled nodes at i^{th} location is given by

$$\Delta_i = \sqrt{\left(\Delta x_{u,i} - \Delta x_{l,i}\right)^2 + \left(\Delta z_{u,i} - \Delta z_{l,i}\right)^2} \quad \textbf{(5.26)}$$

Values of Δ_i parameter were obtained for all node couples ($i = 1, 2, 3 \ldots 23$) and time steps ($t = 0, 10, 20 \ldots 1000$ s). These values were plotted as $\Delta_i(t)$ function.

For the simplicity of determining crack length values, location of node couples should be defined using a length parameter. For this purpose, d parameter was defined as the distance of node couples from constrained end. Since all mesh elements were set to the length of 2,5 mm, conversion was performed easily via formula

$$d = (i - 1) \cdot 2{,}5 \text{ mm} \quad \textbf{(5.27)}$$

Opening lengths of coupled nodes were once again plotted versus distance from constrained edge ($d = 0, 2{,}5, 5 \ldots 55$ mm) and time ($t = 0, 10, 20 \ldots 1000$ s) variables as $\Delta(d, t)$ function.

In order to obtain delamination propagation with a higher sensitivity, Δ values were interpolated with respect to d parameter to have a value at every 0,5 mm. Definitions of $\Delta(d, t)$ function and d distance are shown on the side view portion of mesh model (Figure 5.17).

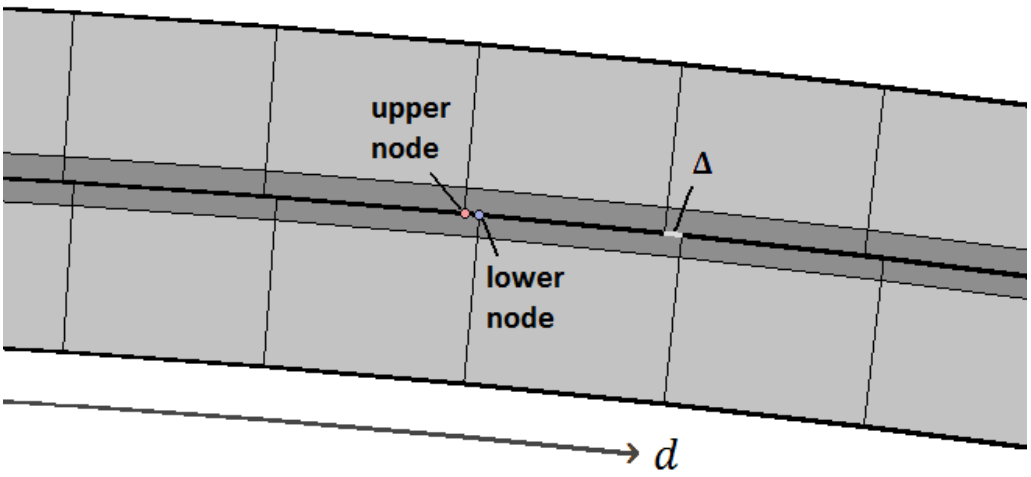

Figure 5.17 : Opening length of coupled nodes (Δ) and distance from constrained edge (d)

After these steps, a filter was developed to pick delamination length (a) values from $\Delta(d,t)$ data. Closest point to constrained edge validating $\Delta > \Delta_c$ criterion was determined and accepted as the tip of the delamination. Δ_c value was chosen as 0,01 mm. This defines crack propagation as having more than 0,01 mm distance between coupled nodes. In accordance with this criterion, delamination length a was obtained for each time step of the simulation as shown in Table 5.6.

Table 5.6 : Delamination length a for all time steps

t (s)	a (mm)	t (s)	a (mm)	t (s)	a (mm)	t (s)	a (mm)	t (s)	a (mm)
0	80	210	132,5	410	134	610	134,5	810	134,5
10	80	220	133	420	134	620	134,5	820	134,5
20	83,5	230	133	430	134	630	134,5	830	134,5
30	102	240	133	440	134	640	134,5	840	134,5
40	111	250	133	450	134	650	134,5	850	134,5
50	117	260	133	460	134	660	134,5	860	134,5
60	120,5	270	133,5	470	134	670	134,5	870	134,5
70	123	280	133,5	480	134	680	134,5	880	134,5
80	124,5	290	133,5	490	134	690	134,5	890	134,5
90	126	300	133,5	500	134,5	700	134,5	900	135
100	127,5	310	133,5	510	134,5	710	134,5	910	135
110	128	320	133,5	520	134,5	720	134,5	920	135
120	129	330	133,5	530	134,5	730	134,5	930	135
130	129,5	340	133,5	540	134,5	740	134,5	940	135
140	130	350	134	550	134,5	750	134,5	950	135
150	130,5	360	134	560	134,5	760	134,5	960	135
160	131	370	134	570	134,5	770	134,5	970	135
170	131,5	380	134	580	134,5	780	134,5	980	135
180	132	390	134	590	134,5	790	134,5	990	135
190	132	400	134	600	134,5	800	134,5	1000	135

5.3.4 Load-displacement data

As mentioned before, z-component of the resultant force on loading point was accepted as load parameter, P. Deformation parameter, δ is given by

$$\delta = 0{,}04\ t \tag{5.28}$$

where 0,04 is value of crosshead rate (mm/s) and t is the time parameter.

All points that have a larger delamination length value from previous rows in Table 5.6 were accepted as propagation points ($PROP$). These points were marked on load-displacement curve (Figure 5.18). However, initiation points (NL, VIS, MAX, C_0 + 5%) were not defined on load-displacement curve, due to the mismatching characteristics with experimental load-displacement data.

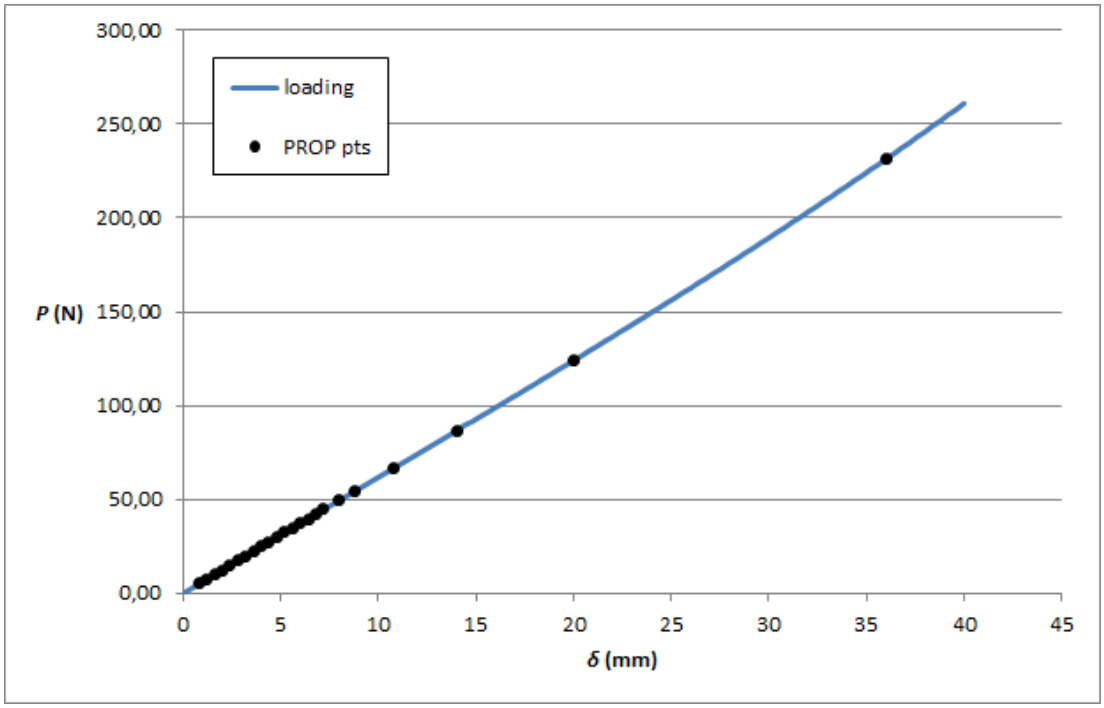

Figure 5.18 : Load-displacement curve of the finite element analysis

6. DISCUSSION

6.1 Experimental Results

First thing that attracts notice while examining calculated values for mode II critical energy release rate, is that the propagation values are 3 to 4 times higher than the values in literature (Figure 6.1) [61, 62]. Another unexpected result is the extreme fluctuations in mode II critical energy release rate values along the specimen length. Several reasons that might have caused this situation are explained.

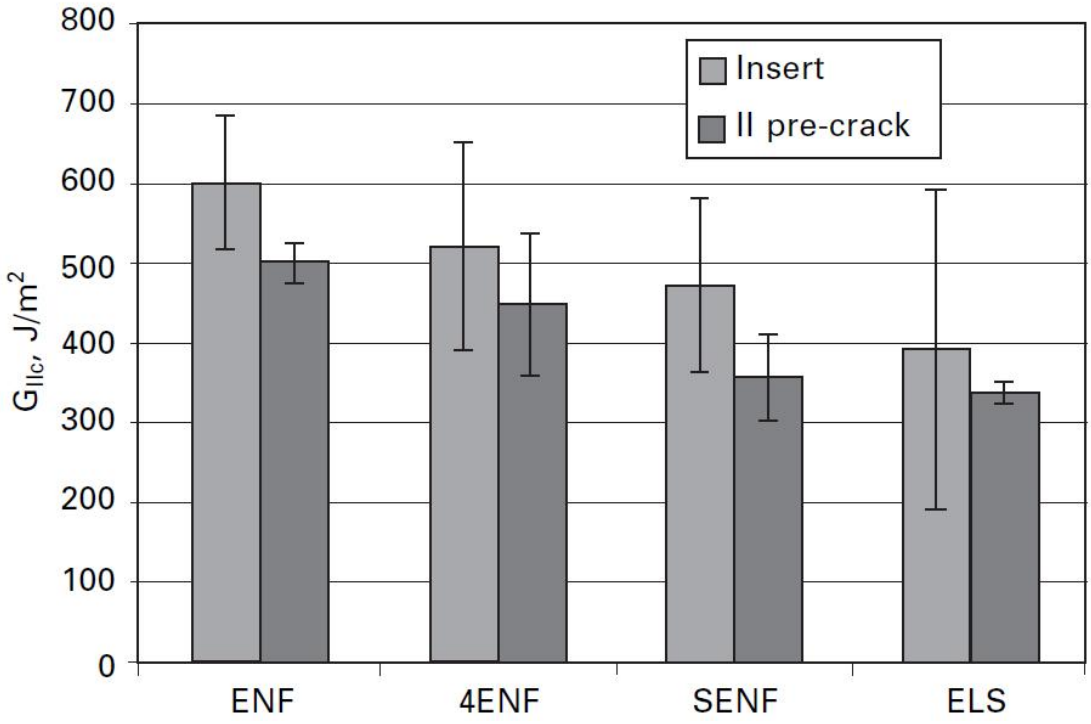

Figure 6.1 : Comparison of mode II critical energy release rates evaluated via different specimens [61]

Materials used for the specimens, carbon fabric and hand-mixed epoxy, may have increased G_{II_c} values due to high matrix volume ratio and using prepregs composites could lower the values due to higher fibre volume ratio. Since interlaminar strength of the material is mostly provided by the matrix phase, lower matrix volume ratio can lead to reducement in interlaminar strength of the composite.

Using prepreg composites along with more standardized manufacturing techniques could also reduce the fluctuations in G_{II_c} values. Although hand lay-up technique has a lower cost, it may cause severe thickness variations and anisotropic material properties in composite.

Another cause of the extreme values may be the thickness of PTFE insert film. As mentioned before, thickness of the film was about 10 times of the thickness value recommended in protocol. This may have disrupted the layers significantly, causing epoxy to fill the gap between layers at the mid-thickness and leading to excessive increments of G_{II_c} values in small-scale bulk epoxy regions.

The cause of large difference between results of two calculation methods, Corrected Beam Theory and Experimental Compliance Method is another point worth investigating. When G_{II_c} versus a curves of each specimen are compared for two methods, it can be observed that the curves are characteristically same for both methods; which indicates that in Experimental Compliance Method formula, one of the multiplied parameters varies greatly. When all the parameters in this equation were examined, m (slope of C versus a^3 plot) parameter was determined as the cause. This indicates that compliance values derived from experimental data are inaccurate and results calculated via Corrected Beam Theory are more efficient.

Additionally; sharp corners in some of the load-displacement curves and discontinuities of the load parameter at increasing or decreasing regions as a general characteristic in all load-displacement curves (Appendix D) indicates that the specimens does not allow proper delamination occurrence. Again, this problem may be the result of material quality and using prepregs would probably help solving it.

6.2 Finite Element Analysis Results

It should be noted that properties of the composite material used in finite element analysis were obtained theoretically and not experimentally. Taking this factor and the variation of material properties between specimens into account; results of this simulation are not expected to be accurate and should be considered coincidental if results match within the smaller accuracy range than 20%.

Results of the finite element analysis were difficult to compare with experimental results. Load-displacement curve based on progression of the initial crack was linear

and the compliance value was constant throughout the simulation. Nodes of the elements on opposite faces were separated at the beginning of simulation and the distance between them grew linearly with respect to time and distance from constrained edge of the specimen. This condition suggests that the analysis is more likely to simulate a condition where two faces are elastically bonded rather than a crack in a brittle material. The reason or the parameter to cause this situation could not be recovered.

On the other hand, reaction force measured on loading point simulating the upper crosshead, was determined to be close to the value obtained from experimental study. Average of maximum load values measured from specimens included in data processing ($i4$, $i6$, $i7$, $p1$, $p3$, $p8$ specimens) is 240 N whereas maximum reaction forced measured on load point in finite element analysis was 261 N. This gives us an accuracy range within 10%, which is considered partially coincidental as noted before. Therefore, the simulation of material softening during crack propagation can be considered successful.

6.3 Summary and Future Work

In this study, mode II delamination resistance of a hand-manufactured unidirectional carbon/epoxy composite material was investigated. Mathematical models regarding to the subject were described. Standardized tests for measuring delamination resistance were summarized. Mode II critical energy release rate, which is the quantity for expressing resilience to mode II delamination, was obtained through experimental study. Experiments were performed in accordance with ESIS protocol for mode II testing using ELS specimen. Material properties of the composite were approximately obtained from material properties of carbon and epoxy provided from suppliers. These properties and results of experimental study were used in finite element modeling. Analysis results were compared with experimental study. Overall results were discussed.

There are a few but important factors that can be improved for this study to be more efficient. First factor is the material quality. Hand-manufactured carbon/epoxy composites may reduce the material quality severely and cause major variations of properties between specimens. Therefore, prepreg composite material and automated manufacturing methods are essential for further studies.

For a study with more reliable results, an automated method to observe and record the crack length during experiments is definitely a priority. A study can be performed to develop an image processing program which reads delamination length values from recorded videos of experiments. Accuracy range of read crack lengths can be minimized by using different criteria for definition of a crack (visually) and comparing the results.

Additionally, a better finite element model can be employed to simulate the behavior of mode II delamination. For instance, fracture mechanics based models can be investigated to compare the results.

As for the future of research subject, test protocols for determination of mode II delamination resistance remains highly controversial. For the standardization of mode II testing, methods to provide more stable propagation are in need. Delamination resistance of cross-ply composites is also an important researching subject, since the application areas of unidirectional composites are quite limited.

REFERENCES

[1] **Paris, P. C. & Sih, G. C.** 1965. Stress analysis of cracks, in *Fracture Toughness Testing and Its Applications*, STP381. American Society for Testing and Materials, 30-83.

[2] **Wang, S. S.** 1984. Edge delamination in Angle-ply Laminates. *AIAA Journal*, **22 (2)**, 256-264.

[3] **Irwin, G. R.** 1957. Analysis of stresses and strains near the end of a crack traversing in a plate. *Journal of Applied Mechanics*, **24**, 351-369.

[4] **Krueger, R.** 2002. The virtual crack closure technique - history, approach and applications. *Applied Mechanics Reviews*, **57 (2)**, 109-143.

[5] **Landes, J. D.** 2000. The Contributions of George Irwin to Elastic-Plastic Fracture Mechanics Development, in *Fatigue and Fracture Mechanics, 31st Volume*, STP1389. American Society for Testing and Materials, 54-63.

[6] **De Morais, A. B., De Moura, M. F., Gonçalves, J. P. M., & Camanho, P. P.** 2003. Analysis of crack propagation in double cantilever beam tests of multidirectional laminates. *Mechanics of Materials*, **35 (7)**, 641-652.

[7] **Liu, P. F., Hou, S. J., Chu, J. K., Hu, X. Y., Zhou, C. L., Liu, Y. L., Zheng, J. Y., Zhao, A., & Yan, L.** 2011. Finite element analysis of postbuckling and delamination of composite laminates using virtual crack closure technique. *Composite Structures*, **93 (6)**, 1549-1560.

[8] **Marat-Mendes, R. M., & Freitas, M. M.** 2010. Failure criteria for mixed mode delamination in glass fibre epoxy composites. *Composite Structures*, **92 (9)**, 2292-2298.

[9] **Shen., F., Lee, K. H., & Tay, T. E.** 2001. Modeling delamination growth in laminated composites. *Composites Science and Technology*, **61 (9)**, 1239-1251.

[10] **Abdullah, E., Ferrero, J. F., Barrau, J. J., & Mouillet, J. B.** 2007. Development of a new finite element for composite delamination analysis. *Composites Science and Technology*, **67 (10)**, 2208-2218.

[11] **Robinson, P., Besant, T., & Hitchings, D.** 2000. Delamination growth prediction using a finite element approach. *European Structural Integrity Society*, **27**, 135-147.

[12] **Park, O., & Sankar, B. V.** 2002. Crack-tip force method for computing energy release rate in delaminated plates. *Composite Structures*, **55 (4)**, 429-434.

[13] **Pietropaoli, E., & Riccio, A.** 2011. Formulation and assessment of an enhanced finite element procedure for the analysis of delamination

growth phenomena in composite structures. *Composites Science and Technology*, **71 (6)**, 836-846.

[14] **Matthews, F. L., Davies, G. A. O., Hitchings, D., & Soutis, C.** 2000. *Finite element modelling of composite materials and structures*. Boca Raton, FL: CRC Press, 158-174.

[15] **Xie, D., & Biggers, S. B., Jr.** 2006. Strain Energy Release Rate calculation for a moving delamination front of arbitrary shape based on the virtual crack closure technique. Part I: formulation and validation. *Engineering Fracture Mechanics*, **73 (6)**, 771-785.

[16] **Xie, D., & Biggers, S. B., Jr.** 2006. Strain Energy Release Rate calculation for a moving delamination front of arbitrary shape based on the virtual crack closure technique. Part II: sensitivity study on modeling details. *Engineering Fracture Mechanics*, **73 (6)**, 786-801.

[17] **SIMULIA** 2010. *Abaqus 6.10 Online Documentation* [User's guide]. Providence, RI: Dassault Systèmes Simulia Corp.

[18] **Xie, D., & Biggers, S. B., Jr.** 2006. Progressive crack growth analysis using interface element based on the virtual crack closure technique. *Finite Elements in Analysis and Design*, **42 (11)**, 977-984.

[19] **Rybicki, E. F., & Kanninen, M. F.** 1977. A finite element calculation of stress intensity factors by a modified crack closure integral. *Engineering Fracture Mechanics*, **9**, 931-938.

[20] **Cherepanov, G. P.** 1967. The propagation of cracks in a continuous medium. *Journal of Applied Mathematics and Mechanics*, **31 (3)**, 503-512.

[21] **Rice, J. R.** 1968. A Path Independent Integral and the Approximate Analysis of Strain Concentration by Notches and Cracks. *Journal of Applied Mechanics*, **35**, 379-386.

[22] **Lonetti, P.** 2010. Dynamic propagation phenomena of multiple delaminations in composite structures. *Computational Materials Science*, **48 (3)**, 563-575.

[23] **Fernlund, G., McCammond, D., & Spelt, J. K.** 1994. Curvilinear formulation of the 3-D J integral: Application to delamination cracking of curved laminates. *Composite Structures*, **28 (2)**, 123-130.

[24] **Yan, X. Q., Du, S., & Duo, W.** 1991. J-Integral criterion of delamination onset in toughened matrix composite laminates. *Engineering Fracture Mechanics*, **40 (1)**, 67-74.

[25] **Chow, W. T., & Atluri, S. N.** 1997. Stress intensity factors as the fracture parameters for delamination crack growth in composite laminates. *Composites Part B: Engineering*, **28 (4)**, 375-384.

[26] **Lee, L. J., & Tu, D. W.** 1993. J integral for delaminated composite laminates. *Composites Science and Technology*, **47 (2)**, 185-192.

[27] **Bruno, D., & Greco, F.** 2000. An asymptotic analysis of delamination buckling and growth in layered plates. *International Journal of Solids and Structures*, **37 (43)**, 6239-6276.

[28] **Turon, A., Camanho, P. & Costa, J.** 2008. *Delamination in composites: simulation of delamination in composites under static and fatigue loading using cohesive zone models*. Saarbrücken: VDM Verlag Dr. Müller, 19-73.

[29] **Samimi, M., Van Dommelen, J. A. W., & Geers, M. G. D.** 2011. A self-adaptive finite element approach for simulation of mixed-mode delamination using cohesive zone models. *Engineering Fracture Mechanics*, **78 (10)**, 2202-2219.

[30] **Turon, A., Dávila, C. G., Camanho, P. P., & Costa, J.** 2007. An engineering solution for mesh size effects in the simulation of delamination using cohesive zone models. *Engineering Fracture Mechanics*, **74 (10)**, 1665-1682.

[31] **Turon, A., Camanho, P. P., Costa, J. & Renart, J.** 2010. Accurate simulation of delamination growth under mixed-mode loading using cohesive elements: Definition of interlaminar strengths and elastic stiffness. *Composite Structures*, **92 (8)**, 1857-1864.

[32] **Ye, Q., & Chen, P.** 2011. Prediction of the cohesive strength for numerically simulating composite delamination via CZM-based FEM. *Composites Part B: Engineering*, **42 (5)**, 1076-1083.

[33] **Borg, R., Nilsson, L., & Simonsson, K.** 2002. Modeling of delamination using a discretized cohesive zone and damage formulation. *Composites Science and Technology*, **62 (10-11)**, 1299-1314.

[34] **Balzani, C., & Wagner, W.** 2008. An interface element for the simulation of delamination in unidirectional fiber-reinforced composite laminates. *Engineering Fracture Mechanics*, **75 (9)**, 2597-2615.

[35] **ASTM** 1994. Standard test method for mode I interlaminar fracture toughness of unidirectional fibre-reinforced polymer matrix composites, D5528. *American Society for Testing and Materials International*, ASTM 1994.

[36] **ISO** 2001. Fibre-reinforced plastic composites - determination of mode I interlaminar fracture toughness, G_{I_c} , for unidirectionally reinforced materials, 15024. *International Organization for Standardization*, ISO 2001.

[37] **ASTM** 2006. Standard Test Method for Mixed Mode I-Mode II Interlaminar Fracture Toughness of Unidirectional Fiber Reinforced Polymer Matrix Composites, D6671. *American Society for Testing and Materials International*, ASTM 2006.

[38] **Brunner, A. J., Blackman, B. R. K., & Davies, P.** 2008. A status report on delamination resistance testing of polymer-matrix composites. *Engineering Fracture Mechanics*, **75**, 2779-2794.

[39] **Russell, A. J. & Street, K. N.** 1982. Factors affecting the interlaminar fracture of graphite/epoxy laminates. *Proceedings of the 4th International Conference on Composite Materials, Tokyo*, 279-286.

[40] **Kageyama, K., Kikuchi, M. & Yanagisawa, N.** 1991. Stabilized end notched flexure test: characterization of mode II interlaminar crack growth, in

Composite Materials: Fatigue and Fracture, 3rd Volume, STP1110. American Society for Testing and Materials, 210-225.

[41] **Martin, R. & Davidson, B. D.** 1997. Mode II fracture toughness evaluation using a four point bend end notch flexure test. *Proceedings 4th International Conference on Deformation and Fracture of Composites, Manchester*, 243-252.

[42] **Jordan, W. M. & Bradley, W. L.** 1987. Micromechanisms of fracture in toughened graphite/epoxy laminates, in *Toughened Composites*, STP937. American Society for Testing and Materials, 95-114.

[43] **O'Brien, T. K.** 1998. Composite interlaminar shear fracture toughness, G_{II_c}: Shear measurement or shear myth?, *in Composite Materials: Fatigue and Fracture, 7th Volume*, STP1330. American Society for Testing and Materials, 3-18.

[44] **Moore, D. R., Pavan, A., Williams, J. G.** (Eds.). 2001. *Fracture mechanics testing methods for polymers, adhesives and composites*. Amsterdam: ESIS Publication, 317-334.

[45] **Kaw, A. K.** 2006. *Mechanics of composite materials* (2nd ed.). Boca Raton, FL: CRC Press, 160-166.

[46] **Babu, P. R. & Pradhan, B.** 2007. Effect of damage levels and curing stresses on delamination growth behaviour emanating from circular holes in laminated FRP composites. *Composites: Part A*, **38**, 2412-2421.

[47] **Hocheng, H. & Tsao, C. C.** 2006. Effects of special drill bits on drilling-induced delamination of composite materials. *Machine Tools & Manufacture*, **46**, 1403-1416.

[48] **Sridharan, S.** (Ed.). 2008. *Delamination behaviour of composites*. Boca Raton, FL: CRC Press, 32-35.

[49] **Chakraborty, D.** 2007. Delamination of laminated fiber reinforced plastic composites under multiple cylindrical impact. *Material and Design*, **28**, 1142-1153.

[50] **Olsson, R.** 2010. Analytical model for delamination growth during small mass impact on plates. *International Journal of Solids and Structures*, **47**, 2884-2892.

[51] **Broek, D.** 1982. *Elementary engineering fracture mechanics* (3rd ed.). Dordrecht: Martinus Nijhoff Publishers, 8-9.

[52] **Newman, J. C., Jr.** 2000. Irwin's stress-intensity factor - a historical perspective, in *Fatigue and Fracture Mechanics, 31st Volume*, STP1389. American Society for Testing and Materials, 39-53.

[53] **Irwin, G. R.** 1956. Relation of Stresses near a Crack to the Crack Extension Force. *Proceedings of the 9th International Congress on Applied Mechanics, Brussels*, 245-251.

[54] **Broek, D.** 1982. *Elementary engineering fracture mechanics* (3rd ed.). Dordrecht: Martinus Nijhoff Publishers, 67-89.

[55] **MSC Software** 2010. *MD/MSC Nastran 2010 Online Documentation* [User's guide]. Santa Ana, CA: MSC Software Corp.

[56] **Tay, T. E.** 2003. Characterization and analysis of delamination fracture in composites: An overview of developments from 1990 to 2001. *Applied Mechanics Reviews*, **56 (1)**.

[57] **Ye, L.** 1988. Role of matrix resin in delamination onset and growth in composite laminates. *Composite Science and Technology*, **33**, 257-277.

[58] **Wu, E. M. & Reuter, R. C. Jr.** 1965. Crack Extension in Fiberglass Reinforced Plastics. *T&AM Report No.* ***275***. Department of Theoretical and Applied Mechanics, University of Illinois, Urbana, IL, February 1965.

[59] **NASA** 1982. Standard test method for mode I interlaminar fracture toughness of unidirectional fibre-reinforced polymer matrix composites, NASA RP-1092. *National Aeronautics and Space Administration*, NASA 1982.

[60] **Moore, D. R., Pavan, A., Williams, J. G.** (Eds.). 2001. *Fracture mechanics testing methods for polymers, adhesives and composites*. Amsterdam: ESIS Publication, 271-275.

[61] **Sridharan, S.** (Ed.). 2008. *Delamination behaviour of composites*. Boca Raton, FL: CRC Press, 65-86.

[62] **Blackman, B. R. K., Brunner, A. J. & Williams, J. G.** 2006. Mode II Fracture testing of composites: a new look at an old problem. *Engineering Fracture Mechanics*, **73**, 2443-2455.

[63] **Dost Kimya** 2011. *3M2 Karbon Fiber Kumaş 300 gr/m^2 UD 12K* [Product information]. İstanbul: Dost Kimya Endüstri Hammadde Sanayi ve Ticaret Ltl. Şti.

[64] **Hexion** 2006. *Laminating resin MGS® L 285* [Product information]. Columbus: Hexion Specialty Chemicals Inc.

[65] **Oras Polimer Plastik** 2011. *PTFE Teflon® Filmler* [Product information]. İstanbul: Oras Polimer Plastik ve Dahili Ticaret Ltd. Şti.

[66] **Heatcon** 2007. *Heated Vacuum Curing Table HCS7500-06-321212* [Operations manual]. Seattle: Heatcon Composite Systems.

[67] **Bosch** 2009. *GGS 27C Professional Die Grinder* [Product Information]. Stuttgart: Robert Bosch GmbH.

[68] **ISO** 2002. Rubber and plastics test equipment - tensile, flexural and compression types, ISO 5893:2002. *International Organization for Standardization*, ISO 2002.

[69] **MTS** 2004. *MTS 322* [System Reference Documentation]. Minneapolis: MTS Systems Corporation.

[70] **ISO** 2008. Plastics – standard atmospheres for conditioning and testing, ISO 291:2008. *International Organization for Standardization*, ISO 2008.

[71] **SAMTECH** 2011. *SAMCEF Field V8.1 Documentation* [User's guide]. Liège: Samtech Group.

[72] **Kaw, A. K.** 2006. *Mechanics of composite materials* (2nd ed.). Boca Raton, FL: CRC Press, 203-313.

[73] **ISO** 1998. Fibre-reinforced plastic composites – Determination of flexural properties, ISO 14125:1998. *International Organization for Standardization*, ISO 1998.

APPENDICES

Appendix A : Detailed dimensioning of plates

Appendix B : Specimen measurements

Appendix C : MTS 322 test machine

Appendix D : Load-displacement curves

Appendix E : Calculation process for experimental results

APPENDIX A

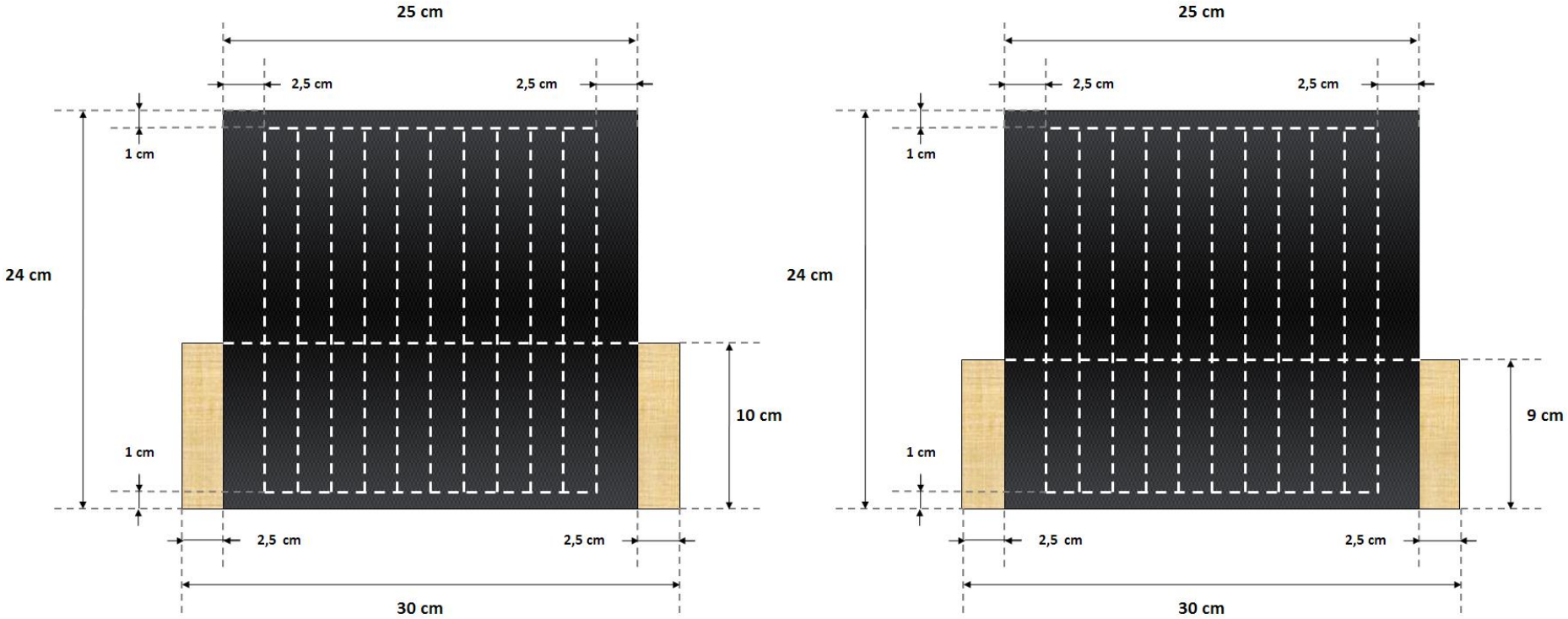

Figure A.1 : Drawings of the designed composite plates

APPENDIX B

Table B.1 : Detailed measurements of specimens with starter film insert (i-specimens)

Specimen code	Length (mm)	Mass (g)		Width and thickness measurements (mm)							Initial delamination	
				start	start 10	1 quarter	half	3 quarter	end 10	end	right	left
i1	220	32	*B*	20,52	20,80	21,08	21,28	21,56	21,84	21,62	88	88
			2h	4,45	4,67	4,85	4,87	4,59	4,42	4,17		
i2	221	30	*B*	20,50	20,70	20,30	19,78	19,80	19,84	19,90	89	89
			2h	4,16	4,51	4,87	4,98	4,67	4,26	3,98		
i3	220	28	*B*	19,00	19,22	19,42	19,94	20,00	20,12	20,16	89	89
			2h	4,09	4,50	4,79	4,88	4,58	4,05	3,88		
i4	221	28	*B*	19,22	19,86	19,96	20,06	20,20	20,90	21,30	89	89
			2h	3,96	4,23	4,66	4,76	4,46	3,90	3,62		
i5	220	28	*B*	20,00	20,50	20,40	20,40	20,18	19,84	19,82	89	89
			2h	3,85	4,04	4,55	4,63	4,32	3,73	3,53		
i6	219	28	*B*	20,52	20,70	20,54	19,90	20,86	20,50	20,72	89	89
			2h	3,83	4,05	4,48	4,55	4,23	3,81	3,54		
i7	219	26	*B*	19,14	19,82	19,56	19,60	19,10	20,24	20,44	89	89
			2h	3,75	3,89	4,30	4,29	4,09	3,70	3,52		
i8	218	26	*B*	18,86	19,08	19,48	20,14	20,50	20,58	20,48	90	90
			2h	3,73	3,90	4,24	4,17	4,03	3,73	3,55		
i9	218	26	*B*	20,32	20,10	20,38	19,56	19,66	19,88	20,00	90	90
			2h	3,71	3,92	4,15	4,01	3,83	3,63	3,52		
i10	218	24	*B*	20,12	20,68	20,40	20,24	19,90	19,88	19,70	90	90
			2h	3,68	3,84	4,12	3,91	3,85	3,69	3,52		

Table B.2 : Detailed measurements of specimens with mode I precrack (p-specimens)

Specimen code	Length (mm)	Mass (g)		Width and thickness measurements (mm)							initial delamination	
				start	start 10	1 quarter	half	3 quarter	end 10	end	right	left
$p1$	219	28	B	19,80	19,66	19,76	19,36	19,62	19,64	19,72	78	77
			$2h$	4,45	4,66	4,83	4,90	4,73	4,34	4,12		
$p2$	219	30	B	19,54	20,00	20,38	20,50	20,40	20,60	20,78	78	78
			$2h$	4,19	4,43	4,76	4,85	4,75	4,31	4,02		
$p3$	218	28	B	19,58	19,92	19,66	19,62	19,48	19,56	19,60	79	78
			$2h$	4,02	4,31	4,78	4,92	4,73	4,17	3,93		
$p4$	219	28	B	19,66	20,50	20,46	20,72	20,30	20,48	20,36	79	78
			$2h$	3,74	4,10	4,62	4,80	4,56	4,04	3,85		
$p5$	219	28	B	19,94	20,42	20,36	19,92	19,52	19,98	20,00	79	79
			$2h$	3,66	3,88	4,48	4,72	4,44	3,90	3,74		
$p6$	219	28	B	20,20	20,34	20,50	20,20	20,40	20,34	20,44	80	80
			$2h$	3,61	3,91	4,36	4,51	4,47	3,85	3,65		
$p7$	219	26	B	19,46	20,14	19,90	20,20	19,92	20,30	20,42	80	80
			$2h$	3,59	3,89	4,32	4,32	4,24	3,82	3,66		
$p8$	219	26	B	19,12	19,80	20,00	19,80	19,74	19,96	20,56	81	81
			$2h$	3,61	3,84	4,23	4,24	4,15	3,76	3,59		
$p9$	219	26	B	19,90	20,06	19,86	19,90	20,10	20,28	20,10	81	81
			$2h$	3,58	3,80	4,10	4,10	3,95	3,82	3,62		
$p10$	219	24	B	19,50	19,82	19,90	20,00	19,62	20,00	20,08	81	81
			$2h$	3,54	3,78	3,94	3,98	3,90	3,75	3,58		

APPENDIX C

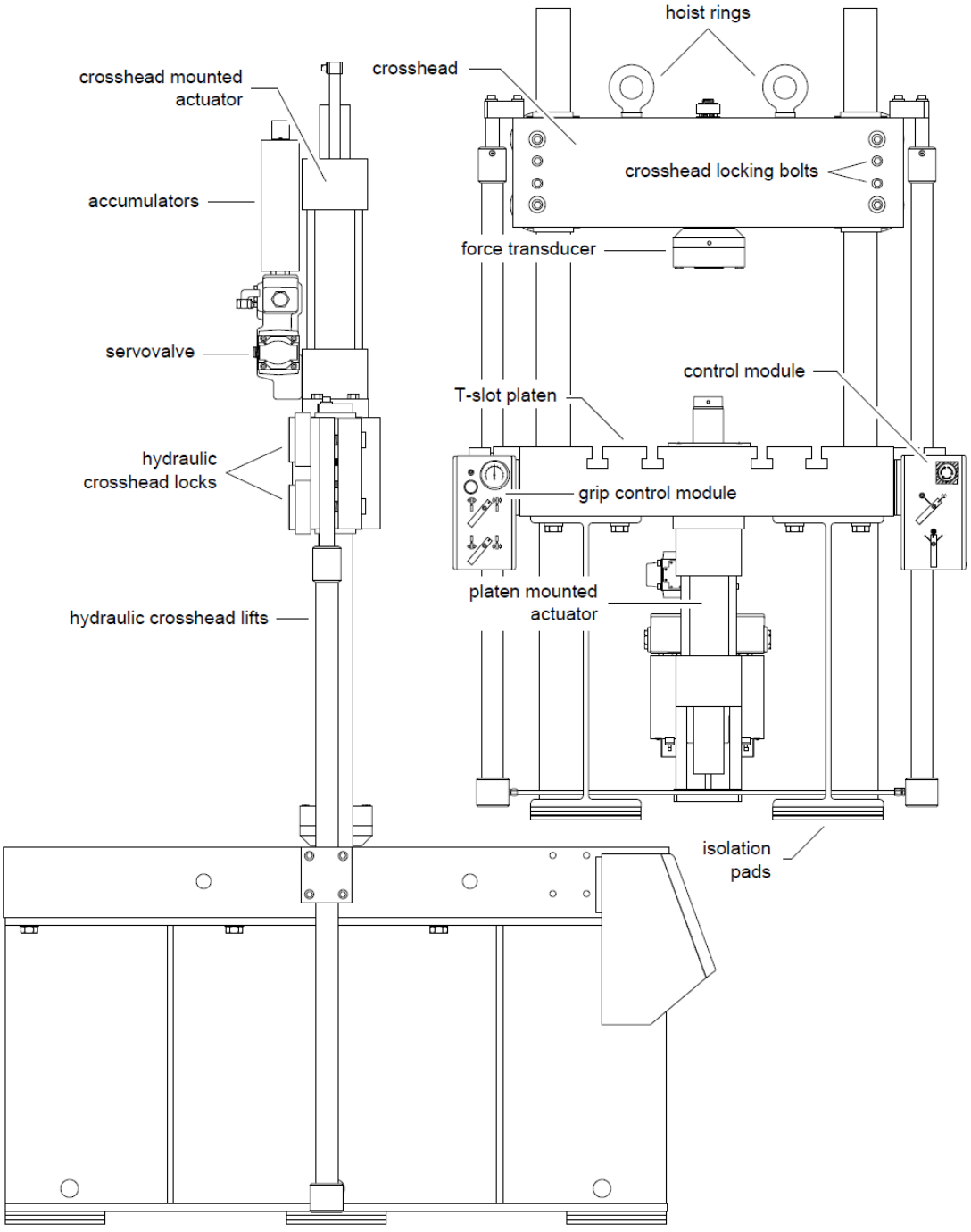

Figure C.1 : Major components of the load cell of MTS 322 test machine [69]

APPENDIX D

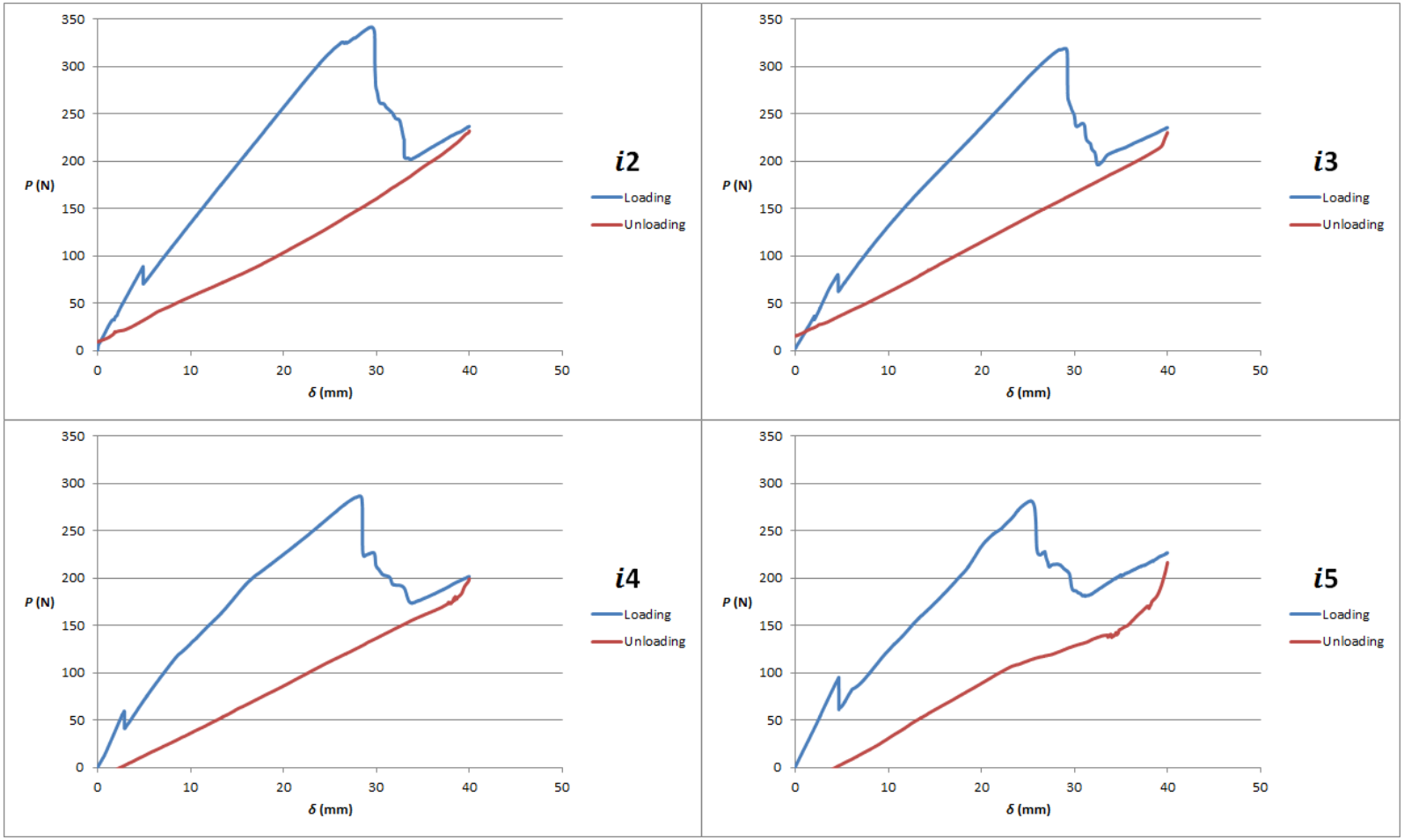

Figure D.1 : Load-displacement curves of *i*2, *i*3, *i*4 and *i*5 specimen

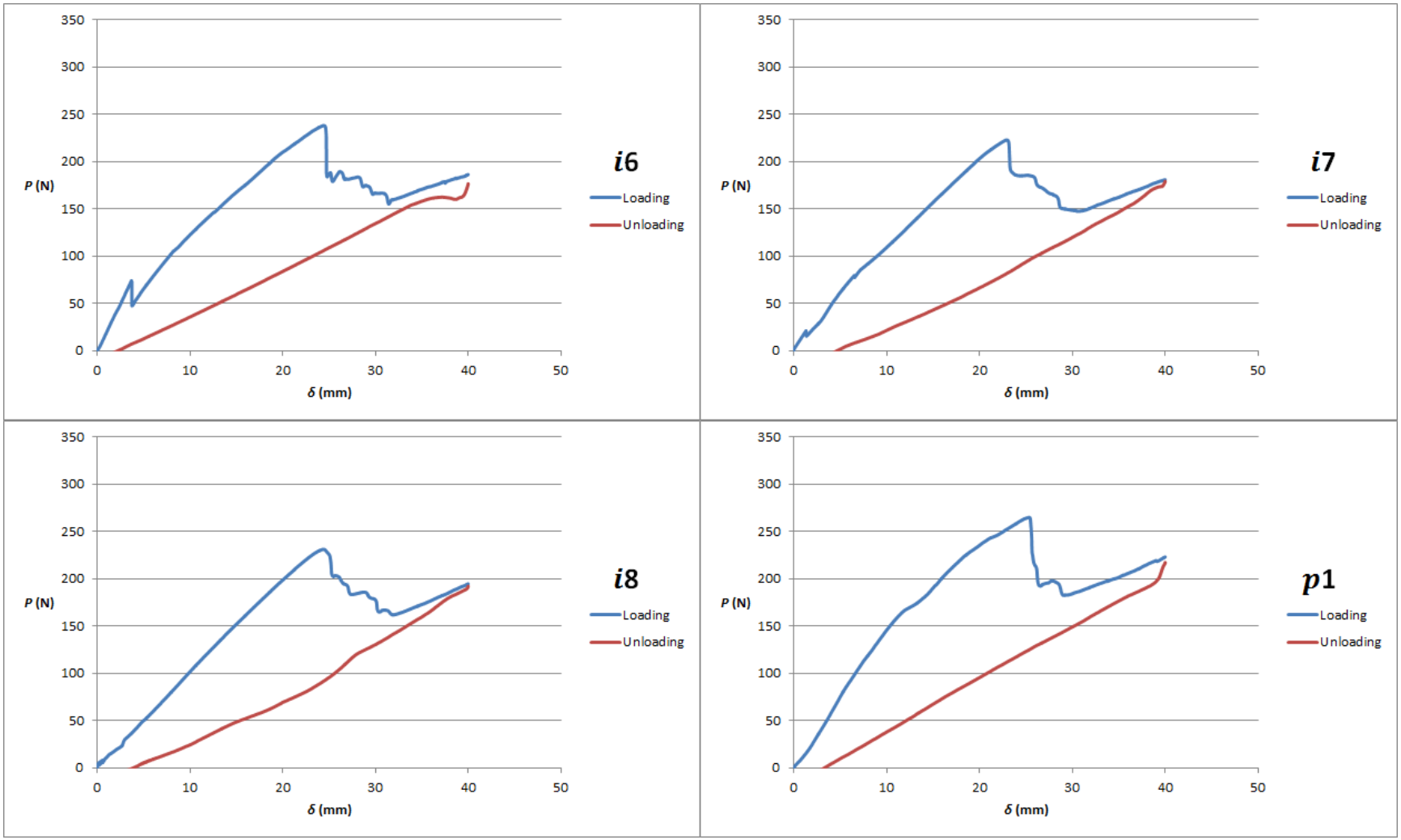

Figure D.2 : Load-displacement curves of $i6$, $i7$, $i8$ and $p1$ specimens

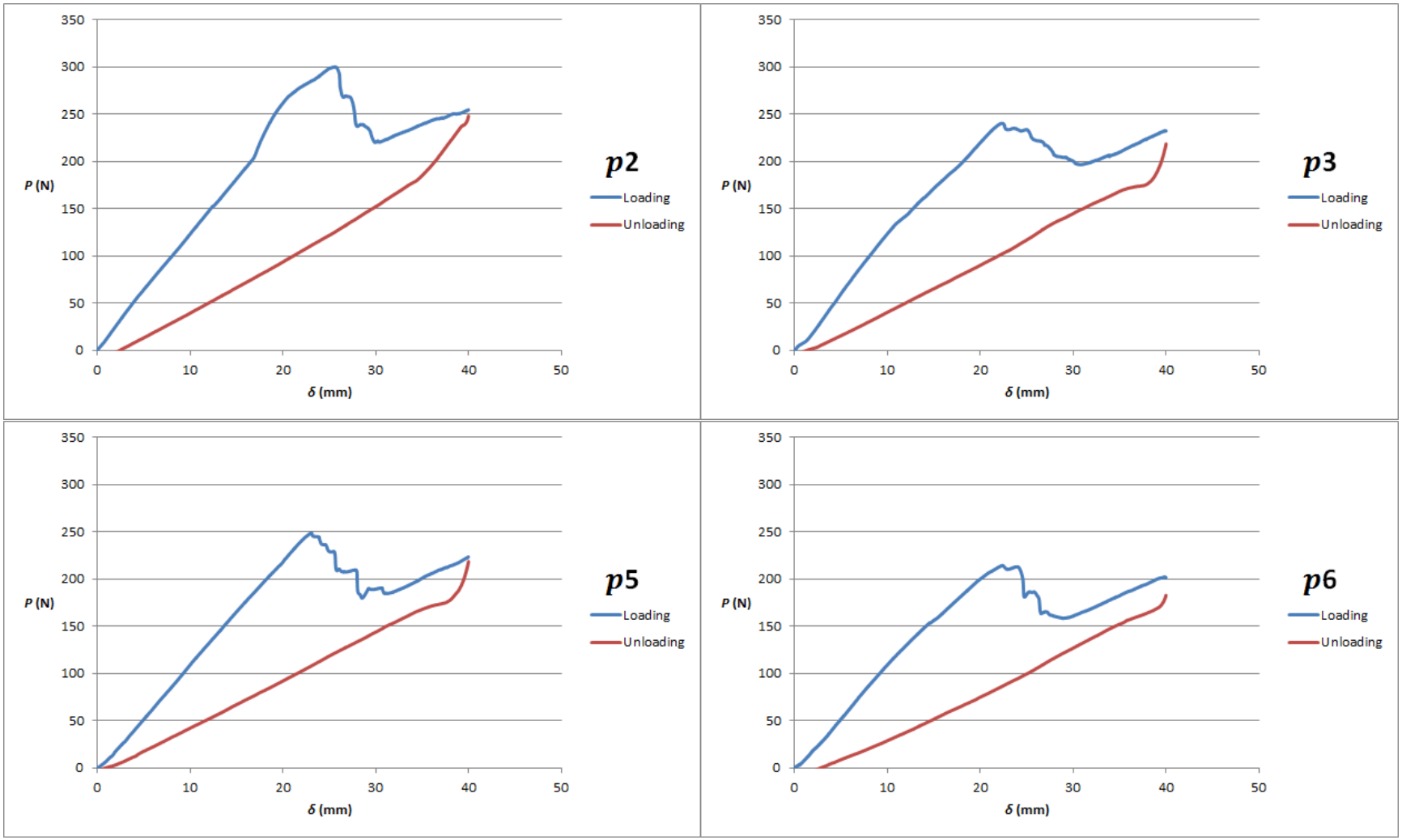

Figure D.3 : Load-displacement curves of $p2$, $p3$, $p5$ and $p6$ specimens

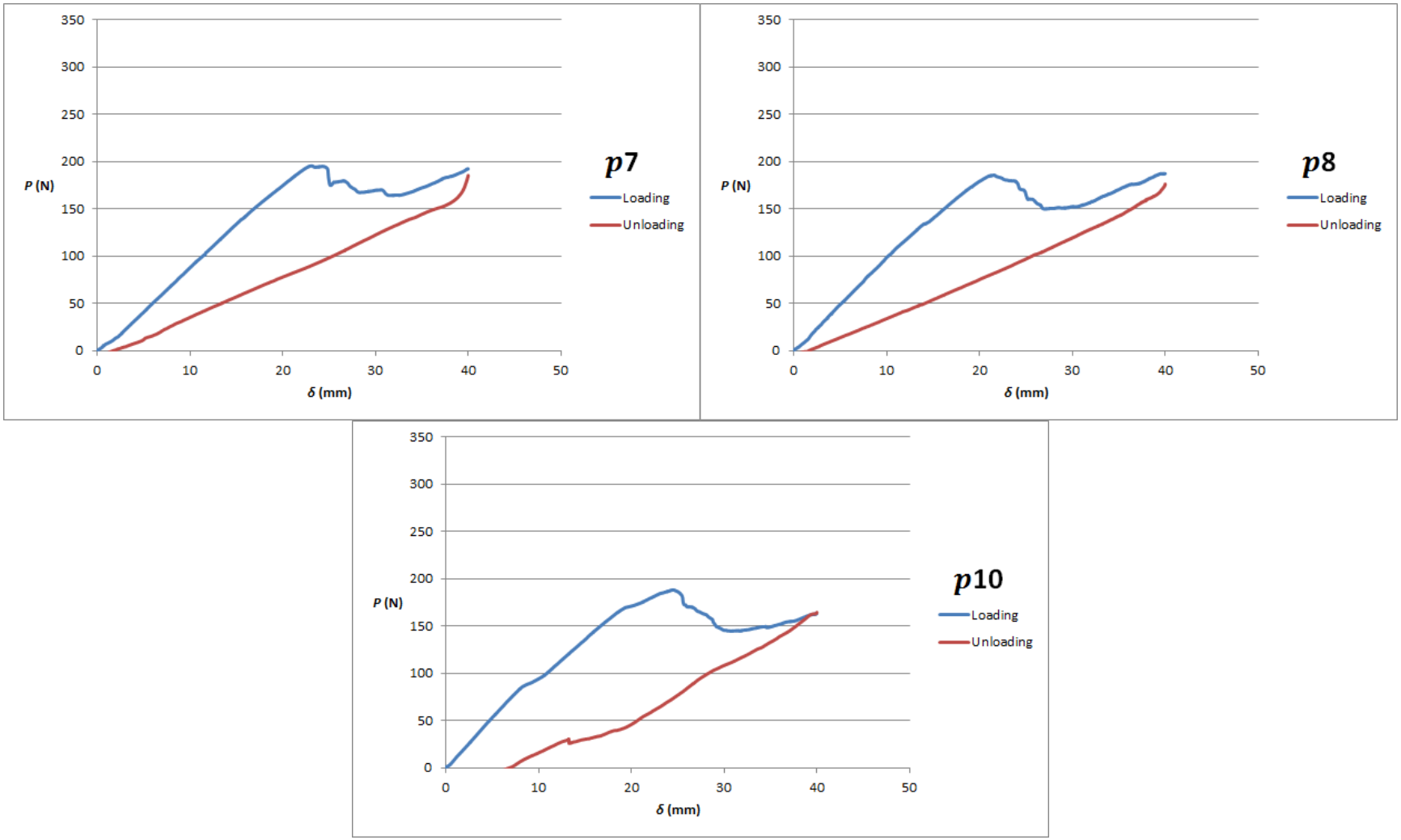

Figure D.4 : Load-displacement curves of $p7$, $p8$, $p10$

APPENDIX E

Table E.1 : Parameter values of $i4$ specimen used in calculation process

Parameter	B	h	I_1	E	m
Value	20,2143	2,1136	17,1136	139,05	53,83E-9
Unit		mm		GPa	1/(N.mm^2)

Table E.2 : Calculation process for $i4$ specimen

Crit. Points	t	δ	P	a	a^3	C	θ_1	θ_2	$G_{\mathrm{II}_c(CBT)}$		$G_{\mathrm{II}_c(ECM)}$	
									-	corr.	-	corr.
NL	389,190	15,563	189,170	80,0	5,12E+05	0,0870	2,2928	-6,4002	961	1021	915	972
MAX	706,690	28,263	286,839	80,0	5,12E+05	0,0986	2,2928	-6,4002	2208	2362	2103	2249
VIS	713,692	28,543	227,781	80,0	5,12E+05	0,1254	2,2928	-6,4002	1393	1489	1326	1418
$PROP$	713,995	28,555	226,478	83,2	5,75E+05	0,1261	2,2306	-6,1204	1488	1584	1417	1508
$PROP$	714,698	28,583	224,921	91,3	7,60E+05	0,1271	2,0607	-5,4603	1767	1863	1683	1774
$PROP$	716,896	28,671	223,455	95,3	8,65E+05	0,1284	1,9729	-5,1590	1902	1997	1811	1901
$PROP$	725,899	29,030	225,007	97,7	9,32E+05	0,1291	1,9209	-4,9896	2026	2121	1929	2020
$PROP$	738,897	29,550	226,936	98,9	9,69E+05	0,1303	1,8931	-4,9013	2114	2210	2013	2105
$PROP$	753,897	30,150	210,526	99,5	9,84E+05	0,1433	1,8818	-4,8658	1839	1919	1751	1828
$PROP$	760,899	30,431	207,010	104,1	1,13E+06	0,1471	1,7810	-4,5590	1948	2025	1855	1929
$PROP$	762,892	30,509	205,940	108,6	1,28E+06	0,1482	1,6855	-4,2820	2098	2175	1998	2071
$PROP$	767,892	30,710	203,824	110,5	1,35E+06	0,1507	1,6469	-4,1731	2126	2200	2024	2095
$PROP$	768,897	30,750	203,603	111,5	1,39E+06	0,1511	1,6257	-4,1141	2161	2235	2058	2129
$PROP$	770,899	30,830	203,162	112,3	1,42E+06	0,1518	1,6087	-4,0670	2184	2258	2080	2150
$PROP$	817,999	32,714	191,988	113,2	1,45E+06	0,1705	1,5912	-4,0190	1980	2040	1886	1942
$PROP$	834,991	33,394	178,390	118,5	1,67E+06	0,1873	1,4859	-3,7348	1875	1924	1786	1832
$PROP$	835,997	33,434	177,274	121,4	1,79E+06	0,1887	1,4324	-3,5937	1942	1990	1849	1895
$PROP$	837,999	33,514	175,786	122,6	1,84E+06	0,1908	1,4098	-3,5347	1948	1995	1855	1900
$PROP$	838,995	33,554	175,135	124,6	1,93E+06	0,1917	1,3736	-3,4408	1997	2044	1902	1947
Unit	s	mm	N	mm	mm^3	mm/N	-		J/m^2			

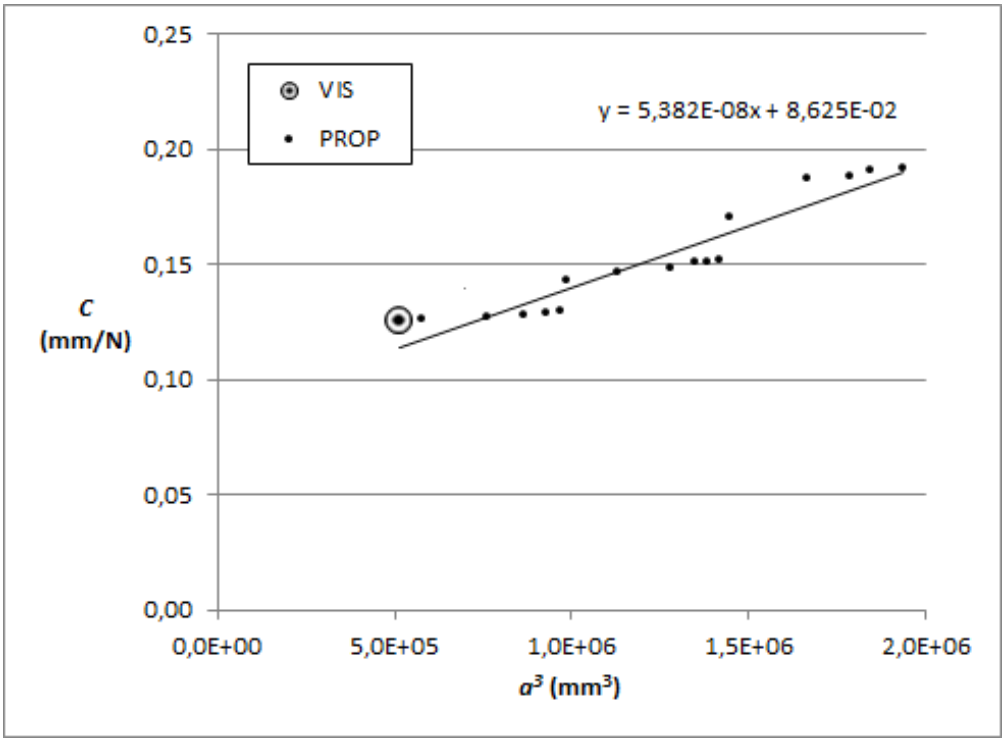

Figure E.1 : Calculation of m for $i4$ specimen

Table E.3 : Parameter values of $i6$ specimen used in calculation process

Parameter	B	h	I_1	E	m
Value	20,5343	2,0350	17,0350	139,05	35,25E-9
Unit		mm		GPa	1/(N.mm^2)

Table E.4 : Calculation process for $i6$ specimen

Crit. Points	t	δ	P	a	a^3	C	θ_1	θ_2	$G_{\mathrm{II}_c(CBT)}$		$G_{\mathrm{II}_c(ECM)}$	
									-	corr.	-	corr.
NL	205,392	8,213	105,107	80,0	5,12E+05	0,0882	2,2928	-6,4002	322	335	182	189
MAX	610,997	24,437	238,253	80,0	5,12E+05	0,1030	2,2928	-6,4002	1654	1772	935	1002
VIS	615,694	24,626	236,275	80,0	5,12E+05	0,1047	2,2928	-6,4002	1627	1743	920	985
$PROP$	616,495	24,657	234,296	82,6	5,63E+05	0,1057	2,2424	-6,1715	1705	1820	964	1029
$PROP$	617,491	24,697	228,015	85,6	6,27E+05	0,1088	2,1811	-5,9147	1735	1845	981	1043
$PROP$	618,497	24,737	186,715	87,7	6,73E+05	0,1333	2,1381	-5,7456	1220	1294	690	732
$PROP$	620,499	24,817	184,182	89,0	7,06E+05	0,1356	2,1085	-5,6340	1225	1298	693	734
$PROP$	624,591	24,981	186,424	93,6	8,19E+05	0,1348	2,0107	-5,2860	1386	1461	784	826
$PROP$	627,491	25,098	188,026	98,2	9,48E+05	0,1343	1,9087	-4,9504	1553	1631	878	922
$PROP$	630,597	25,222	186,371	99,3	9,80E+05	0,1361	1,8847	-4,8747	1560	1637	882	926
$PROP$	631,593	25,262	183,287	101,1	1,03E+06	0,1387	1,8467	-4,7569	1563	1637	884	926
$PROP$	632,599	25,302	180,828	103,9	1,12E+06	0,1408	1,7859	-4,5734	1607	1680	909	950
$PROP$	633,595	25,342	179,515	105,4	1,17E+06	0,1420	1,7536	-4,4783	1630	1702	921	962
$PROP$	669,591	26,783	181,697	108,5	1,28E+06	0,1483	1,6883	-4,2901	1769	1841	1000	1041
$PROP$	685,597	27,422	182,270	111,4	1,38E+06	0,1514	1,6282	-4,1209	1876	1948	1061	1102
$PROP$	694,591	27,781	183,014	114,4	1,50E+06	0,1527	1,5677	-3,9546	1994	2067	1128	1169
$PROP$	700,597	28,022	183,675	121,4	1,79E+06	0,1535	1,4314	-3,5909	2265	2339	1281	1322
$PROP$	710,597	28,423	180,833	122,8	1,85E+06	0,1581	1,4068	-3,5268	2244	2314	1269	1309
Unit	s	mm	N	mm	mm^3	mm/N	-		J/m^2			

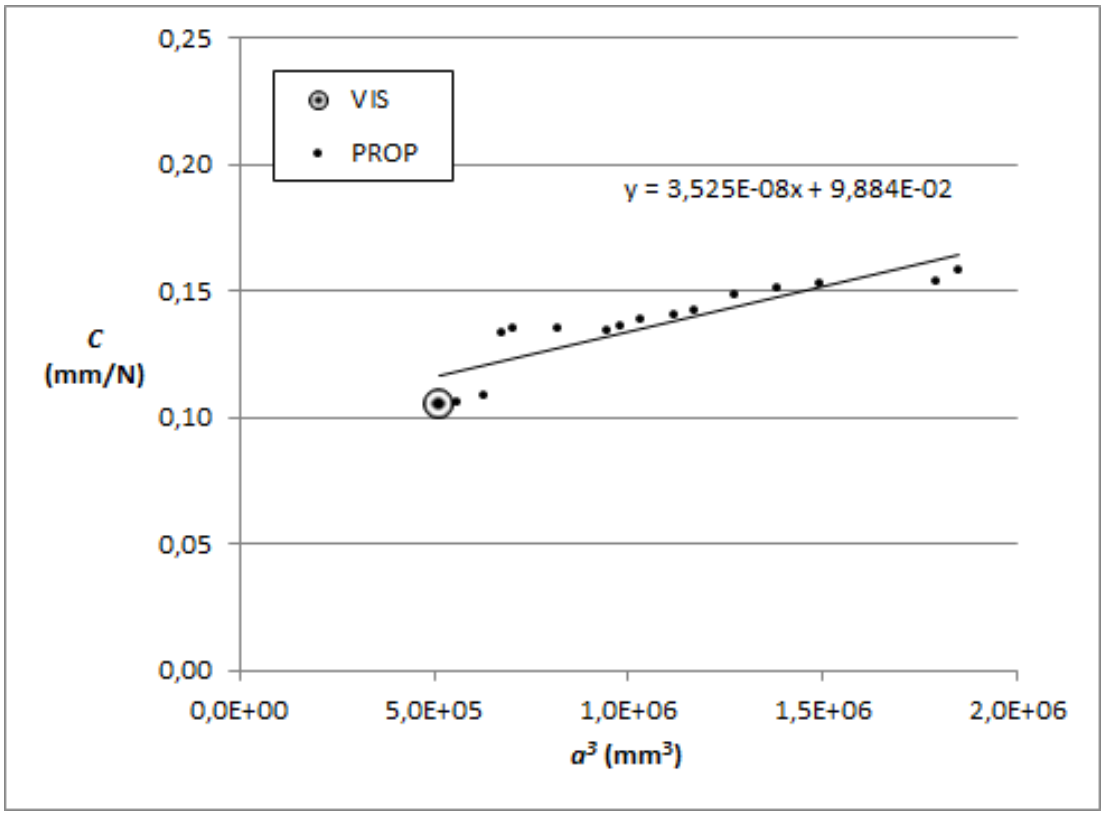

Figure E.2 : Calculation of m for $i6$ specimen

Table E.5 : Parameter values of $i7$ specimen used in calculation process

Parameter	B	h	I_1	E	m
Value	19,7000	1,9671	16,9671	139,05	17,92E-9
Unit		mm		GPa	1/(N.mm^2)

Table E.6 : Calculation process for $i7$ specimen

Crit. Points	t	δ	P	a	a^3	C	θ_1	θ_2	$G_{\mathrm{II}_c(CBT)}$		$G_{\mathrm{II}_c(ECM)}$	
									-	corr.	-	corr.
NL	181,593	7,260	86,253	80,0	5,12E+05	0,0839	2,2928	-6,4002	261	270	65	67
MAX	573,399	22,934	222,964	80,0	5,12E+05	0,1029	2,2928	-6,4002	1743	1866	434	465
VIS	583,995	23,357	190,956	80,0	5,12E+05	0,1223	2,2928	-6,4002	1278	1369	318	341
$PROP$	584,591	23,381	190,487	84,1	5,94E+05	0,1228	2,2128	-6,0447	1404	1496	350	373
$PROP$	585,196	23,405	189,938	88,0	6,83E+05	0,1232	2,1297	-5,7138	1532	1625	382	405
$PROP$	586,192	23,445	189,501	89,9	7,27E+05	0,1237	2,0900	-5,5658	1590	1683	396	419
$PROP$	588,292	23,529	188,722	92,0	7,79E+05	0,1247	2,0450	-5,4047	1651	1744	411	434
$PROP$	590,294	23,609	187,967	95,3	8,65E+05	0,1256	1,9729	-5,1589	1758	1851	438	461
$PROP$	600,294	24,010	185,527	98,0	9,42E+05	0,1294	1,9132	-4,9649	1812	1903	451	474
$PROP$	602,296	24,089	185,422	99,3	9,80E+05	0,1299	1,8844	-4,8739	1858	1950	463	486
$PROP$	609,298	24,369	185,003	101,2	1,04E+06	0,1317	1,8443	-4,7497	1919	2011	478	501
$PROP$	616,300	24,649	185,054	101,9	1,06E+06	0,1332	1,8287	-4,7020	1948	2039	485	508
$PROP$	625,294	25,009	185,596	105,7	1,18E+06	0,1348	1,7460	-4,4560	2110	2202	525	549
$PROP$	627,296	25,089	185,752	106,9	1,22E+06	0,1351	1,7222	-4,3871	2158	2251	538	561
$PROP$	629,298	25,169	185,706	112,3	1,42E+06	0,1355	1,6086	-4,0668	2383	2477	594	617
$PROP$	632,296	25,289	185,556	113,2	1,45E+06	0,1363	1,5906	-4,0171	2417	2511	602	626
$PROP$	636,300	25,448	185,222	113,3	1,46E+06	0,1374	1,5881	-4,0104	2414	2507	601	624
$PROP$	644,298	25,769	184,450	115,3	1,53E+06	0,1397	1,5489	-3,9036	2477	2570	617	640
$PROP$	645,294	25,809	184,160	116,8	1,59E+06	0,1402	1,5200	-3,8257	2533	2625	631	654
$PROP$	646,300	25,849	183,998	117,8	1,64E+06	0,1405	1,4996	-3,7711	2574	2667	641	664
$PROP$	648,292	25,928	183,243	122,4	1,83E+06	0,1415	1,4135	-3,5442	2756	2848	686	709
$PROP$	650,294	26,009	181,897	122,8	1,85E+06	0,1430	1,4056	-3,5236	2734	2825	681	704
$PROP$	661,300	26,449	173,551	124,4	1,92E+06	0,1524	1,3776	-3,4509	2553	2635	636	656
Unit	s	mm	N	mm	mm^3	mm/N	-		J/m^2			

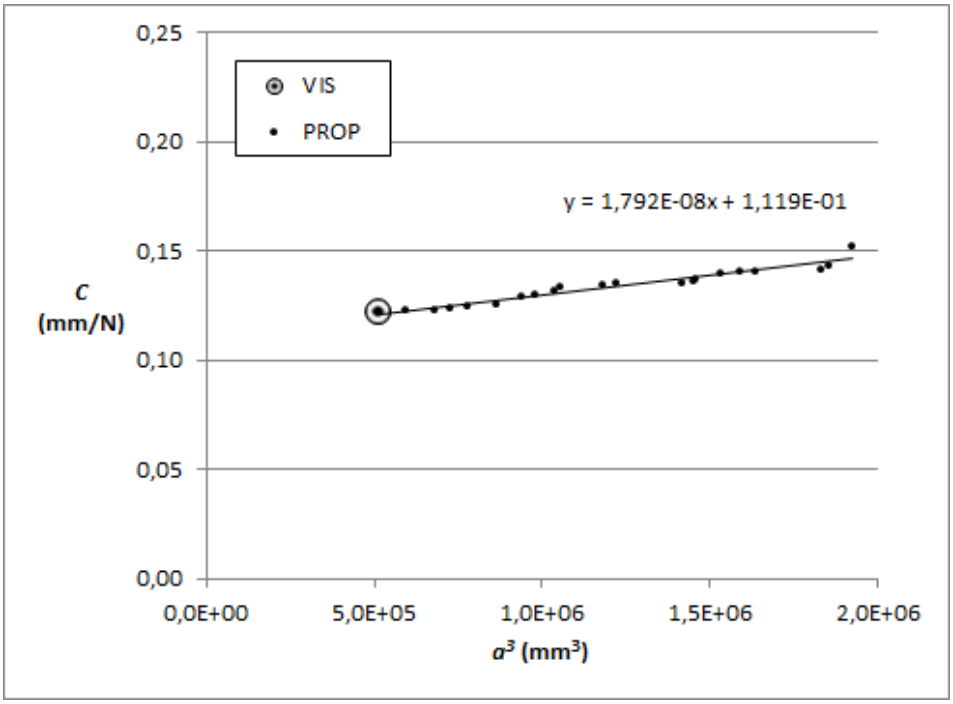

Figure E.3 : Calculation of m for $i7$ specimen

Table E.7 : Parameter values of $p1$ specimen used in calculation process

Parameter	B	h	I_1	E	m
Value	19,6514	2,2879	17,2879	138,67	32,01E-9
Unit		mm		GPa	1/(N.mm^2)

Table E.8 : Calculation process for $p1$ specimen

Crit. Points	t	δ	P	a	a^3	C	θ_1	θ_2	$G_{\mathrm{II}_c(CBT)}$		$G_{\mathrm{II}_c(ECM)}$	
									-	corr.	-	corr.
NL	293,399	11,732	164,938	80,0	5,12E+05	0,0677	2,2928	-6,4002	611	644	425	448
MAX	634,093	25,361	265,060	80,0	5,12E+05	0,0957	2,2928	-6,4002	1578	1693	1099	1179
VIS	637,394	25,493	262,822	80,0	5,12E+05	0,0970	2,2928	-6,4002	1551	1664	1080	1159
$PROP$	637,794	25,509	260,899	83,1	5,74E+05	0,0978	2,2316	-6,1248	1650	1763	1149	1228
$PROP$	637,999	25,518	259,750	84,1	5,94E+05	0,0982	2,2124	-6,0432	1673	1786	1165	1244
$PROP$	638,399	25,534	257,679	85,7	6,30E+05	0,0991	2,1784	-5,9037	1712	1824	1192	1270
$PROP$	638,995	25,557	254,659	86,9	6,56E+05	0,1003	2,1538	-5,8066	1718	1828	1197	1273
$PROP$	639,493	25,577	251,773	88,3	6,89E+05	0,1016	2,1242	-5,6928	1734	1842	1208	1283
$PROP$	639,796	25,589	249,731	94,3	8,38E+05	0,1024	1,9950	-5,2327	1945	2053	1355	1430
$PROP$	640,196	25,605	246,946	96,3	8,94E+05	0,1037	1,9504	-5,0848	1985	2091	1383	1456
$PROP$	641,300	25,649	232,713	101,9	1,06E+06	0,1102	1,8287	-4,7022	1973	2068	1374	1440
$PROP$	643,292	25,729	224,935	103,9	1,12E+06	0,1144	1,7857	-4,5731	1916	2005	1334	1396
$PROP$	646,300	25,850	217,368	104,9	1,15E+06	0,1189	1,7641	-4,5092	1824	1907	1270	1328
$PROP$	647,296	25,890	216,039	108,3	1,27E+06	0,1198	1,6922	-4,3011	1920	2003	1337	1395
$PROP$	651,300	26,050	213,376	111,7	1,39E+06	0,1221	1,6221	-4,1042	1992	2073	1387	1444
$PROP$	653,292	26,130	211,850	112,3	1,42E+06	0,1233	1,6091	-4,0680	1986	2066	1383	1439
$PROP$	657,296	26,290	196,944	114,8	1,51E+06	0,1335	1,5584	-3,9293	1794	1864	1249	1298
$PROP$	664,298	26,570	192,416	120,7	1,76E+06	0,1381	1,4454	-3,6277	1892	1959	1317	1364
$PROP$	670,294	26,810	194,184	123,4	1,88E+06	0,1380	1,3946	-3,4950	2016	2084	1404	1451
$PROP$	677,296	27,090	195,033	124,3	1,92E+06	0,1389	1,3784	-3,4530	2063	2132	1437	1485
$PROP$	681,300	27,250	195,550	125,0	1,95E+06	0,1393	1,3666	-3,4225	2096	2165	1460	1508
Unit	s	mm	N	mm	mm^3	mm/N	-		J/m^2			

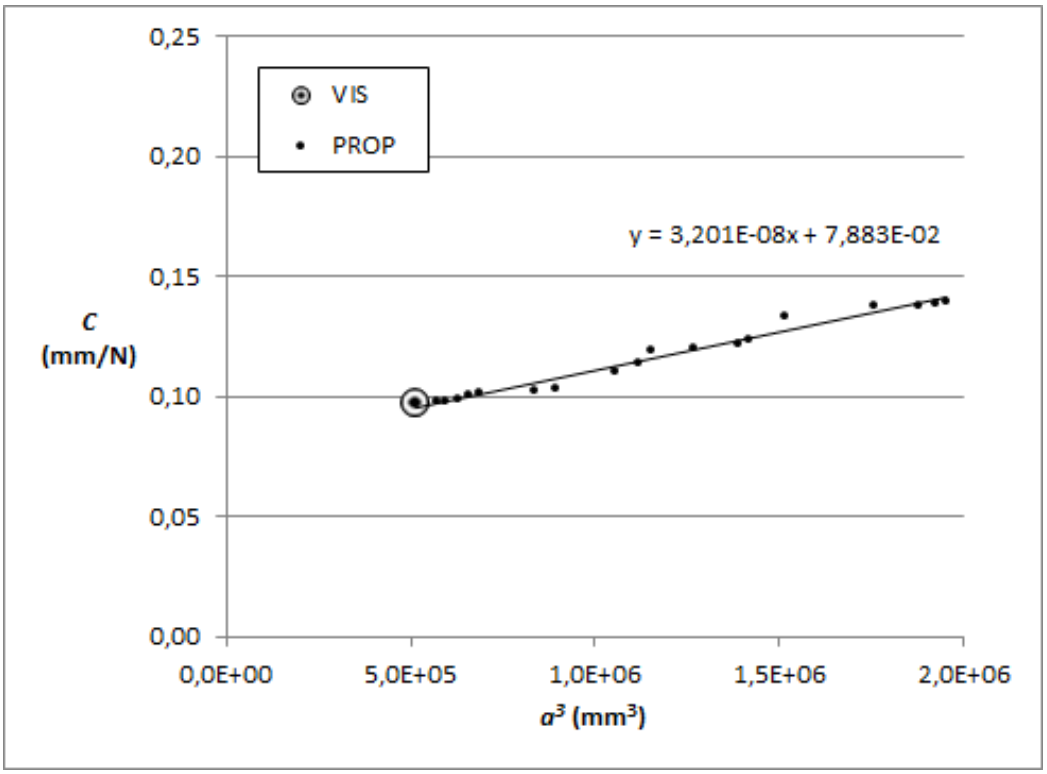

Figure E.4 : Calculation of m for $p1$ specimen

Table E.9 : Parameter values of $p3$ specimen used in calculation process

Parameter	B	h	I_1	E	m
Value	19,5029	2,0950	17,0950	138,67	48,74E-9
Unit		mm		GPa	1/(N.mm^2)

Table E.10 : Calculation process for $p3$ specimen

Crit. Points	t	δ	P	a	a^3	C	θ_1	θ_2	$G_{\mathrm{II}_c(CBT)}$		$G_{\mathrm{II}_c(ECM)}$	
									-	corr.	-	corr.
NL	271,298	10,850	133,159	80,0	5,12E+05	0,0777	2,2928	-6,4002	526	553	425	447
MAX	558,300	22,334	240,464	80,0	5,12E+05	0,0929	2,2928	-6,4002	1717	1839	1387	1486
VIS	564,892	22,597	238,678	80,0	5,12E+05	0,0947	2,2928	-6,4002	1691	1812	1367	1464
$PROP$	566,698	22,669	235,967	87,6	6,72E+05	0,0961	2,1397	-5,7521	1981	2104	1601	1700
$PROP$	579,696	23,188	233,862	88,0	6,81E+05	0,0991	2,1316	-5,7209	1963	2084	1586	1684
$PROP$	591,698	23,670	235,231	88,3	6,90E+05	0,1006	2,1234	-5,6899	2004	2126	1619	1718
$PROP$	605,692	24,230	233,123	88,7	6,99E+05	0,1039	2,1151	-5,6586	1985	2105	1604	1701
$PROP$	610,692	24,430	232,551	91,7	7,71E+05	0,1050	2,0518	-5,4287	2109	2229	1704	1801
$PROP$	612,694	24,510	232,690	95,5	8,71E+05	0,1053	1,9686	-5,1446	2291	2413	1851	1950
$PROP$	633,690	25,350	229,760	99,3	9,78E+05	0,1103	1,8859	-4,8784	2414	2533	1950	2047
$PROP$	650,800	26,034	222,194	101,3	1,04E+06	0,1172	1,8415	-4,7411	2351	2462	1899	1989
$PROP$	654,794	26,194	221,927	103,8	1,12E+06	0,1180	1,7879	-4,5795	2461	2572	1989	2078
$PROP$	703,798	28,155	205,904	106,8	1,22E+06	0,1367	1,7237	-4,3915	2243	2335	1812	1887
$PROP$	731,796	29,275	203,944	110,9	1,36E+06	0,1435	1,6374	-4,1465	2374	2461	1918	1989
$PROP$	733,798	29,355	203,842	112,0	1,40E+06	0,1440	1,6157	-4,0864	2417	2504	1953	2024
$PROP$	734,794	29,395	203,490	113,3	1,45E+06	0,1444	1,5889	-4,0125	2466	2553	1993	2063
$PROP$	735,800	29,435	203,062	115,9	1,56E+06	0,1449	1,5372	-3,8720	2569	2656	2076	2146
$PROP$	736,894	29,480	202,619	117,7	1,63E+06	0,1455	1,5011	-3,7751	2641	2727	2134	2204
$PROP$	740,897	29,640	202,240	119,9	1,72E+06	0,1465	1,4598	-3,6656	2728	2814	2205	2274
$PROP$	756,894	30,280	197,823	124,5	1,93E+06	0,1530	1,3763	-3,4476	2812	2893	2272	2337
Unit	s	mm	N	mm	mm^3	mm/N	-		J/m^2			

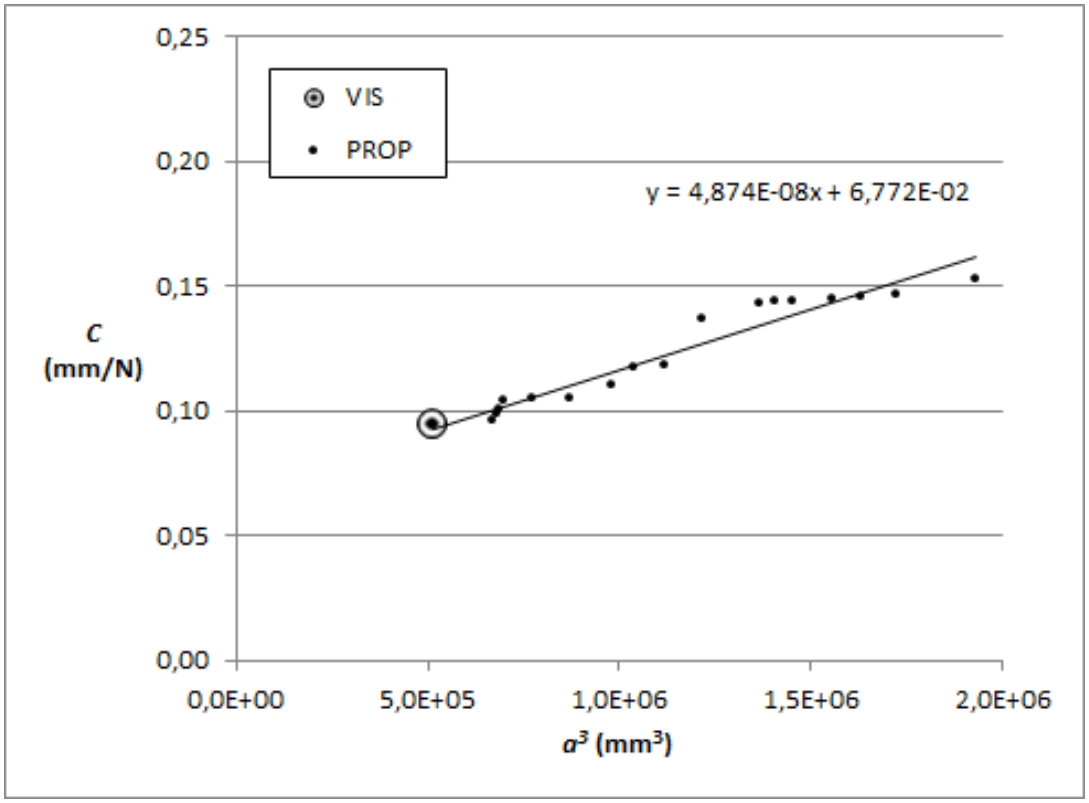

Figure E.5 : Calculation of m for $p3$ specimen

Table E.11 : Parameter values of $p8$ specimen used in calculation process

Parameter	B	h	I_1	E	m
Value	19,8543	1,9586	16,9586	138,67	30,06
Unit		mm		GPa	1/(N.mm^2)

Table E.12 : Calculation process for $p8$ specimen

Crit. Points	t	δ	P	a	a^3	C	θ_1	θ_2	$G_{\mathrm{II}_c(CBT)}$		$G_{\mathrm{II}_c(ECM)}$	
									-	corr.	-	corr.
NL	349,093	13,960	133,697	80,0	5,12E+05	0,1019	2,2928	-6,4002	627	663	260	275
MAX	539,991	21,598	185,823	80,0	5,12E+05	0,1163	2,2928	-6,4002	1211	1295	502	537
VIS	559,894	22,394	182,637	80,0	5,12E+05	0,1227	2,2928	-6,4002	1170	1252	485	519
$PROP$	560,899	22,435	182,537	84,5	6,03E+05	0,1230	2,2044	-6,0100	1302	1386	540	575
$PROP$	561,896	22,475	182,217	86,4	6,44E+05	0,1234	2,1649	-5,8501	1357	1442	563	598
$PROP$	563,897	22,555	181,733	87,3	6,66E+05	0,1242	2,1448	-5,7718	1380	1465	572	607
$PROP$	565,899	22,634	181,239	89,6	7,19E+05	0,1250	2,0966	-5,5900	1445	1530	599	634
$PROP$	567,892	22,714	180,969	91,5	7,66E+05	0,1256	2,0561	-5,4441	1501	1587	622	658
$PROP$	569,894	22,793	180,797	93,2	8,08E+05	0,1261	2,0197	-5,3168	1554	1640	644	680
$PROP$	573,897	22,954	180,541	95,3	8,65E+05	0,1272	1,9729	-5,1590	1622	1708	672	708
$PROP$	584,894	23,394	179,887	96,7	9,04E+05	0,1301	1,9425	-5,0593	1657	1743	687	723
$PROP$	594,894	23,794	179,571	101,2	1,04E+06	0,1326	1,8440	-4,7487	1809	1895	750	786
$PROP$	595,899	23,834	179,594	104,1	1,13E+06	0,1328	1,7810	-4,5590	1915	2002	794	830
$PROP$	597,892	23,913	178,968	106,6	1,21E+06	0,1337	1,7270	-4,4009	1995	2082	827	863
$PROP$	607,892	24,314	171,675	107,6	1,25E+06	0,1417	1,7058	-4,3399	1870	1951	775	809
$PROP$	610,997	24,437	170,751	108,9	1,29E+06	0,1432	1,6790	-4,2636	1895	1974	785	818
$PROP$	614,991	24,597	170,378	111,1	1,37E+06	0,1445	1,6333	-4,1352	1963	2043	814	847
$PROP$	620,997	24,838	169,352	113,5	1,46E+06	0,1468	1,5846	-4,0007	2024	2103	839	872
$PROP$	626,993	25,078	162,870	115,5	1,54E+06	0,1541	1,5441	-3,8907	1940	2013	804	834
$PROP$	628,995	25,158	161,136	119,5	1,71E+06	0,1562	1,4673	-3,6855	2032	2103	842	872
$PROP$	635,099	25,402	160,657	123,7	1,89E+06	0,1582	1,3906	-3,4847	2162	2234	896	926
$PROP$	649,093	25,961	158,372	125,0	1,95E+06	0,1640	1,3666	-3,4225	2147	2216	890	919
Unit	s	mm	N	mm	mm^3	mm/N	-		J/m^2			

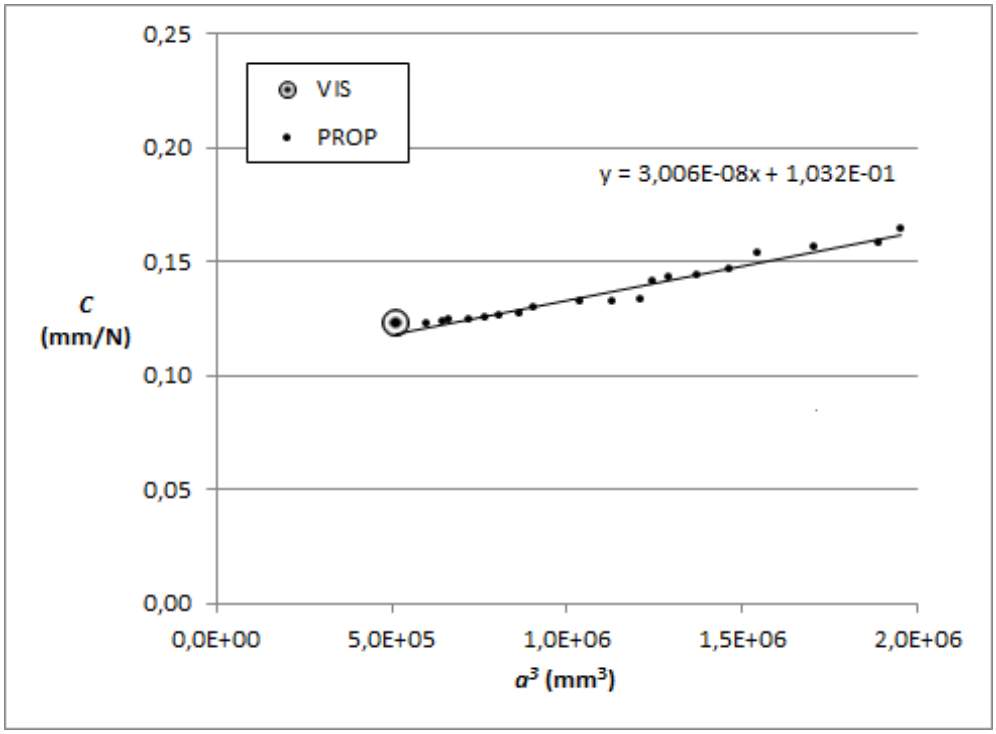

Figure E.6 : Calculation of m for $p8$ specimen

CURRICULUM VITAE

Candidate's full name:	İdil Sezer
Place and date of birth:	29.10.1987, İstanbul
Permanent Address:	Halkalı Merkez Mah. İkitelli Cad. Ihlamur Evleri Sit. Küçükçekmece, İST.
Universities and Colleges attended:	Istanbul Technical University, Aeronautical Engineering Bachelor's Degree, 2004-2008. Istanbul Technical University, Aeronautics and Astronautics Engineering MSc programme, 2008-present.
Publications:	